Control Laws for Autonomous Racing

Master's Thesis

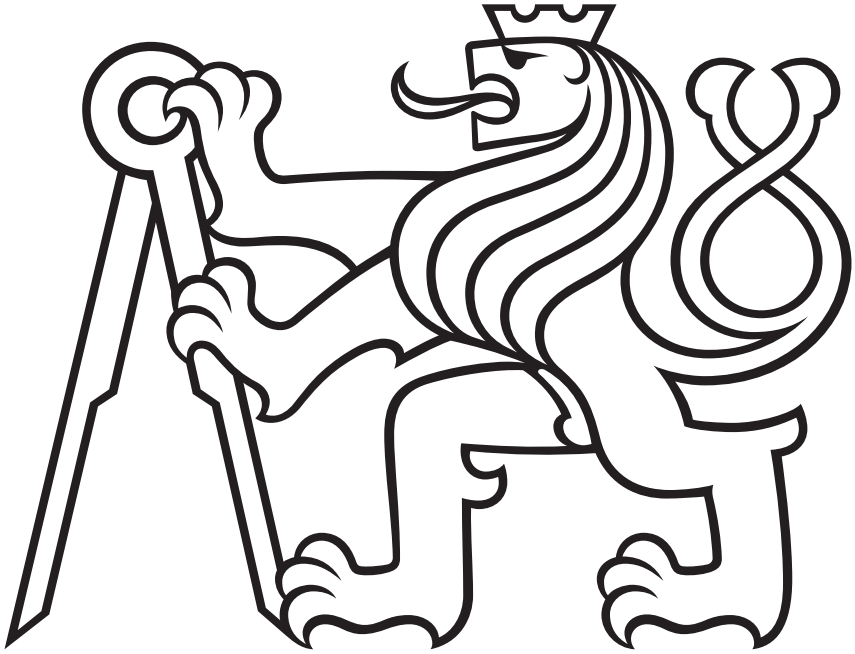

Author: Bc. Dominik Filyó
Supervisor: doc. Ing. Martin Hromčík, Ph.D.
Field of Study: Cybernetics and Robobotics

Czech Technical University in Prague
Faculty of Electrical Engineering
Department of Control Engineering

May, 2020

MASTER'S THESIS ASSIGNMENT

I. Personal and study details

Student's name: **Filyó Dominik** Personal ID number: **438666**

Faculty / Institute: **Faculty of Electrical Engineering**

Department / Institute: **Department of Control Engineering**

Study program: **Cybernetics and Robotics**

Branch of study: **Cybernetics and Robotics**

II. Master's thesis details

Master's thesis title in English:

Control laws for autonomous racing

Master's thesis title in Czech:

Řídicí zákony pro autonomní soutěžní vozy

Guidelines:

The goal of the thesis is to develop control algorithms suitable for fast dynamic autonomous driving. The motivation comes from the recent development in the student formula competition and the CVUT FEL eForce team's efforts towards autonomous racing involvment.
1. Implement the simulation framework, based on either available tools (e.g. the new Automotive Toolbox and Autonomous Driving Toolbox for
MATLAB) or your own custom-builty MATLAB/Simulink solutions.
2. Get familiar with existing longitudinal control solutions (like ABS, ESR). Implement simulation models implementing selected functionalities.
3. Get familiar with existing lateral control algorithms. Implement simulation models implementing selected functionalities.
4. Validate the developed functionalities experimentally on a subscape vehicle (modified and implemented RC car)

Bibliography / sources:

[1] Kiencke, Uwe, Nielsen, Lars, Automotive Control Systems, Springer-Verlag Berlin Heidelberg, 2005, ISBN 978-3-540-23139-4
[2] Franklin, Gene F.; Powell, J. David; Emami-Naeini, Abbas, Feedback Control of Dynamic Systems, Global Edition, Pearson Education Limited, 2019, ISBN: 9781292274522

Name and workplace of master's thesis supervisor:

doc. Ing. Martin Hromčík, Ph.D., Department of Control Engineering, FEE

Name and workplace of second master's thesis supervisor or consultant:

Date of master's thesis assignment: **13.02.2020** Deadline for master's thesis submission: **22.05.2020**

Assignment valid until:
by the end of summer semester 2020/2021

doc. Ing. Martin Hromčík, Ph.D.	prof. Ing. Michael Šebek, DrSc.	prof. Mgr. Petr Páta, Ph.D.
Supervisor's signature	Head of department's signature	Dean's signature

III. Assignment receipt

The student acknowledges that the master's thesis is an individual work. The student must produce his thesis without the assistance of others, with the exception of provided consultations. Within the master's thesis, the author must state the names of consultants and include a list of references.

. _____
Date of assignment receipt

_____
Student's signature

Declaration

I declare that the presented work was developed independently and that I have listed all sources of information used within it in accordance with the methodical instructions for observing the ethical principles in the preparation of university theses.

Bc. Dominik Filyó

Prague, 22.5.2020

Acknowledgements

Firstly, I would like to express my sincere gratitude to my supervisor doc. Ing. Martin Hromčík, Ph.D. for his valuable advice and guidance on writing this thesis. Special thanks belongs to Ing. Tomáš Haniš, Ph.D. for his objective view on the topic. Also, my thanks go to my university colleagues and friends.

Last but not least, I would like to thank my whole family for their continuous encouragement and supporting me throughout studying the university.

Abstract

Fully autonomous driving under any conditions and circumstances is a challenging task on which experts from all over the world work. It is assumed that fully autonomous cars will not drive on the roads in the coming years. This thesis focuses mainly on a single part of the complex topic. The aim of this work is to explore existing control laws for autonomous vehicles and design a simple, yet robust control system for a racing car. The greatest emphasis is given to the classical control theory, although other methods are also mentioned here. After the control system is designed, it is validated and tested in the MATLAB environment. A sports vehicle Porsche 911 is selected as the test car due to its convenient properties.

Keywords: trajectory tracking, autonomous vehicle, autonomous racing, racing vehicle, vehicle control, longitudinal control, lateral control, vehicle dynamics

Abstrakt

Plně autonomní řízení za jakýchkoli podmínek a okolností je náročný úkol, na kterém pracují odborníci z celého světa. Předpokládá se, že v nadcházejících letech ještě nebudou jezdit na silnicích plně autonomní auta. Tato práce se zaměřuje především na jednu část tohoto komplexního tématu. Cílem práce je prozkoumat existující řídící zákony pro autonomní vozidla a navrhnout jednoduchý, ale robustní řídicí systém pro závodní auto. Největší důraz je kladen na klasickou teorii řízení, i když jsou zde zmíněny i jiné metody. Poté, co je řídicí systém navržen, je validován a testován v prostředí MATLAB. Sportovní vůz Porsche 911 je vybrán jako testovací auto díky svým vhodným vlastnostem.

Klíčová slova: sledování trajektorie, autonomní vozidlo, autonomní závodění, závodní vozidlo, řízení vozidla, podélné řízení, příčné řízení, dynamika vozidla

Překlad názvu: Řídicí zákony pro autonomní soutěžní vozy

Contents

1 Introduction **1**
1.1 Motivation . . . 1
1.2 Problem definition . . . 2
1.3 Outline . . . 3

2 Objectives **5**

3 Self-driving Cars **7**
3.1 History . . . 7
3.2 Classification . . . 8
3.3 Legislation . . . 12
3.4 Autonomous racing . . . 13

4 Vehicle Modeling **15**
4.1 Nonlinear single-track model . . . 15
4.2 Vehicle dynamics . . . 16
4.3 Kinematics and wheel modeling . . . 18
4.4 Tire modeling . . . 19
4.5 Linear single-track model . . . 21

5 Vehicle Control **23**
5.1 Longitudinal control . . . 23
5.1.1 Active safety systems . . . 23
5.1.2 Reference speed generation . . . 26
5.1.3 Reference speed tracking . . . 30
5.2 Lateral control . . . 34
5.2.1 Geometric controllers . . . 35
5.2.2 Other controllers . . . 39

6 Control Strategy **43**
6.1 Straight segments . . . 43
6.2 Curved segments . . . 45

7 Simulations and Experiments **49**
7.1 Simulation framework . . . 49
7.2 Simulation results . . . 50
7.2.1 Longitudinal tracking . . . 50
7.2.2 Lateral tracking . . . 54
7.2.3 Combined tracking . . . 59

8 Results **65**

9 Conclusion **67**

A List of Acronyms and Symbols **68**

B Vehicle Parameters in Simulations **71**

C Content of the Attached Disc **72**

References **73**

List of Figures

1.1 Experimental 1:5 RC platform created during a faculty project 2
1.2 Simplified autonomous car architecture 3
3.1 Almost hundred years of development of self-driving cars 8
3.2 Bird eye view of the Tesla car 9
3.3 US map with autonomous vehicle legislation 13
4.1 Vehicle coordinate system 16
4.2 Top view of the single-track model with the global coordinate system . . . 17
4.3 Block diagram of the nonlinear single-track model 18
4.4 Example of dependency of the slip ratio λ and the longitudinal force F_x using Magic Formula 20
4.5 Example of dependency of the slip angle α and the lateral force F_y using Magic Formula 20
4.6 Example of dependency of the slip angle α and the aligning torque M using Magic Formula 20
4.7 Friction ellipse of the j-th tire with generated force F 21
5.1 Lateral stability defined by the phase plane $\beta - \dot{\beta}$ 27
5.2 Racing track and optimal path with apex in the middle 28
5.3 Structure of the longitudinal controller 31
5.4 Slip circles with points representing tire states 32
5.5 Understeer and oversteer 34
5.6 Simple geometric model of a vehicle with Ackermann steering 35
5.7 Pure pursuit geometry 36
5.8 Dependency of the look-ahead distance on the tracking quality 37
5.9 Stanley geometry 38
5.10 Phase plane with the sliding surface. 40
6.1 Longitudinal slip curve with a grey area representing the operating space of ABS 45
6.2 Diagram of longitudinal control on curved segments 45
6.3 Nonlinear mapping function $f : (-\infty, e_{c_{ref}}\rangle \rightarrow \langle -1, 1\rangle$ with deadband and saturation 46
7.1 Porsche 911 Carrera 49
7.2 Simulation framework 51
7.3 Performance of the PI regulator on gravel ($\mu = 0.5$) 52
7.4 Performance of the PI regulator on wet asphalt ($\mu = 0.75$) 52
7.5 Performance of the PI regulator on asphalt/concrete ($\mu = 1$) 53
7.6 Dependence of the parameter I on the tracking performance (P = 100, $\mu = 0.5$) 53

7.7 Vehicle variables for braking with ABS 55
7.8 Top view of the actual path when cornering and braking 55
7.9 Testing lap for lateral controllers 56
7.10 Pure pursuit tracking quality for different constants k_d 57
7.11 Stanley tracking quality for different constants k_d and k_{ss} 58
7.12 Dependence of the parameter $k_{d,yaw}$ on the performance of Stanley controller with high gain k_d 59
7.13 Testing lap for combined control 59
7.14 Tracking quality of the proposed controller in three different cases 61
7.15 Slip circles of the proposed controller for a changing parameter P 62
7.16 Slip circles of the car affected by a negative longitudinal force 63
7.17 Tracking quality of the proposed method in a bend with the car affected by a positive longitudinal force 64
7.18 Comparison of vehicle variables without the slip controller and with the slip controller 64

List of Tables

1 SAE international's levels of driving automation for on-road vehicles 10
2 Autonomous vehicle market penetration projections 12
3 Estimated crash reduction (%) by four-wheel ABS for cars and LTVs . . . 24
4 Estimated crash reduction (%) by combined ABS and ESC for cars and LTVs 25
5 Parameters of the ABS for simulation 54
6 Pure pursuit quality indicators 57
7 Stanley quality indicators 57
8 Quality indicators of the proposed controller without disturbances 60
9 Quality indicators of the proposed controller with a negative longitudinal force 63

1 Introduction

Cybernetics and robotics are one of the most perspective scientific areas in the world. Nowadays, more people are interested in modern technology than ever before. It is given by the fact that cybernetics influences our everyday lives since the new millennium. Let us mention the internet, where searching and advertisement are not imaginable without advanced knowledge in cybernetics, more specifically Artificial Intelligence (AI). Not everyone is interested in modern technology, but everyone must have noticed that robots are taking our jobs. According to [1], about 47 percent of US jobs were at risk in 2013 because of computerization. We can be sure that this trend will continue in the future.

This leads us to the topic of this thesis. Not only many employments are at risk, but also activities as driving. Huge research is being conducted at universities around the world. Czech Technical University in Prague (CTU), Faculty of Electrical Engineering (FEE) created a new centre for research of full authority vehicle control system layer named Smart Driving Solutions[1]. Not only car manufacturers invest billions of dollars in the development of self-driving cars. In 2019, investment into self-driving cars achieved $100 billion [2]. Companies that invested over $1 billion to autonomous driving are Volkswagen, Samsung, Ford, Toyota, Daimler, BMW, Audi, Honda, Softbank, Kia, Hyundai, Uber, Generals Motors and Apple (in descending order).

The main reason for the deployment of autonomous vehicles is the safety of passengers and pedestrians. A secondary goal is to make the journey more pleasant for passengers. With the expansion of wireless networks (5G), cars will be able to share information with other cars (car-to-car) and with infrastructure (infrastructure-to-car) [3, 4]. That will prevent traffic congestions and overall improve the traffic on highways and in big cities. Deploying of connected cars is also associated with a reduction in fuel consumption and therefore a reduction of fossil fuel emissions [5].

1.1 Motivation

The idea for this thesis came naturally as a continuation of our project at the Department of Control Engineering [6]. The research was supported by Toyota Motor Engineering and Manufacturing Europe as a part of Toyota Research Lab[2]. Toyota Research Lab is a network of top European workplaces in the area of autonomous driving (University of Cambridge, ETH Zürich, KU Leuven, Max-Planck Institut Saarbruecken, Czech Technical University in Prague). The cooperation with Toyota started already in 2003 thanks to prof. Ing. Jiří Matas, Ph.D from Center for Machine Perception. In 2018, the cooperation of the prof. Matas' team and Toyota expanded even further.

The goal of the project was to develop and test a 1:5 RC platform (see Fig. 1.1). The

[1]See the website http://sds.felk.cvut.cz/ for more information.
[2]See the website https://www.trace-lab.com/ for more information.

(a) Interior **(b)** Exterior

Fig. 1.1: Experimental 1:5 RC platform created during a faculty project. *Source:* Michal Bahník, 2020

created platform is built around commercially available RC car model Losi Desert Buggy. On top of the platform, there is mounted ZED stereo camera for collecting images of the surface in front of the car. The camera is also able to make depth maps and perform motion tracking together with 3D mapping. The platform contains two computers. The central unit is Nvidia Jetson Xavier with a powerful GPU which is responsible for gathering image data from the camera, data from the second computer Raspberry Pi3 with shield Navio2, and reference signals from the RC receiver. Navio2 is a board with its own ARM CPU for processing data from IMU and GPS units. The platform is used for developing and testing of various control systems.

The interest in dynamic driving at CTU FEE has been present for several years. In the master's thesis [7], the author explores laterally unstable vehicles and their stabilization by the active steering system. The thesis [8] aims to trajectory tracking of autonomous vehicles with a predictive controller. Last but not least, in [9], the author created a 1:10 RC platform for validating control algorithms. The reason for making the larger platform was to get closer to the real car's behavior and also insufficient computing power required for image processing and neural network operation. In 2020, at the time of writing this thesis, the student team eForce[3] from CTU FEE is developing the first autonomous vehicle for international races of self-driving formulas. The competitions will take place in the Czech Republic, Germany, and Spain in the summer. We have agreed on mutual cooperation on the formula project and the RC platform project. The results of this thesis may be used as inspiration or a starting point of developing the autonomous formula controllers.

1.2 Problem definition

The main output of the thesis is to develop longitudinal and lateral controllers for an autonomous racing vehicle. Our interest is to improve behavior of such a vehicle for fast

[3]See the website https://eforce.cvut.cz/en/ for more information.

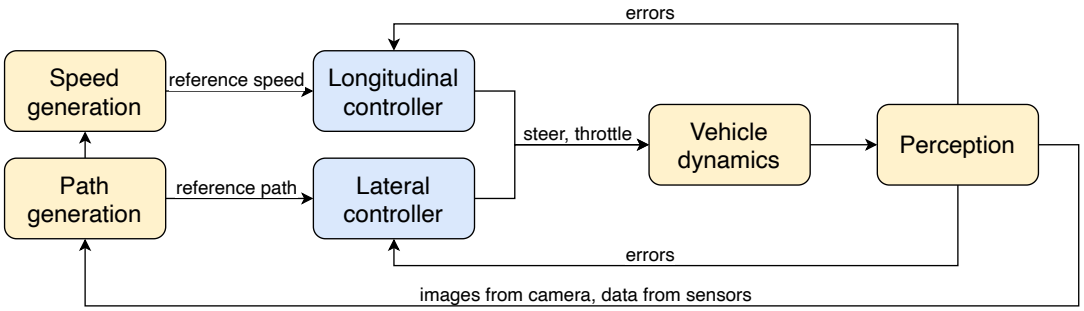

Fig. 1.2: Simplified autonomous car architecture. Longitudinal and lateral controllers are scope of this work. This design assumes simplification in form of decoupled longitudinal and lateral dynamics.

dynamic racing given a reference path. Dynamics of every vehicle change significantly with parameters such as weight distribution, or vehicle states such as velocity. Fig. 1.2 shows a simplified self-driving car architecture which is the same as a scheme of any mobile robot. Sensor measurements and the reference path enter both blocks with controllers. Sensor measurements consist of data from a stereo camera, IMU, and GPS. Based on this information, the car is supposed to follow the path while minimizing defined errors, for example, a perpendicular distance between the path and the center of the vehicle.

1.3 Outline

This work is organized as follows. After the objectives, it continues with an introductory chapter to self-driving cars (Chapter 3). This chapter provides a background of autonomous technology in terms of history, classification, and legislation. Information about autonomous racing is also presented there. The next two chapters are devoted to technical aspects of autonomous driving – mathematical modeling of vehicle dynamics (Chapter 4) and algorithms for vehicle control, together with methods for reference speed generation (Chapter 5). Vehicle control is discussed for both longitudinal and lateral dynamics. Chapter 6 describes our proposed solution for trajectory tracking of an autonomous vehicle. The last chapter before results and conclusions (Chapter 7) shows experiments made for the verification of employed control laws under different conditions.

2 Objectives

The thesis consists of several tasks which are listed below:

- Get familiar with existing longitudinal control solutions (like ABS, ESC). Implement simulation models implementing selected functionalities.
- Get familiar with existing lateral control algorithms. Implement simulation models implementing selected functionalities.
- Implement the simulation framework, based on either available tools (e.g. the new Automotive Toolbox and Autonomous Driving Toolbox for MATLAB) or your own custom-built MATLAB/Simulink solutions.
- Validate the developed functionalities experimentally on a subscale vehicle (modified and implemented RC car).

3 Self-driving Cars

The chapter introducing self-driving cars is divided into five sections that are focused on individual aspects of these types of vehicles. In the thesis, there are several designations for cars without a driver or for cars with driver and control system cooperation. We do not distinguish among self-driving, autonomous, and driverless cars/vehicles. There are many summary publications on the topic of autonomous driving. An overview of energy, environmental, and sustainability implications is given in [10]. The new book [11] presents comprehensively legal, technical, societal, and political impacts of road vehicle automation. Many surveys have been done on a technical aspect of automated driving, e.g. [12, 13].

3.1 History

The era of driverless cars began almost a hundred years ago. Francis P. Houdina developed the first car without a driver in 1925. It was a radio-operated automobile Chandler with a receiving antenna on the back of the car (see Fig. 3.1). The other car with a transmitting antenna had to follow the first car as shown in the image. At that time, radio signals reached only a few meters. The signals were driving small electric motors via analog components [14]. Automated guided cars were exhibited at the World's Fair in 1939. The vehicles were navigated via electromagnetic fields from coils built into the road [15].

The first promising experiments with real driverless cars began in the 1950s. In 1953, RCA Labs managed to build a small car that followed a pattern on the floor without outside intervention. Since then, there was no need to drive autonomous vehicles remotely. This company went further in development, and in 1957, they presented a full-size self-driving car. The demonstration took place on a 120-meter stretch of highway in Nebraska, US. In the same period, General Motors developed Firebirds, experimental cars described as "electronic guide system that can rush it over an automatic highway while the driver relaxes" [16].

In the early 1960s, the installation of automatic roads was first considered. Authorities began to see the potential of automated driving systems. Research laboratories around the world started to develop their solutions for autonomous driving, which at that time were based on the principle of guiding via electromagnetic interaction with the road (Ohio State University, Bendix Corporation, Citroën) [15]. In addition to technical research, semantic modeling techniques developed for a deductive question-answering system has also been studied since 1970 (intelligent automated logic) [17].

The 1980s and 1990s were revolutionary years for autonomous driving. Not only computing power reached a sufficient value, but also all types of commercial sensors have been developed since then (LiDAR, camera). Notable projects from the 1980s are the Mercedes-Benz robotic van capable of driving on empty roads and DARPA-funded

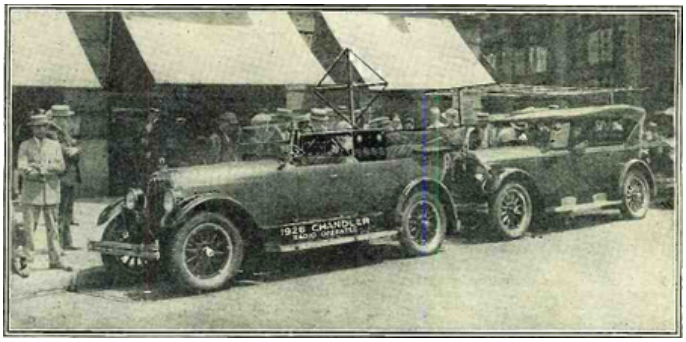

(a) 1926 Chandler

(b) Tesla Model 3

Fig. 3.1: Almost hundred years of development of self-driving cars. Image (a) shows the first car without a driver and (b) is an example of a modern self-driving car.

Autonomous Land driven Vehicle (ALV) [18, 19]. ALV utilized new modern technology as LiDAR, computer vision, and autonomous robotic control developed at prestigious universities in the USA (e.g. University of Maryland and Carnegie Mellon University). Two years after the introduction of ALV, in 1985, HRL Laboratories designed the first off-road autonomous navigation on the ALV [20]. Maximal speed of the ALV was 31 km/h, on complex terrain only 3.1 km/h [15]. The first neural network used for steering a vehicle was introduced in 1989 [21]. With today's perspective, the input image resolution was only 30×32 px, and it was connected, together with a laser rangefinder, to a fully connected neural network. It was one of the first usages of a neural network in control engineering (data-driven control [22]).

In 1994, the robot vehicle VaMP by Mercedes-Benz was driving on a three-lane highway in Paris performing challenging actions such as overtaking other cars [23]. Great success was achieved in 1995, when the project NavLab drove autonomously from the East Coast to the West Coast in the US [24]. The NavLab was powered by the system called RAPLH [25]. The only information available to the system was the curvature estimation and the lateral offset of the vehicle relative to the reference lane center. However, for security reasons, only steering was controlled by the system, but throttle and brakes were human-controlled. Unlike today, research on self-driving cars in the United States was funded mainly by DARPA, the US Army, and the US Navy until 2005. National Research Council published a guide for the military use of unmanned vehicles in 2002 [26].

3.2 Classification

The automotive industry uses many terms that are not precisely defined, and thus confusion can arise. An example of such a designation is "autonomous". There are individuals or companies that refer to autonomous vehicles as vehicles without a human driver, and other individuals or companies mean vehicles equipped with the Automated Driving Sys-

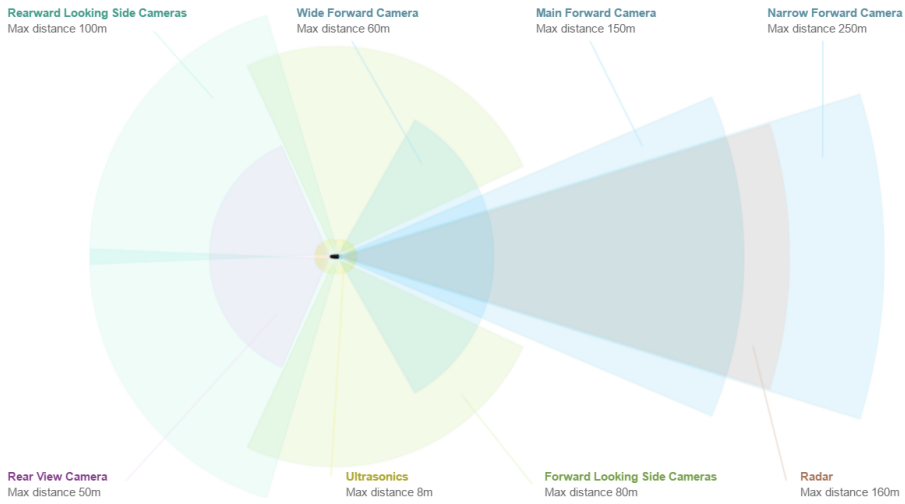

Fig. 3.2: Bird eye view of the Tesla car. The car is equipped with many sensors with different properties. Elon Musk claims that Tesla is currently working on level 5 autopilot [30]. *Source:* Tesla, 2020.

tem (ADS) in any form, e.g. Lane Keeping Assistant (LKA). Calling semi-autonomous cars autonomous can even lead to serious traffic accidents [27]. To avoid such confusion, National Highway Traffic Safety Administration (NHTSA) published the first classification system of self-driving vehicles [28]. The policy does not deal only with classification, but also with research, licensing, safety issues, and regulation.

In 2014, Society of Automotive Engineers (SAE) defined its own classification system with six levels of vehicle's autonomy – *Taxonomy and Definitions for Terms Related to On-Road Motor Vehicle Automated Driving Systems* [29]. Lowest level 0 means no automation, and the scale goes up to level 6 that means full automation. The classification table grouped by four parameters is shown in Tab 1. SAE updates the document as needed, but the essence remains the same. New versions of the text were published in 2016 and 2018. The second version was adopted by NHTSA, and since 2016, SAE's ranking is widely used among manufacturers and researchers.

This system categorizes cars according to the level of human-computer interaction. Basically, the capabilities and equipment of the car do not matter. A brief description of each category with examples follows:

- **Level 0** – Majority of today's vehicles are still level 0. In level 0 cars, there is no automation at all. The driver must rely only on himself, all tasks (braking, steering, parking, maneuvering, and accelerating) are performed by the driver. Auxiliary systems like ABS or conventional cruise control are not considered as automation, hence all vehicles equipped only with auxiliary systems fall into this category.

- **Level 1 ("hands-on")** – Middle-class cars have basic driving assistants implemented. Lane Keeping Assistant (LKA), Adaptive Cruise Control (ACC), Collision

SAE level	Name	Execution of Steering and Acceleration/ Deceleration	Monitoring of Driving Environment	Fallback Performance of Dynamic Driving Task	System Capability (Driving Modes)
Human driver monitors the driving environment					
0	No Automation	Human driver	Human driver	Human driver	N/A
1	Driver Assistance	Human driver and system	Human driver	Human driver	Some driving modes
2	Partial Automation	System	Human driver	Human driver	Some driving modes
Automated driving system monitors the driving environment					
3	Conditional Automation	System	System	Human driver	Some driving modes
4	High Automation	System	System	System	Some driving modes
5	Full Automation	System	System	System	All driving modes

Tab. 1: SAE international's levels of driving automation for on-road vehicles. *Source:* SAE International, 2014.

Avoidance System (CAS), and parking assistance are the most widespread level 1 assistants. Although they are autonomous systems, the driver still has to perform most operations. Drivers are expected to keep their hands on the steering wheel. Cars without any crash avoidance technology cannot qualify for the four-star safety rating or higher [31].

  - **LKA** helps the driver to stay in the traffic lane. The system alerts the driver when the car drives out the lane and turns wheels to correct the error. A vehicle equipped with LKA cannot keep itself centered in the lane.
  - **ACC** speeds up and slows down the car to keep a safe distance from the car in front of it. In addition, improved ACC systems are able to stop the car completely and then continue driving which is useful in traffic jams. It was shown that vehicles equipped with ACC are not string stable[4] [32].
  - **CAS**, also called Automatic Emergency Braking, is a system that prevents collisions between cars. If the front car starts to brake strongly, the system detects imminent crash, and it apply maximum braking force available. Since both ACC and CAS use the same forward-looking sensors, they are often installed together.
  - **Parking assistant** steers the car to the desired parking space while the driver adjusts the speed.

- **Level 2 ("hands-off")** – Vehicles in this category are able to perform both steering

[4]String stability – Any nonzero position, speed, and acceleration errors of an individual vehicle in a string do not amplify when they propagate upstream.

and accelerating on its own without driver intervention. However, the driver still has to monitor the driving environment and take control whenever needed. Level 2 autonomy is already considered as vehicle autopilot (basic Tesla Autopilot is classified as level 2, newer hardware achieves level 3 capabilities). At minimum, level 2 cars must be equipped with the improved stop-and-go ACC and Automated Lane Centering (ALC). Some level 2 cars include features as lane changes or automatic parking.

  - Unlike level 1 LKA, **ALC** follows the road or highway lane and keeps the vehicle centered. It is able to steer the car on roads with sharp turns. The driver must always be careful, because the system may not work in difficult conditions due to poor quality road signs or bad weather.

- **Level 3 ("eyes-off")** – Starting from level 3, vehicles monitor the driving environment. Level 3 is a boundary between semi-autonomous and fully autonomous cars. They still require the presence of a human driver who can intervene if necessary. This autonomy level is the most controversial because a person is still responsible for the car, but that person can read a book or watch a movie. The only requirement is that the driver stays conscious during the route. If a problem occurs, it may be difficult for the driver to react in split-seconds which can lead to severe accidents. Car manufacturers therefore often skip level 3 and develop level 4 directly (Ford, Volvo). Despite the disadvantages, some cars still offer level 3 capabilities (Audi A8, forthcoming BMW iNEXT) [33].

- **Level 4 ("mind-off")** – Level 4 provides robust self-driving capabilities in most conditions. However, a human still has the option to drive the car manually. The driver is even allowed to sleep while driving, and thus he becomes a passenger. Level 4 cars can handle road construction sites and other tricky situations as long as the manufacturer's terms are met. On the other hand, they still have problems driving through torrential rain and snow. No commercial level 4 car is available in 2020, but several models are expected to come in a few years (Google's Waymo, Volvo, and Baidu joint project). Services like autonomous taxi and ridesharing seem to be perspective use of the level 4 technology.

- **Level 5** – Full level of automation. In comparison to level 4 cars, level 5 cars are able to perform full dynamic driving under any circumstances. They are able to drive in heavily populated urban areas with heavy traffic with minimal risk of an accident. Level 5 cars are not expected to be developed earlier that in 2025 [34]. According to European Union (EU), they are expected to show on roads around 2030 [35]. Tab. 2 shows the prediction of deployment of level 5 cars [36]. Human occupants of this type of vehicle will be just passengers, and they will never be

Stage	Decade	New sales	Fleet	Travel
Available with large price	2030s	2-5%	1-2%	1-4%
Available with moderate price	2040s	20-40%	10-20%	10-30%
Available with minimal price	2050s	40-60%	20-40%	30-50%
Standard feature included on most new vehicles	2060s	80-100%	40-60%	50-80%
Saturation (everybody who wants it has it)	2070s	-	-	-
Required for all new and operating vehicles	-	100%	100%	100%

Tab. 2: Autonomous vehicle market penetration projections. *Source:* Victoria Transport Policy Institute, 2017

involved in driving. Most likely, level 5 cars will not even have a steering wheel and pedals since they will not be needed.

Automated cars with the level of autonomy 1 or higher are also distinguished according to a level of assistance to the driver. Advanced Driver Assistance System (ADAS) corresponds to level 1 or level 2 cars. It is a system that assists the driver while driving but does not take responsibility for the car. Automated Driving System (ADS) involves systems that take control of the vehicle under defined conditions.

3.3 Legislation

The incremental cost is not the only factor that prevents the wider spread of autonomous cars in the world. As technology goes forward, there is a need for the regularization of self-driving cars and implement them into laws. Because this is a relatively new technology, legal aspects hamper the deployment of autonomous cars. Governments around the world are aware that autonomous driving is inevitable in the future. Both US and EU published documents that are devoted to the future of autonomous cars [37, 38]. Strategic Transport Research and Innovation Agenda (STRIA) roadmap for connected and automated transport was published recently in 2019 [39].

In the US, driverless car manufacturers must follow the policy of the federal government and also the laws of the state in which the car operates. In 2015, the US states California, Florida, Michigan, Nevada, Virginia, and Washington, DC, allowed the testing of self-driving cars on public roads. Year later, in 2016, the Obama's Administration released the first report which introduced the regularization of autonomous cars [40]. Since then, the Trump's Administration, specifically NHTSA together with US Department of Transportation (DOT), published follow-up reports that updates its regulatory guidance. They limit the federal regulatory role in overseeing of autonomous vehicles while giving more competences to DOT. This department now addresses the impact of autonomous technology on commercial trucks, public transit, rail, and ships [41]. The map of US states with the level of regularization is shown in Fig. 3.3.

In the study by the EU, law and policy, together with limitations and gaps in the

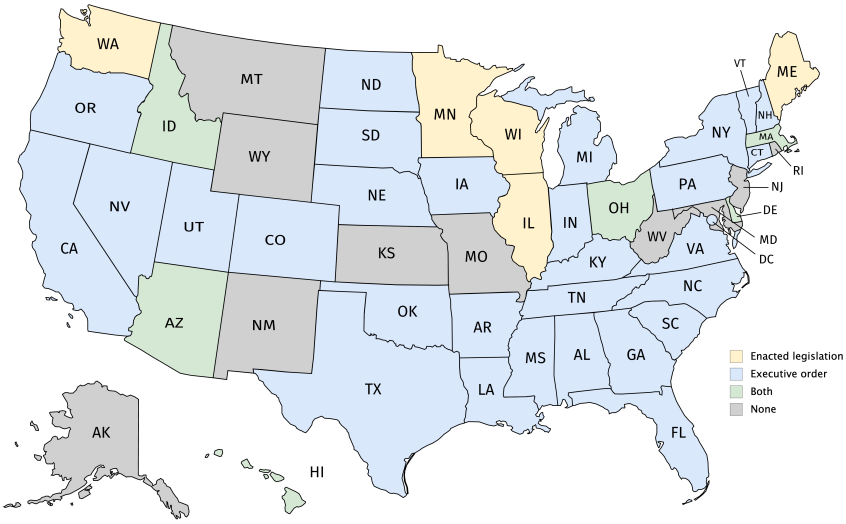

Fig. 3.3: US map with autonomous vehicle legislation. *Source:* National Conference of State Legislatures, 2020.

current framework, are discussed [42]. In 2017, 29 countries of the EU signed a document on testing and large scale demonstration of connected and automated driving [43]. This cooperation among European countries will help to develop and expand new technology faster. Furthermore, in the same year, the European Parliament adopted civil law rules for robotic systems and AI [44]. The EU also cooperates to develop the next generation of broadband infrastructure useful for connected driving of self-driving cars [45].

Ethical and legal issues are not included in this work. These questions are discussed for instance in [11, 46, 47].

3.4 Autonomous racing

Autonomous racing is a very complex discipline which consists of several challenging tasks. First, the high-level planner must generate the optimal trajectory using sensors mounted on the racing car. The low-level planner then executes dynamic objectives like overtaking other vehicles and obstacle avoidance. The planner provides reference inputs to longitudinal and lateral control systems. Throughout the racing, the system performs Simultaneous Localization And Mapping (SLAM) from camera data. This work focuses mainly on control algorithms for autonomous racing vehicles.

Autonomous racing is a relatively new sport discipline that is spreading all over the world. A number of events are organized every year, including both professional competitions and student competitions [48]. One of the most prestigious competitions of autonomous vehicles is DARPA Grand Challenge. The US congress supports this challenge to reduce the gap between academic research and military use. DARPA offers the winners a high financial reward ($2 million for the first place). Each year, the goal of the competition is different. The first two years in 2004 and 2005 were held on off-road

tracks. Two years later, in 2007, the contest is known as the "Urban Challenge", indicating that it was held in an urban environment. The competition also focused on humanoid robots, defense systems, or satellites in the past. In the last years, from 2017 to 2021, the task is to build a robotic system that autonomously searches and explores subterranean environments [49].

The DARPA Grand Challenge contributes to progress in robotics and artificial intelligence. Many novel algorithms have been developed within the event [50]. In 2005, the Stanley car by Stanford University managed to defeat all 23 opponents and completed the 212 km off-road track with the best time [51]. Their algorithm is named after the race car, and it is still a widely utilized algorithm for path tracking. Stanford's rivals from Carnegie Mellon University got second place in the race. Along with other lateral control algorithms, the Stanley controller is discussed in Chapter 5.

The first global championship for autonomous cars racing on a racetrack is called Roborace[5]. The first season took place in 2019, and only two teams participated – Technical University of Munich and Team Arrival. The number of participants will surely increase in the future. In the Roborace championship, all teams have the same starting conditions. They use a chassis and powertrain designed by the organizer, and their task is to create the best control algorithms. The newest racing vehicle called DevBot 2.0 is all-electric and runs on the Nvidia DRIVE platform. The DevBot holds a Guinness World Record for the highest speed achieved by a self-driving car (282.42 km/s) [52].

Not only full-size car races are organized, but also RC cars races. The best-known competition of this type is F1TENTH[6] organized by two US universities – University of Virginia, University of Pennsylvania, and Italian University of Modena and Reggio Emilia. For the race, an autonomous F1/10 platform was developed [53]. All participating teams use similar hardware, and the goal is to design the best perception, planning, and control for the vehicle. CTU FEE also periodically participates in the race with good results (Portugal 2018 – 1st, Italy 2018 – 3rd place, New York 2019 – 3rd place).

[5]See the website https://roborace.com/ for more information.
[6]See the website http://f1tenth.org/ for more information.

4 Vehicle Modeling

Longitudinal and lateral dynamics of vehicles have been studied since the 1940s. The first mathematical model was made by German engineers Riekert and Schunk [54]. This very idealized model works only for later acceleration up to 4 m/s^2 [55]. Since then, researchers have created many models that differ by a number of Degrees of Freedom (DOF), from the simplest ones to very complex models capturing detailed dynamics. The single-track model is a simple representation of a bicycle-like vehicle, but it can also be used for car-like vehicles. It simplifies the system by having only two wheels connected by a rigid bar. The single-track representation does not take into account effects like body roll and redistribution of weight in the lateral direction. There is a linear version with 2 DOF (e.g. absolute speed and yaw) and a nonlinear version with 3-7 DOF [55]. This chapter focuses on the nonlinear single-track model with 3 DOF by Denis Efremov from CTU FEE [7].

Other model options of car-like vehicles include the twin-track model that has considerably more DOF (from 14 to 30), and it can thus cover more dynamic effects. The disadvantage is the high complexity and hence the necessity to use modern computer software. There are even more sophisticated methods for modeling a vehicle with more than 500 DOF. These models, such as the finite-element model or the hybrid model, are intended e.g. for aerodynamics testing. For this work, it is unnecessary to deal with something more complex than the nonlinear single-track model which captures all dynamic behavior. A detailed description of single-track and twin-track models is included in [55].

4.1 Nonlinear single-track model

The classical nonlinear single-track model is used for a description of a vehicle in the planar plane. The model is not complex and yet captures the main vehicle dynamics. It is therefore popular among many researchers for designing stabilization systems [56]. The derivation is based on the following simplifications:

- All lifting, rolling and pitching motions are neglected.
- The vehicle's mass is assumed to be concentrated at the Center of Gravity (CG).
- The front and the rear tires are represented as one single tire on each axle. The imaginary tire contact points, which the tire forces are to act upon, lie along the center of the axle.
- The pneumatic trail and the aligning torque resulting from the slip angle of the tire is neglected.
- The wheel-load distribution between the front and the rear axle is assumed to be constant.

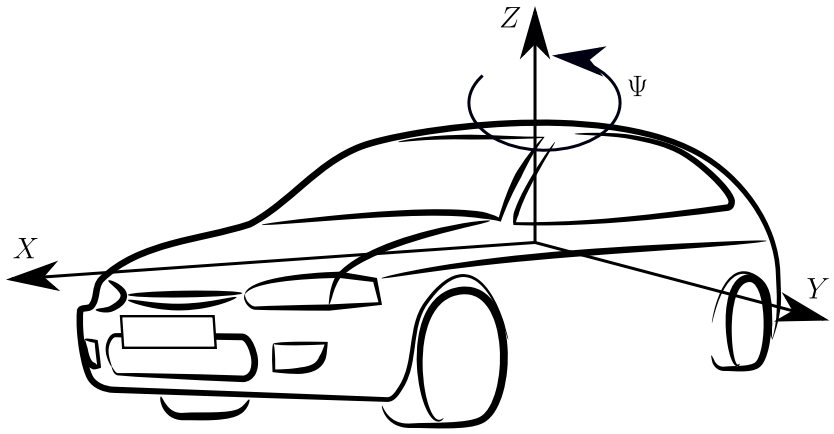

Fig. 4.1: Vehicle coordinate system

The local coordinate system is shown in Fig. 4.1. There is used the right-handed coordinate system. The X axis lies in the longitudinal direction with the car. The Y axis points to the left, and Z axis points up. The positive direction of rotation Ψ is when the car turns left. The index g in Fig. 4.2 denotes the global coordinate system.

4.2 Vehicle dynamics

In the vehicle coordinate system, the velocity $\vec{v}$ is computed as

$$\vec{v} = \begin{pmatrix} v\cos\beta \\ v\sin\beta \\ 0 \end{pmatrix}. \tag{4.1}$$

The acceleration of the Center of Gravity (CG) is given by by the sum of the normal acceleration and the tangential acceleration:

$$\begin{aligned} \vec{a} &= \underbrace{\frac{\mathrm{d}\vec{v}}{\mathrm{d}t}}_{a_t} + \underbrace{\vec{\omega}\times\vec{v}}_{a_n} = \begin{pmatrix} \dot{v}\cos\beta - v\dot{\beta}\sin\beta \\ \dot{v}\sin\beta + v\dot{\beta}\cos\beta \\ 0 \end{pmatrix} + \begin{pmatrix} 0 \\ 0 \\ \dot{\psi} \end{pmatrix} \times \begin{pmatrix} v\sin\beta \\ v\cos\beta \\ 0 \end{pmatrix} \\ &= \begin{pmatrix} \dot{v}\cos\beta - v(\dot{\beta}+\dot{\psi})\sin\beta \\ \dot{v}\sin\beta + v(\dot{\beta}+\dot{\psi})\cos\beta \\ 0 \end{pmatrix} \end{aligned} \tag{4.2}$$

The equation of translational motion for this system has the form $\vec{F} = m\vec{a}$. Plugging Eq (4.2) to this formula results in

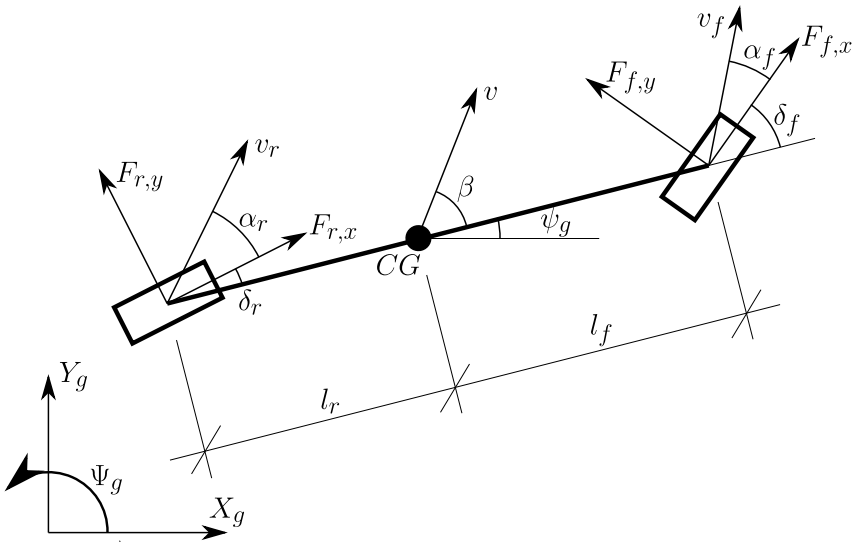

Fig. 4.2: Top view of the single-track model with the global coordinate system

$$m \begin{pmatrix} \dot{v}\cos\beta - v(\dot{\beta}+\dot{\psi})\sin\beta \\ \dot{v}\sin\beta + v(\dot{\beta}+\dot{\psi})\cos\beta \\ 0 \end{pmatrix} = \begin{pmatrix} F_x \\ F_y \\ 0 \end{pmatrix}. \tag{4.3}$$

In addition to the linear motion, the car can rotate around the Z axis, and therefore third motion equation is in the form $M = I\ddot{\psi}$. If we organize all the equations, we can write one Newton's matrix equation to describe the dynamics of the planar vehicle with three DOF as

$$\begin{pmatrix} mv(\dot{\beta}+\dot{\psi}) \\ m\dot{v} \\ I\ddot{\psi} \end{pmatrix} = \begin{pmatrix} -\sin\beta & \cos\beta & 0 \\ \cos\beta & \sin\beta & 0 \\ 0 & 0 & 1 \end{pmatrix} \begin{pmatrix} F_x \\ F_y \\ M \end{pmatrix}, \tag{4.4}$$

where m is the vehicle mass, v is the absolute speed of CG, β is the side-slip angle (the angle between the speed vector and the vector parallel to the vehicle), ψ is the yaw angle, I is the moment of inertia of the vehicle around the Z axis, F_x and F_y are forces acting on the CG, and M is the moment of force acting around the Z axis.

The forces F_x, F_y and the moment M acting on the body are determined from so-called steering angle projection

$$\begin{pmatrix} F_x \\ F_y \\ M \end{pmatrix} = \begin{pmatrix} \cos\delta_f & -\sin\delta_f & \cos\delta_r & -\sin\delta_r \\ \sin\delta_f & \cos\delta_f & \sin\delta_r & \cos\delta_r \\ l_f\sin\delta_f & l_f\cos\delta_f & -l_r\sin\delta_r & -l_r\cos\delta_r \end{pmatrix} \begin{pmatrix} F_{f,x} \\ F_{f,y} \\ F_{r,x} \\ F_{r,y} \end{pmatrix}, \tag{4.5}$$

where δ_f and δ_r are the steering angles on front and rear wheels, l_f, and l_r are the distances from the CG to the front axle and rear axle respectively. $F_{f,x}, F_{f,y}, F_{r,x}, F_{r,y}$ are the forces

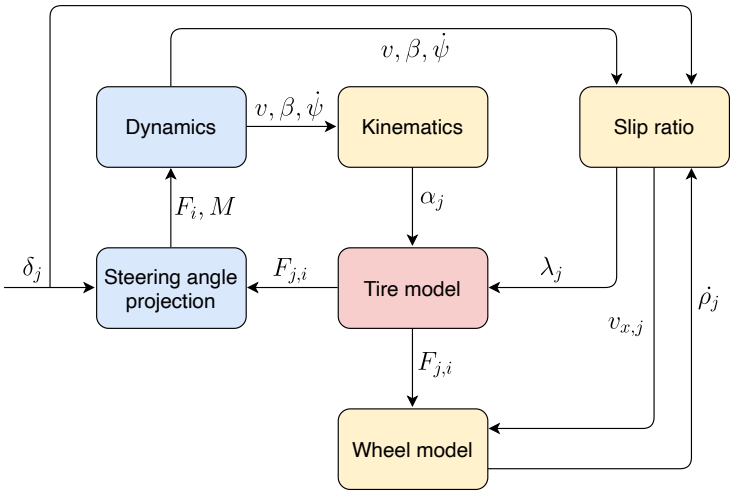

Fig. 4.3: Block diagram of the nonlinear single-track model. Blue blocks are discussed in Section 4.2, yellow blocks in Section 4.3 and red block in Section 4.4. Indices j denote the front or the rear wheel ($j \in \{r, f\}$), and indices i denote the axis ($i \in \{x, y\}$).

acting parallel and perpendicular to the wheels heading. These forces depend on the used tire model. Tire modeling is discussed in Section 4.4. After merging Eq (4.4) and Eq (4.5) and simple reordering, we get a system of nonlinear equations describing dynamics of the vehicle under specified conditions:

$$\begin{aligned}\dot{x_1} = -x_3 &+ \frac{\cos\beta}{mv}(F_{f,x}\sin\delta_f + F_{f,y}\cos\delta_f + F_{r,x}\sin\delta_r + F_{r,y}\cos\delta_r) \\ &- \frac{\sin\beta}{mv}(F_{f,x}\cos\delta_f - F_{f,y}\sin\delta_f + F_{r,x}\cos\delta_r - F_{r,y}\sin\delta_r)\end{aligned} \tag{4.6a}$$

$$\begin{aligned}\dot{x_2} = &\frac{\sin\beta}{m}(F_{f,x}\sin\delta_f + F_{f,y}\cos\delta_f + F_{r,x}\sin\delta_r + F_{r,y}\cos\delta_r) \\ &+ \frac{\cos\beta}{m}(F_{f,x}\cos\delta_f - F_{f,y}\sin\delta_f + F_{r,x}\cos\delta_r - F_{r,y}\sin\delta_r)\end{aligned} \tag{4.6b}$$

$$\dot{x_3} = \frac{1}{I}(F_{f,x}l_f\sin\delta_f + F_{f,y}l_f\cos\delta_f - F_{r,x}l_r\sin\delta_r - F_{r,y}l_r\cos\delta_r) \tag{4.6c}$$

This set is called state transition equation with 3 states. The states are defined as $x_1 = \beta$, $x_2 = v$ and $x_3 = \dot{\psi}$.

4.3 Kinematics and wheel modeling

The vehicle kinematics consists of computation of slip angles α_f and α_r. A slip angle is defined as a ratio between the lateral velocity of the wheel $v_{j,y}$ and the forward velocity $v_{j,x}$ ($v_j = \sqrt{v_{j,y}^2 + v_{j,x}^2}$). The index j denotes the front or the rear wheel ($j \in \{r, f\}$). The

slip angle α_j is defined as

$$\alpha_j = -\arctan\frac{v_{j,y}}{|v_{j,x}|} = -\arctan\frac{(v\sin\beta + l_j\dot{\psi})\cos\delta_j - v\cos\beta\sin\delta_j}{|(v\sin\beta + l_j\dot{\psi})\sin\delta_j + v\cos\beta\cos\delta_j|}. \tag{4.7}$$

Consequence of the slip angle is the cornering force which makes the car to turn. The cornering force is linear to the slip angle first few degrees and then it increases nonlinearly until it reaches its maximum value. The force decreases behind the peak as shown further in Section 4.4 [57].

The principle of moment conservation apply for both wheels:

$$J_j\ddot{\rho}_j = \tau_j - R_jF_{j,x} - \mathrm{sgn}(\dot{\rho})\tau_{Bj} - k_jv_{j,x} \tag{4.8}$$

Here, J_j is the moment of inertia of the j-th wheel around the axis that passes through the center of the wheel, $\ddot{\rho}_j$ is the angular acceleration, τ_j is the torque produced by the engine, R_j is the radius of the wheel, $F_{j,x}$ is the force acting on the wheel in the longitudinal direction, $\dot{\rho}$ is the angular velocity, τ_{Bj} is the breaking torque produced by brakes, k_j is the coefficient of the road drag, and $v_{j,x}$ is the forward velocity of the wheel.

The slip ratio λ has a similar meaning for longitudinal dynamics as the slip angle for lateral dynamics. In the tire modeling, the slip angle α_j is used for determining of the lateral wheel force $F_{j,y}$, while the slip ratio λ_j is used for determining of the longitudinal wheel force $F_{j,x}$. Furthermore, the slip ratio is necessary for designing effective ABS. Let us define the tangential velocity of the j-th wheel as $v_{Tj} = \dot{\rho}_jR_j$. The slip ratio is then defined as a ratio between the tangential velocity and the forward velocity $v_{j,x}$:

$$\lambda_j = \frac{v_{Tj} - v_{j,x}}{\max(|v_{j,x}|, v_{Tj})} = \frac{\dot{\rho}_jR_j - v_{j,x}}{\max(|v_{j,x}|, v_{Tj})} \tag{4.9}$$

The slip ratio is bounded as $\lambda_j \in \langle -1, 1\rangle$. Zero slip ratio means that there is no sliding between the wheel and the road. In that case, the whole force is transferred from the wheel to the road, and thus no adhesion is lost. If $\lambda_j = 1$, the wheels move but the car remains motionless. This extreme case may occur when a high-performance car starts on slippery surfaces such as gravel or ice. If $\lambda_j = -1$, the car moves but the wheels do not, e.g. during heavy braking on low friction surfaces.

4.4 Tire modeling

Tire modeling is a complex task important for the realistic car model behavior. The task is to determine forces F_x, F_y and the aligning torque M produced by the tire. Many papers on tire modeling have been published since 1950s [58]. Overview of the tire models is given in [59]. In this thesis, we aim only on the model by Dutch professor Hans B. Pacejka who dedicated his career to vehicle system dynamics. The first models by Pacejka

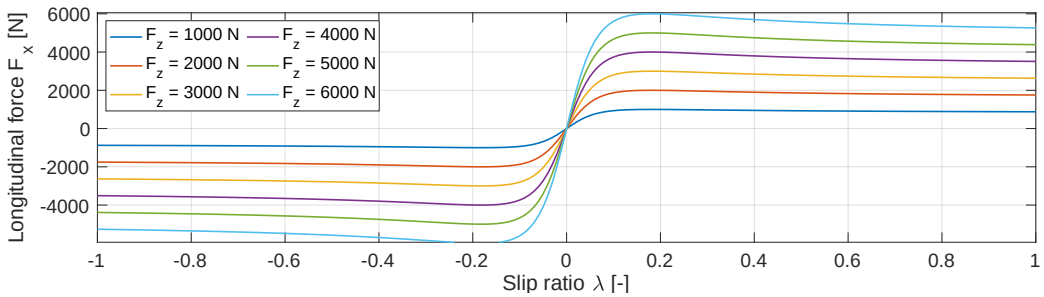

Fig. 4.4: Example of dependency of the slip ratio λ and longitudinal force F_x using Magic Formula with parameters $B = 0.15, C = 2, D = 1, E = 0.95$

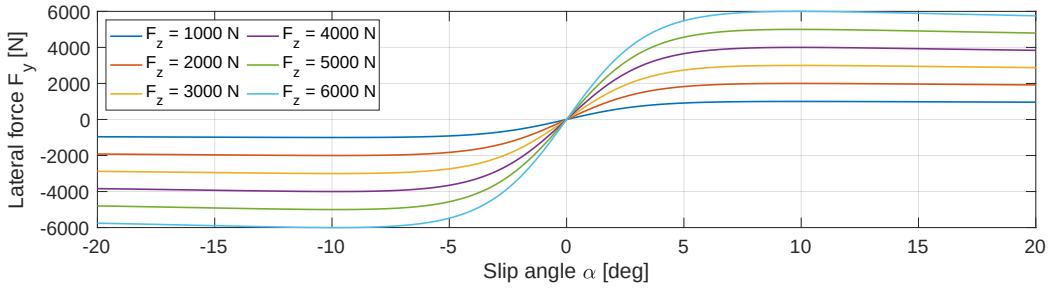

Fig. 4.5: Example of dependency of the slip angle α and lateral force F_y using Magic Formula with parameters $B = 12, C = 1.4, D = 1, E = 0.1$

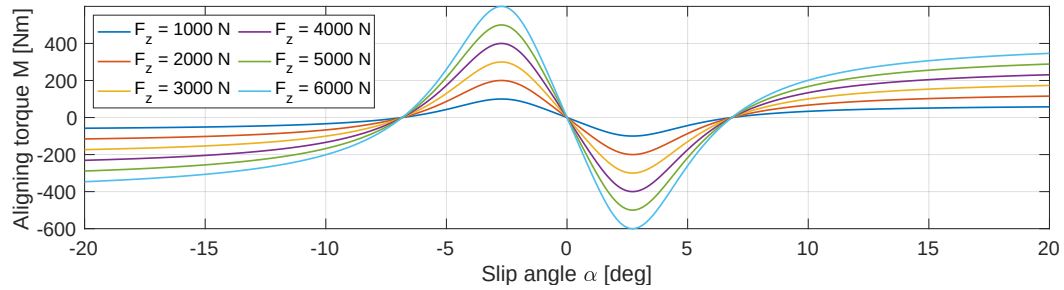

Fig. 4.6: Example of dependency of the slip angle α and aligning torque M using Magic Formula with parameters $B = 0.2, C = 2.5, D = -10, E = -4$

contained 10-20 coefficients to describe the characteristics of the tire [57].

In 1987, Pacejka with his co-wokers introduced the famous "Magic Formula" to model a tire effectively using as few coefficients as possible [60]. He updated the formula several times to ensure higher similarity with a real tire. In 1992, a third version, which is still in use today, was published [61]. Since Pacejka introduced his tire model, it became the most predominating model due to its versatility and simplicity. This method, unfortunately, does not work at low speeds, and that is the main drawback. Engineers use alternatives as the brush tire model for low-speed applications [62].

Pacejka's Magic Formula utilizes only four coefficients to describe a tire behavior. It

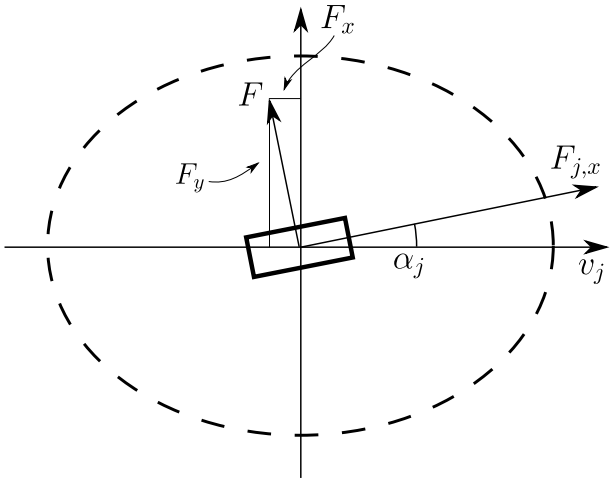

Fig. 4.7: Friction ellipse of the j-th tire with generated force F

has the form

$$y(x) = F_z D \sin(C \arctan(Bx - E(Bx - \arctan(Bx)))), \tag{4.10}$$

where the pair (y, x) can be (F_x, λ), (F_y, α), or (M, α). The parameter B is the stiffness factor, C is the shape factor, D is the peak factor, and E is the curvature factor. The set of parameters is unique for each F_x, F_y or M, and it is generally not dependent solely on the characteristics of the tire, but also on the load F_z and the surface. Examples of the generated forces and the moment for different loads are shown in Fig. 4.4, Fig. 4.5, Fig. 4.6.

The horizontal force generated by the tire cannot be higher than the vertical force generated by the load F_z. This restriction can be represented geometrically by the friction ellipse. The friction ellipse is a boundary around the tire which limits the vector of the horizontal force (see Fig. 4.7). It can be calculated as

$$|\vec{F}| = \sqrt{\frac{F_x^2}{D_x^2} + \frac{F_y^2}{D_y^2}} \leq F_z, \tag{4.11}$$

where D_x and D_y are Magic Formula coefficients D for longitudinal force and lateral force respectively.

4.5 Linear single-track model

Linear models are especially suitable for designing control algorithms. Linearization of the Newton's matrix equation Eq. (4.4) for small side-slip angles $\beta < 10°$ is

$$\begin{pmatrix} mv(\dot{\beta} + \dot{\psi}) \\ m\dot{v} \\ I\ddot{\psi} \end{pmatrix} = \begin{pmatrix} -\beta & 1 & 0 \\ 1 & \beta & 0 \\ 0 & 0 & 1 \end{pmatrix} \begin{pmatrix} F_x \\ F_y \\ M \end{pmatrix}. \tag{4.12}$$

Another assumption is a constant speed v that is used as a model parameter. With $\beta = 0$, the previous matrix equation transforms to

$$\begin{pmatrix} mv(\dot{\beta} + \dot{\psi}) \\ I\ddot{\psi} \end{pmatrix} = \begin{pmatrix} F_y \\ M \end{pmatrix}. \tag{4.13}$$

The original steering angle projection (Eq. (4.5)) is linearized for small steering angles as

$$\begin{pmatrix} F_x \\ F_y \\ M \end{pmatrix} = \begin{pmatrix} 1 & 0 & 1 & 0 \\ 0 & 1 & 0 & 1 \\ 0 & l_f & -0 & -l_r \end{pmatrix} \begin{pmatrix} F_{f,x} \\ F_{f,y} \\ F_{r,x} \\ F_{r,y} \end{pmatrix}, \tag{4.14}$$

Linear forms for side slip angles α_f and α_r are

$$\alpha_f = \delta_f - \beta - \frac{l_f\dot{\psi}}{v}, \tag{4.15a}$$

$$\alpha_f = \delta_r - \beta + \frac{l_r\dot{\psi}}{v}. \tag{4.15b}$$

The tire dynamics is approximated using the linear tire model as

$$F_{j,y} = C_j\alpha_j, \tag{4.16}$$

where C_j is the tire stiffness for the j-th tire. We obtain the linear vehicle model by merging Eq. (4.13), Eq. (4.14), Eq. (4.15), and Eq. (4.16). The final state-space representation has the form

$$\overbrace{\begin{pmatrix} \dot{\beta} \\ \ddot{\psi} \end{pmatrix}}^{\dot{\mathbf{x}}} = \overbrace{\begin{pmatrix} a_1 & a_2 \\ a_3 & a_4 \end{pmatrix}}^{\mathbf{A}} \overbrace{\begin{pmatrix} \beta \\ \dot{\psi} \end{pmatrix}}^{\mathbf{x}} + \overbrace{\begin{pmatrix} b_1 & b_2 \\ b_3 & b_4 \end{pmatrix}}^{\mathbf{B}} \overbrace{\begin{pmatrix} \delta_f \\ \delta_r \end{pmatrix}}^{\mathbf{u}}, \tag{4.17}$$

where

$$\begin{gathered} a_1 = -\frac{C_f + C_r}{mv},\ a_2 = \frac{l_rC_r - l_fC_f}{mv^2} - 1,\ a_3 = \frac{l_rC_r - l_fC_f}{I},\ a_4 = -\frac{l_f^2C_f + l_r^2C_r}{vI}, \\ b_1 = \frac{C_f}{mv},\ b_2 = \frac{C_r}{mv},\ b_3 = \frac{l_fC_f}{I}\ b_4 = \frac{l_rC_r}{I}. \end{gathered} \tag{4.18}$$

5 Vehicle Control

Existing vehicle control solutions are presented in this chapter. We divided the chapter into two categories, according to the axis in which the control system works. Longitudinal control adjusts car speed by changing the engine torque. Since the power train dynamics is not in the scope of this work, we assume that we can directly control the torque of the front axle τ_f and torque of the rear axle τ_r, together with the breaking torques τ_{Bf} and τ_{Br}. Lateral control systems regulate wheels rotation to achieve the best possible tracking of the reference path.

Control systems are typically formulated as feedback systems with a defined error that they try to eliminate. Since a vehicle is a nonholonomic, strongly nonlinear, and complex system, longitudinal and lateral dynamics cannot be separated. The coupling effects appear at three locations. First, it is kinematic and dynamic coupling given by the motion in the yaw plane caused by wheels. This effect can be immediately seen from the wheel model in Section 4.3. The second coupling effect appears in the tire dynamics (Section 4.4), where the friction ellipse limits longitudinal and lateral tire forces. The last effect is weight redistribution when decelerating or accelerating that creates coupling due to modification in the normal tire forces [63]. Engineers must therefore take into account these effects when designing vehicle control systems.

5.1 Longitudinal control

Vehicle longitudinal control systems, as well as vehicle lateral control systems, can have a different level of autonomy (viz. Section 3.2). Two categories are discussed in this part – active safety systems and reference speed tracking together with the generating of the speed profile. Active safety systems include level 0 systems as Anti-lock Brake System (ABS), Traction Control System (TCS), stability enhancement system, or collision warning system. Semi-automated control systems such as Adaptive Cruise Control (ACC) are not discussed since they are not important to the assignment of the thesis. There are many papers devoted to technology and trends of ACC, e.g. a review on a novel approach where vehicles communicate with each other [64].

5.1.1 Active safety systems

Auxiliary vehicle systems are designed to improve vehicle behavior under difficult conditions. Vehicles equipped with some level 0 technology are not considered as autonomous vehicles. During regular situations, a driver does not recognize that the system is activated because it does not interfere in driving. ABS is considered a core security system, and almost all cars and trucks that occur on roads in developed countries are equipped at least with it. Studies on the effectiveness of ABS were conducted by NHTSA [65].

Fatal crash involvements				
	All roads		Wet, snowy or icy roads	
	Cars	LTVs	Cars	LTVs
All fatal involvements	1	-1	-1	-6
All non-control-group involvements	1	-1	-1	-6
All run-off-road crashes	**-9**	-6	**-34**	-10
– Side impacts with fixed objects	**-30**	0	**-85**	-4
– First-event rollovers	-11	-10	**-52**	**-31**
– All other run-off-road crashes	-3	-5	**-17**	-3
Pedestrian/bicyclist/animal	**13**	**14**	0	-14
Culpable involvements with other vehicles	4	-1	**12**	-6
All crash involvement				
All fatal involvements	**6**	**8**	**16**	**14**
All non-control-group involvements	**13**	**15**	**21**	**19**
All run-off-road crashes	-1	11	-13	3
– Side impacts with fixed objects	**-20**	-9	**-43**	-15
– First-event rollovers	3	17	-12	6
– All other run-off-road crashes	5	15	-3	9
Pedestrian/bicyclist/animal	-8	**-42**	-8	-10
Culpable involvements with other vehicles	**17**	**20**	**37**	**36**

Tab. 3: Estimated crash reduction (%) by four-wheel ABS for cars and Light Trucks and Vans (LTVs). Green font indicates a significant reduction and red font indicates a significant increase. *Source:* National Highway Traffic Safety Administration, 2009

According to them, ABS have almost zero effect on fatal crash involvements, but it has a substantial effect on nonlethal accidents. See Tab. 3 for detailed comparison.

ABS prevents loss of wheel adhesion during braking on slippery surfaces like ice, snow, and gravel. Wheel slipping may also occur when a layer of water forms on the road during rain. ABS tries to keep wheels in the area with the largest braking force, and thus the car brakes earlier. The braking force depends on the tire model, specifically the slip ratio. According to Fig. 4.4, it is best to hold slip ration between 0.1 and 0.2 in this example. Every slip curve has a similar shape with an increasing region and a decreasing region.

However, ABS has another effect in addition to a shorter braking distance (in certain situations, it may even increase). Imagine an emergency situation where an obstacle appears in front of the vehicle. Every driver begins to brake hard, locking the wheels, which results in loss of control of the vehicle. If the front wheels are locked, the vehicle continues to drive in a straight line. In this situation, the driver cannot affect the behavior of the vehicle, and if it fails to brake, it will hit the obstacle. If the rear wheel locks, the vehicle may uncontrollably spin and go into a skid. ABS detects if some wheel is about to lock and release the brake on that wheel. Holding and releasing the brake is repeated cyclically many times per second.

ABS can be divided according to the number of individually controlled valves [66]. The best scheme is so-called four-channel, four-sensor ABS. In this system, every wheel

Fatal crash involvements						
	ABS		ESC		Combined	
	Cars	LTVs	Cars	LTVs	Cars	LTVs
All fatal involvements	1	-1	14	28	15	27
All run-off-road crashes	-9	-6	36	70	30	68
Culpable involvements with other vehicles	4	-1	19	34	22	33
All crash involvements						
All fatal involvements	6	8	8	10	14	17
All run-off-road crashes	-1	11	45	72	44	75
Culpable involvements with other vehicles	17	20	13	16	28	33

Tab. 4: Estimated crash reduction (%) by combined ABS and ESC for cars and Light Trucks and Vans (LTVs). *Source:* National Highway Traffic Safety Administration, 2009

Algorithm 1 Simple ABS

Require: MaxBrakeTorque, $k \in \langle 0, 1 \rangle$
  while Car Not Stationary **do**
    if CurrentBrakeTorque < MaxBrakeTorque **then**
      CurrentBrakeTorque++
    end if
    if WheelSpeed == 0 **then**
      CurrentBrakeTorque $\leftarrow k \cdot$ CurrentBrakeTorque
    end if
  end while

has its own tachometer and a separate valve. This setup guarantees the best possible performance. Other possible setups are three-channel, three-sensor, and one-channel, one-sensor ABS. In the first case, there are two valves for front wheels and only one valve for both rear wheels. The last scheme consists of a valve and a sensor on the rear axle. The second and third setup can be commonly found on pickup trucks.

There are many different versions of algorithms behind ABS. Of course, more expensive cars, which have better and more accurate sensors, have more efficient safety systems. A simple implementation of ABS is shown in Alg. 1 [67]. This algorithm utilizes a tachometer on wheels and an accelerometer on the vehicle chassis. The accelerometer is used for determining the vehicle speed by double integration. Except for the maximum braking torque, the only parameter, the algorithm uses, is the coefficient k. k determines how much the brake is released when the wheel is locked. It is always between 0 (the braking force always returns to zero) and 1 (the brake remains at the same level). The improved version, we created for the RC platform, is presented in Chapter 6.

Another active safety system similar to ABS is called Traction Control System (TCS). It prevents wheels from spinning during acceleration on slippery surfaces. TCS utilizes the same sensors and controllers as ABS. If a fault occurs in ABS, TCS stops working as well, and vice versa. Since the systems work on the same principle, we do not discuss it separately. The vast majority of modern cars are equipped with both discussed systems.

Extension of longitudinal active safety systems is Electronic Stability Control (ESC). ESC provides the vehicle additional stability control by detecting loss of traction in bends. This system has a big impact on traffic accidents compared to ABS (viz. Tab. 4).

5.1.2 Reference speed generation

An important topic is tracking a reference trajectory with an autonomous car. A trajectory consists of a path (sequence of points in space) and a speed profile. Each reference position is associated with the given speed. Path generation from sensors (stereo camera, IMU, GPS) in real-time is a complex task. For this reason, we assume that the path is generated off-line, and it is used as the input to the control algorithm. A subsequent task is generation of the speed profile on the defined path. Generating the feasible trajectory is an important process because no controller can provide stability if the cruise speed is excessive. There may be different requirements for the generated speed depending on the deployment of the car. Our interest is in racing cars, hence the objective is the minimum-time trajectory.

The problem of generating the reference speed v_{ref} for the given path can be solved using several approaches. Two simple approaches based on different criteria are described in [68]. Both are not computationally demanding and can therefore be calculated on-line on any hardware. The easiest solution is a purely geometric trajectory generation. It is based on the assumption that the speed should be reduced when approaching a bend. Daimler-Chrysler defined the maximum admissible speed to be inversely proportional to the curvature as

$$v_{max} = \sqrt{\frac{g\mu}{\kappa}}, \tag{5.1}$$

where g is the gravitational constant, μ is the friction coefficient between the tire and the surface, and κ is the curvature. Curvature is defined as $\kappa = \frac{1}{R}$, where R is the radius of the osculating circle that has first and second derivatives equal to the path derivatives near the touch point. The curvature of a twice differentiable plane curve parameterized as $\gamma(s) = (x(s), y(s))$ is [69]

$$\kappa = \frac{|\dot{x}\ddot{y} - \dot{y}\ddot{x}|}{\sqrt{(\dot{x}^2 + \dot{y}^2)^3}}. \tag{5.2}$$

The admissible speed given by Eq (5.1) has only one parameter, and that is the road curvature. This model is incomplete in some situations, and it needs to be improved by including other variables. NHTSA therefore recommends their description for the

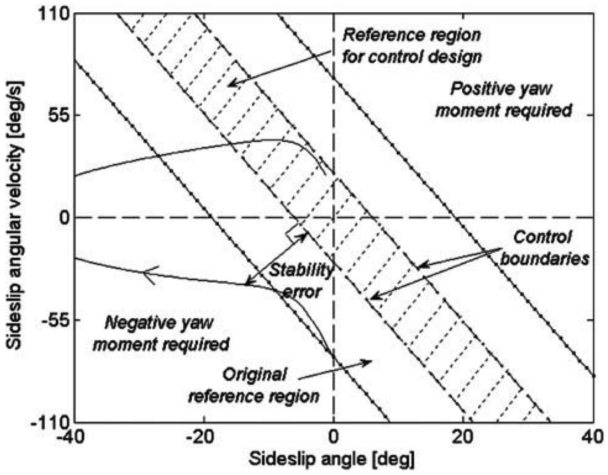

Fig. 5.1: Lateral stability defined by the phase plane $\beta - \dot{\beta}$. *Source:* [70] , 2006.

calculation of the maximum speed in bends:

$$v_{max} = \sqrt{\frac{g(\phi + \mu)}{\kappa(1 - \phi\mu)}}, \tag{5.3}$$

Here, a new parameter ϕ is considered. The road camber angle ϕ is the angle between the road and the horizontal plane. Note that at zero camber angle, Eq (5.3) becomes Eq (5.1). Then, as recommended by NHTSA, the acceleration a to achieve the right cruise speed should be less then

$$a_{max} = \sqrt{\frac{v^2 - v_{max}^2}{2(d - t_v v)}}, \tag{5.4}$$

where v is the current speed, v_{max} is the maximum admissible speed, t_v is the time delay due to driver reaction, and d is the distance to the summit of the bend. Such an improved geometric model is still not ideal as it does not take into account the dynamics of the vehicle.

The second approach discussed in [68] is based on the lateral dynamics criterion. Knowledge of the vehicle's lateral behavior helps to maintain lateral stability. Different lateral dynamics indicators available to us by measurements or state observer can be used to determine the suitable speed real-time. In [70], authors use $\beta - \dot{\beta}$ phase plane to keep the vehicle stable. When the vehicle lies in the bounded area, it is considered to be lateral stable. This can be written by inequality

$$|\dot{\beta} + k_{\beta\dot{\beta}}\beta| \leq b, \tag{5.5}$$

where β is the side-slip angle, $\dot{\beta}$ is the side-slip velocity, and b and $k_{\beta\dot{\beta}}$ are parameters defining stability region boundaries. The reference plane is illustrated in Fig. 5.1. A complete analysis of the phase plane stability criterion is done in [71].

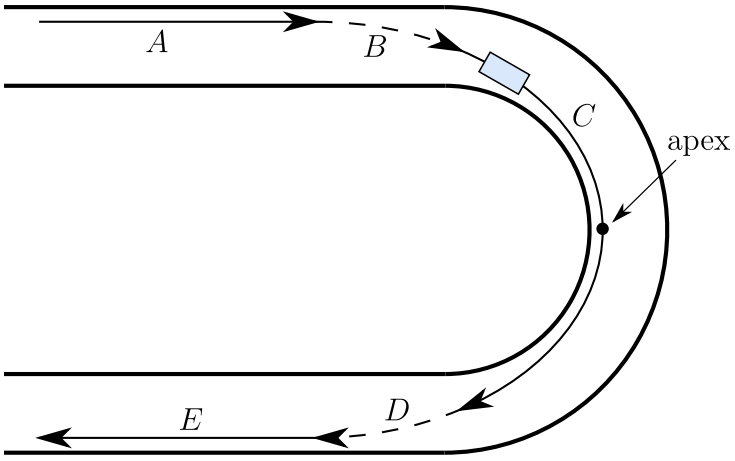

Fig. 5.2: Racing track and optimal path with apex in the middle. A – maximum acceleration ($a_x = a_{x_{max}}, a_y = 0$), B – combined breaking + cornering ($-a_{x_{max}} < a_x < 0, a_y < a_{y_{max}}$), C – maximum cornering ($a_x = 0, a_y = a_{y_{max}}$), D – combined acceleration + cornering ($0 < a_x < a_{x_{max}}, a_y < a_{y_{max}}$), E – maximum acceleration ($a_x = a_{x_{max}}, a_y = 0$)

Another criterion associated with lateral dynamics is a limitation of the side-slip angle depending on the speed. Because of nonlinearity of the system, we can consider quadratic dependence

$$\beta \leq a - cv^2, \tag{5.6}$$

where a, b, c are parameters that depend on the dynamics of the car. In [70], the authors suggest parameters $a = 10, c = 7/16000$. For low speeds, the second term has a negligible effect and thus $\beta \leq a$. When the speed increases, the term starts to limit the side-slip angle to preserve the stability. Conditions given by equations and inequalities (5.3), (5.4), (5.5), (5.6) and many others, not covered in this work, can be evaluated in a parallel way for greater robustness.

A paper on autonomous vehicle control at the limits of handling [69] tries to mimic a racing driver's behavior. Professional drivers can hold the maximum possible force that can be generated by tires throughout the race. This force is given by the friction ellipse introduced in Section 4.4. The concept of the $g-g$ diagram as the operational envelope is presented in the paper. The $g-g$ diagram represents the acceleration limits of the vehicle. In contrast with the friction ellipse, the $g-g$ diagram shows only vehicle's limits as a whole and does not detect if some tire exceeded its peak force. In order to ensure the best lap time, the path must consist of straight segments where the maximum speed is reached, arc segments with apex[7] in the center, and two transition curves between the straight line and bend entry, bend exit respectively (see Fig. 5.2 for an example). Generating the right speed is crucial because if the car approaches the bend too fast, tracking of the optimal path becomes impossible.

[7] Apex – A point on the racing line closest to the edge of the track.

To control longitudinal and lateral movement separately, the combined acceleration must lie inside the $g-g$ diagram with some safety margin. If the acceleration is too close to the border, longitudinal and lateral dynamics became strongly coupled resulting in a risk of skidding and therefore loss of stability. A mathematical relation between the longitudinal acceleration a_x and the lateral acceleration a_y adapted from Eq (4.11) is

$$a_x^2 + a_y^2 \leq (\mu g)^2. \tag{5.7}$$

Let $\gamma(s) = (x(s), y(s))$ be a twice differentiable plane path with a single parameter s describing the traveled distance from the start. Then, for the segment C (Fig. 5.2) holds:

$$a_y(s) = \frac{v_{ref}(s)^2}{R(s)},\ a_x(s) = 0 \tag{5.8}$$

Plugging the accelerations from Eq (5.8) to Eq (5.7) yields

$$v_{ref} < \sqrt{\mu g R(s)}. \tag{5.9}$$

This result corresponds to the recommendation from Eq (5.1).

To find the reference velocity on the segment where both accelerations act (B and D), the calculation starts by substituting the lateral acceleration a_y from Eq (5.8) to Eq (5.7) and moving a_x to the left-hand side:

$$a_x(s) = \sqrt{\mu^2 g^2 - \kappa(s)^2 v_{ref}(s)^4} \tag{5.10}$$

For the longitudinal acceleration a_x holds

$$a_x(s) = \frac{\mathrm{d}v_{ref}(s)}{\mathrm{d}t} = \frac{\mathrm{d}v_{ref}(s)}{\mathrm{d}s}\frac{\mathrm{d}s}{\mathrm{d}t} = \frac{\mathrm{d}v_{ref}(s)}{\mathrm{d}s} v_{ref}(s). \tag{5.11}$$

Merging Eq (5.10) and Eq (5.11) and considering the border of the $g-g$ diagram obtains an ordinary differential equation of the first order

$$\frac{\mathrm{d}v_{ref}(s)}{\mathrm{d}s} = \frac{\sqrt{\mu^2 g^2 - \kappa(s)^2 v_{ref}(s)^4}}{v_{ref}(s)}. \tag{5.12}$$

Eq (5.12) can be solved in real time by utilizing backward integration (segment B) or forward integration (segment D). Nevertheless, two things remain to be clarified. An initial condition is necessary to solve the equation. $v_{ref}(0)$, $v_{ref}(l)$ respectively (l is the length of the segment) are found from the constant radius segment C. The last essential task is defining the transition curves. To make the algorithm robust without unintended stability impacts, the best candidate is a curve with a linear curvature change. Such a

curve is called a clothoid, and it is defined with Fresnel integrals as [69]

$$x = C(cs) = \frac{1}{c}\int_0^{cs} \cos(q^2)\,\mathrm{d}q, \tag{5.13a}$$

$$y = S(cs) = \frac{1}{c}\int_0^{cs} \sin(q^2)\,\mathrm{d}q, \tag{5.13b}$$

where c is the only parameter of the clothoid describing its shape, and s is the distance along the clothoid.

In [8], the author solves the problem of generating the speed profile with a simple point-mass vehicle as the optimization problem

$$\min_{\mathbf{u}(t)} \quad t' \tag{5.14a}$$

$$\text{subject to} \quad s(t') = s', \tag{5.14b}$$

$$\dot{\mathbf{x}}(t) = f(\mathbf{x}(t), \mathbf{u}(t)), \tag{5.14c}$$

$$g(\mathbf{x}(t), \mathbf{u}(t)) \leq 0, \tag{5.14d}$$

where t' is the lap time, s' is the lap length, $\mathbf{x}$ is the state vector, and $\mathbf{u}$ is the input vector. Eq (5.14c) represents the vehicle dynamics and Eq (5.14d) describes all types of constraints including vehicle handling limits and initial conditions.

5.1.3 Reference speed tracking

The longitudinal dynamics control, as well as the control of lateral dynamics, can be done using either classical control theory or optimal control theory. The second approach may deal with complex nonlinear systems with many DOF better, but often, a computationally challenging problem arises. Popular optimal control methods are Model Predictive Control (MPC), Linear Quadratic Control (LQR), and H_∞ control. This thesis aims only on the classical control strategy since it is more intuitive, and high-quality results (minimum errors) can be achieved with the classical control as well as with the optimal control. We suggest a reader to see [8, 72] for the optimal control employed in the area of vehicle control.

A longitudinal controller receives the reference speed v_{ref} as the input. The objective of the controller is minimizing the error e_v defined as

$$e_v = v_{ref} - v_x = v_{ref} - v\cos\beta, \tag{5.15}$$

where v_{ref} is the reference speed generated by any method, whether mentioned in Section 5.1.2 or not, v_x is the forward speed, v is the size of the velocity vector, and β is the

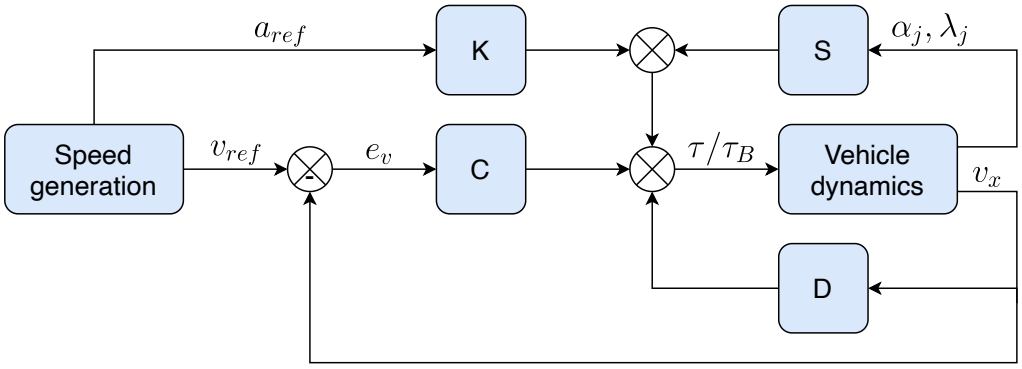

Fig. 5.3: Structure of the longitudinal controller. C is a classical feedback controller, K is a feedforward controller which sets the vehicle to the pre-calculated state, S helps to keep the vehicle stable based on defined conditions, and D is drag compensator.

side-slip angle.

As already mentioned, this work does not address the mapping from the reference torque to the actual motor torque (we can assume $\tau_{ref} = \tau$). The most straightforward design of the longitudinal controller includes only a single feedback controller C (see Fig. 5.3). It was shown by many researchers that a PID controller is a suitable controller for the task of speed tracking [73, 74]. The control law of a feedback PID controller is given by the equation

$$u_C(t) = K_\mathrm{P} e_v(t) + K_\mathrm{I} \int_0^t e_v(t')\,\mathrm{d}t' + K_\mathrm{D} \frac{\mathrm{d}e_v(t)}{\mathrm{d}t}, \tag{5.16}$$

where $K_\mathrm{P}, K_\mathrm{I}, K_\mathrm{D}$ are nonnegative coefficients for the proportional, integral, and derivative terms. Because the model has a separate brake input, another supplementary control law must be added:

$$\tau, \tau_B = \begin{cases} u, 0 & \text{if } u > 0, \\ 0, -u & \text{if } u < 0, \\ 0, 0 & \text{if } u = 0 \end{cases} \tag{5.17}$$

If the speed profile is available, computing of the acceleration profile is not a difficult task since $a_{ref} = \dot{v}_{ref}$ [69]. The computed a_{ref} can be utilized as a feedforward part of the controller (see the controller K in Fig. 5.3). The feedforward controller would be satisfactory on its own with a perfect model in the ideal world, but due to model and measurement errors, the feedback part compensates the errors. The two-controller model is sufficient for certain situations, but it is not suitable for fast driving at the limits of handling. Hence two additional control laws are implemented to improve the vehicle behavior.

The feedback controller S in Fig. 5.3 prevents tires from getting into saturation while ensuring that the tires operate at the limits. When the slip controller detects that the

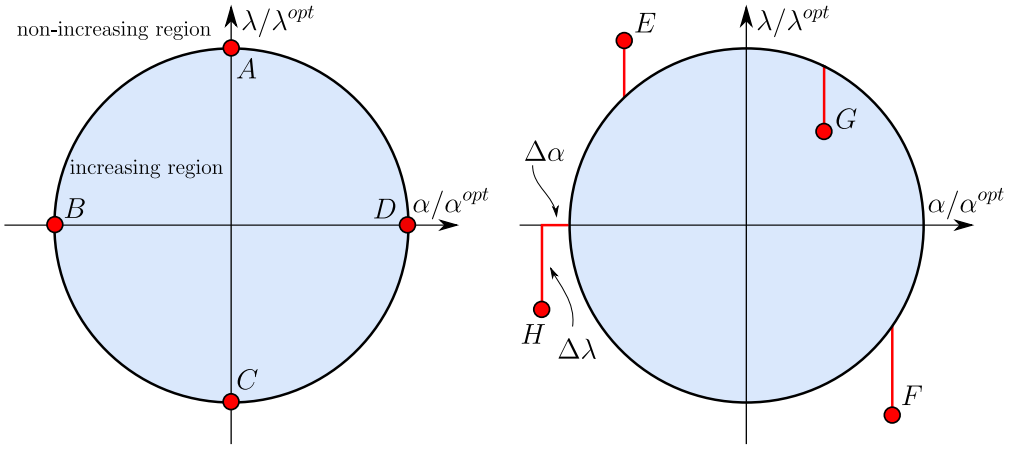

(a) A – maximum acceleration, B – maximum cornering to the left, C – maximum breaking, D – maximum cornering to the right

(b) E, F, H – the tire is saturated, the combined acceleration needs to be reduced, G – the tire is able to provide more combined acceleration

Fig. 5.4: Slip circles with points representing tire states. The red distance is used for computing the motor input by the feedback slip-based controller.

vehicle does not turn as it should, it reduces the amount of the longitudinal acceleration to increase the lateral acceleration. On contrary, when the controller detects that some tire does not operate at the limit, it provides the additional force. Let α_j^{opt} denote the slip angle when the vehicle achieves the maximum lateral tire force generated by the tire j (approximately 10° in Fig. 4.5). The optimal slip ratio λ_j^{opt} is then defined the same way but with the longitudinal tire force instead of the lateral force (approximately 0.2 in Fig. 4.4). A slip circle is designed to represent the combined lateral and longitudinal slip (see Fig. 5.4). This circle is a normalized friction ellipse with the unit distance to the edge of the circle. Any point that satisfies the equation

$$\left(\frac{\lambda_j}{\lambda_j^{opt}}\right)^2 + \left(\frac{\alpha_j}{\alpha_j^{opt}}\right)^2 = 1 \tag{5.18}$$

produces the optimal peak force. In practise, operating at the edge edge of the slip circle is not a suitable method since the rear axle saturation can lead to vehicle instability [69]. Therefore, some safety margin should be always considered. The values of $\alpha_f^{opt}, \alpha_r^{opt}, \lambda_f^{opt}, \lambda_r^{opt}$ should be chosen with respect to the application from experiments.

The algorithm generates the motor input according to the distance between the vehicle state and the edge of the unit circle. The relative longitudinal distance $\Delta\lambda$ is defined as

$$\Delta\lambda = \begin{cases} \left|\frac{\lambda_j}{\lambda_j^{opt}}\right| - \sqrt{1 - \left|\frac{\alpha_j}{\alpha_j^{opt}}\right|^2} & \text{if } \left|\frac{\alpha_j}{\alpha_j^{opt}}\right| \leq 1, \\ \left|\frac{\lambda_j}{\lambda_j^{opt}}\right| & \text{if } \left|\frac{\alpha_j}{\alpha_j^{opt}}\right| > 1, \end{cases} \tag{5.19}$$

and the relative lateral distance $\Delta\alpha$ as

$$\Delta\alpha = \begin{cases} 0 & \text{if } \left|\frac{\alpha_j}{\alpha_j^{opt}}\right| \leq 1, \\ \left|\frac{\alpha_j}{\alpha_j^{opt}}\right| - 1 & \text{if } \left|\frac{\alpha_j}{\alpha_j^{opt}}\right| > 1. \end{cases} \tag{5.20}$$

When $|\alpha_j/\alpha_j^{opt}| \leq 1$ and the point is outside the circle (points E, F in Fig. 5.4), the j-th axle is saturated. In this case, the controller computes only $\Delta\lambda$ and proportionally reduces/increases the amount of throttle. If the tire is in the state G, it does not operate at the peak force, thus the controller adjusts the amount of the throttle so that the tire reaches its limit. The last case is when $|\alpha_j/\alpha_j^{opt}| > 1$ meaning that the tire slips. Then, the throttle command is computed from both distances $\Delta\lambda$ and $\Delta\alpha$. The control law based on the slip circle is

$$u_S(t) = \begin{cases} K_\lambda \Delta\lambda(t) + K_\alpha \Delta\alpha(t) & \text{if } \left|\frac{\lambda_j}{\lambda_j^{opt}}\right| \leq 1, \\ -K_\lambda \Delta\lambda(t) - K_\alpha \Delta\alpha(t) & \text{if } \left|\frac{\lambda_j}{\lambda_j^{opt}}\right| > 1, \end{cases} \tag{5.21}$$

where K_λ and K_α are the slip controller gains.

Notice that the half-plane given by $\lambda_j/\lambda_j^{opt} < 0$ represents braking. A natural part of this algorithm is therefore a simple version of ABS. This nature also implies the traction control for the positive acceleration. The slip control does not affect the lateral slip α, only the steering input has control over α. Even if only the front axle is steered, as in any commercial car, the controller evaluates slips on both axles separately to stabilize all wheels (4 wheels when the twin-track model is used). When both axles are saturated, the controller focuses on stabilizing the front axle first [69].

The last optional improvement is focused on drag compensation. The drag is mainly caused by the aerodynamic force F_A, but also by the wheels rolling resistance F_R and other physical phenomena. The drag can be expressed by equation

$$F_D = -F_A - F_R = -\frac{1}{2}\rho v_x^2 C_D A - C_r F_z, \tag{5.22}$$

where ρ is the density of air, v_x is the forward velocity, C_D is the drag coefficient, A is the cross sectional area, C_r is the rolling resistance coefficient, and F_z is the normal force. The drag force F_D acts against the longitudinal acceleration a_x. The drag compensation is the function $u_D = f(F_D) = f(v_x)$. The complete longitudinal control law has the form

$$u(t) = u_C(e_v(t)) + u_S(\alpha_j(t), \lambda_j(t)) + u_K(a_{ref}(t)) + u_D(v_x(t)), \tag{5.23}$$

together with Eq (5.17).

Of course, except the discussed control strategy, there are many other methods for

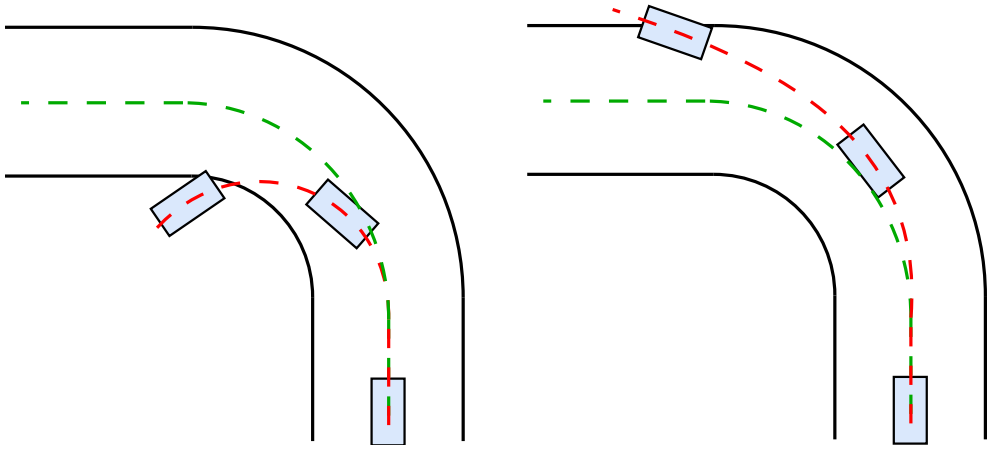

(a) Understeer is caused by the loss of adhesion on the rear axle

(b) Oversteer is caused by the loss of adhesion on the front axle

Fig. 5.5: Understeer and oversteer. The green line represents the optimal path and the read line the real path.

reference speed tracking. A popular method from the category of robust control is Sliding Mode Control (SMC). The sliding mode technique forces the vehicle to follow a defined trajectory in the phase plane. See [75] for an implementation of SMC for vehicle longitudinal control. In [76], authors use the Lyapunov approach to design automated vehicle guidance.

5.2 Lateral control

Vehicle lateral control or steering control ensures that the autonomous vehicle follows the path produced by the path planner. A review of path tracking strategies can be found in [77]. As already mentioned, it is not possible to control lateral dynamics without affecting longitudinal dynamics, and vice versa. Hence both lateral and longitudinal controllers must cooperate to provide the robust trajectory tracking. It is important to note that the path tracking has a higher priority than the velocity tracking. Speed should always be adapted with respect to vehicle's capabilities. For this reason, the slip-based controller was introduced in the last chapter.

Important concepts related to lateral dynamics are understeering/oversteering. These terms indicate sensitivity of any vehicle to steering. When a car tends to oversteer, it does not turn enough, and it can leave the road on the outer side. On the contrary, a result of understeer is leaving the road on the inner side and possible spin of the vehicle (see Fig. 5.5). This property is defined for each vehicle by the gradient K [7]. It depends mainly on the distribution of mass. Racing cars and formulas with a heavy engine placed above the rear axle are configured for understeer. A significant drawback of an understeering vehicle is instability, and that is why most commercial cars tend to oversteer.

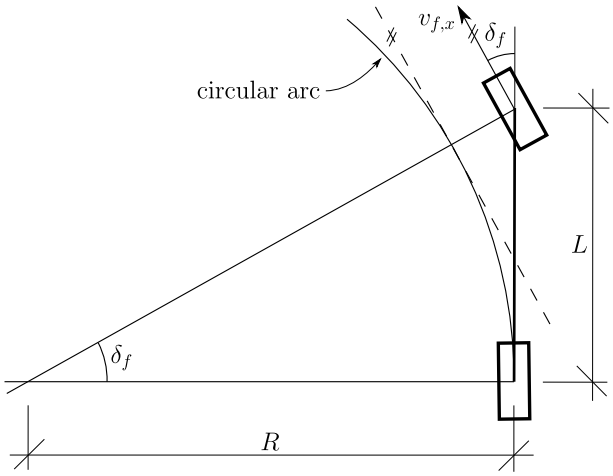

Fig. 5.6: Simple geometric model of a vehicle with Ackermann steering

5.2.1 Geometric controllers

The discussed algorithms for lateral control are distinguished according to the principle into geometric path trackers and others. Geometric controllers are popular for the simplicity of implementation. They are based on geometric relationships between the vehicle and the road. The basic assumption for the derivation of geometric path trackers is the kinematic vehicle model (Ackermann steered vehicle [78]), but there are also various extensions for dynamic models. Further in this chapter, we assume that only the front axle is operable and therefore $\delta_r = 0$. From the assumptions of Ackermann steering geometry and plane movement, the relation among the steering angle δ_f, the radius of the arc R that the rear axle follows, and the wheelbase[8] L can be written as

$$\tan \delta_f = \frac{L}{R}. \tag{5.24}$$

The Ackermann geometry is shown in Fig. 5.6. The main drawback of this simple model is a good approximation only for low speeds and moderate steering angles.

Pure pursuit is a basic geometric path tracker developed already in early 1990s [79]. It is based on the principle of determining the curvature of the circular arc that connects the rear axle with so-called look-ahead point. The look-ahead point is a point on the desired path which is at the constant time distance from the rear axle. The steering angle is calculated so that the car constantly pursues the point. The geometry of the Pure pursuit algorithm is shown in Fig. 5.7. The distance l_d is called the look-ahead distance, and it is the only input parameter.

According to the sine rule applied to the triangle OPQ in Fig. 5.7, the following

[8]Wheelbase – The distance between the front axle and the rear axle.

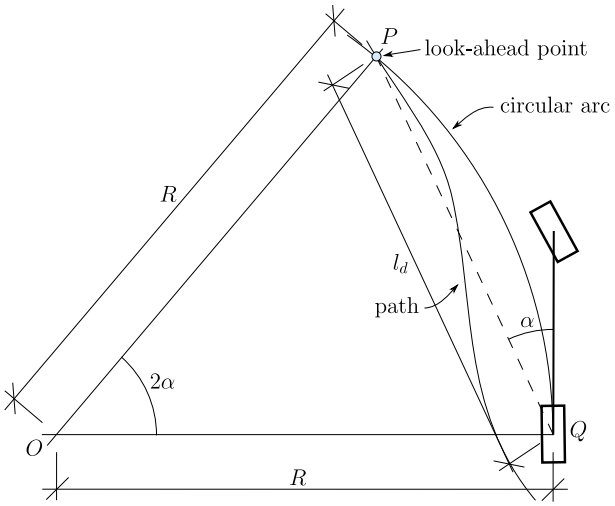

Fig. 5.7: Pure pursuit geometry

equation holds:

$$\frac{l_d}{\sin 2\alpha} = \frac{R}{\sin(\frac{\pi}{2} - \alpha)} \tag{5.25}$$

Applying the double-angle formulae to the left-hand side of Eq (5.25) and phase shift of sine to the right-hand side results in

$$\begin{aligned} \frac{l_d}{2\sin\alpha\cos\alpha} &= \frac{R}{\cos\alpha}, \\ \frac{2\sin\alpha}{l_d} &= \underbrace{\frac{1}{R}}_{\kappa}. \end{aligned} \tag{5.26}$$

Using the Ackermann assumption from Eq (5.24), we can write

$$\delta_f(t) = \arctan(\kappa L) = \arctan\left(\frac{2L\sin\alpha(t)}{l_d}\right). \tag{5.27}$$

It is a common practice to choose the look-ahead distance l_d with respect to the forward velocity of the vehicle v_x. Unwanted behavior could occur for low and high speeds if the distance was constant. After this improvement, the final law is given by

$$\delta_f(t) = \arctan\left(\frac{2L\sin\alpha(t)}{k_d v_x(t)}\right), \tag{5.28}$$

where k_d is a constant influencing the look-ahead distance. Choosing the right k_d is important for correct path tracking. A small value of the k_d causes oscillations along the path as the car always overshoots the tracked point. The oscillations decrease when the parameter increases, however, curvatures near corners decrease as well. This results in nonprecise path tracking mainly around bends as shown in Fig. 5.8. The whole process is

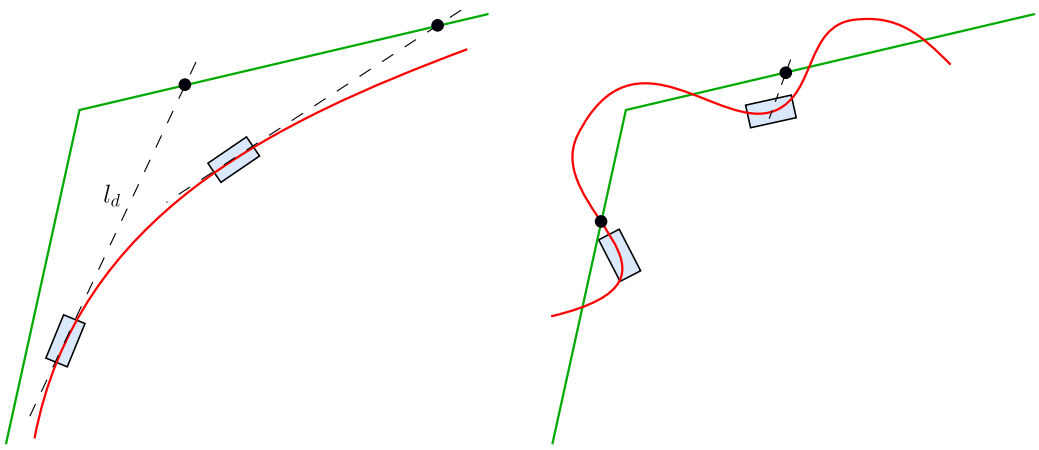

(a) Small look-ahead distance **(b)** Large look-ahead distance

Fig. 5.8: Dependency of the look-ahead distance on the tracking quality. The green line represents the desired path, and the read line represents the real path. The black points symbolize look-ahead points.

Algorithm 2 Pure pursuit

Require: $k_d \in (0, \infty)$
  while True **do**
    $v_x, \psi_g \leftarrow$ SensorFusion()
    $Q \leftarrow$ CurrentVehiclePosition()
    $P \leftarrow$ LookAheadPointPosition(Q, k_d, v_x)
    $\alpha \leftarrow$ CalculateAngle(Q, P, ψ_g)
    $\delta_f \leftarrow$ SteeringCommand(α, k_d, v_x)
  end while

shown in Alg. 2 where ψ_g denotes the yaw of the vehicle in the global coordinate system (as shown in Fig. 4.2). Of course, calculations can be performed in the local coordinate system of the vehicle using transformations.

The original Pure pursuit method disregards the curvature of the road and other potentially useful factors. It is hence natural that many algorithms have been developed to extend the original algorithm [80]. Let us mention, for example, vector pursuit algorithm based on the theory of screws. It generates the steering command based on the vehicle's immediate location relative to the position of the look-ahead point and the desired orientation along the path at that point [81]. Another path tracker based on the Pure pursuit is CF-pursuit [82]. The authors incorporated the path's curvature into their system. A major improvement of CF-pursuit is also replacing circular arcs with clothoid curves (Eq. 5.13) in order to reduce fitting errors and a fuzzy controller to tune the look-ahead distance.

Stanley is next very popular geometric path tracker [83]. This algorithm was developed by the Stanford team for the DARPA Grand Challenge in 2005. The autonomous car equipped with the Stanley defeated all 23 competitors and won the race. Since then,

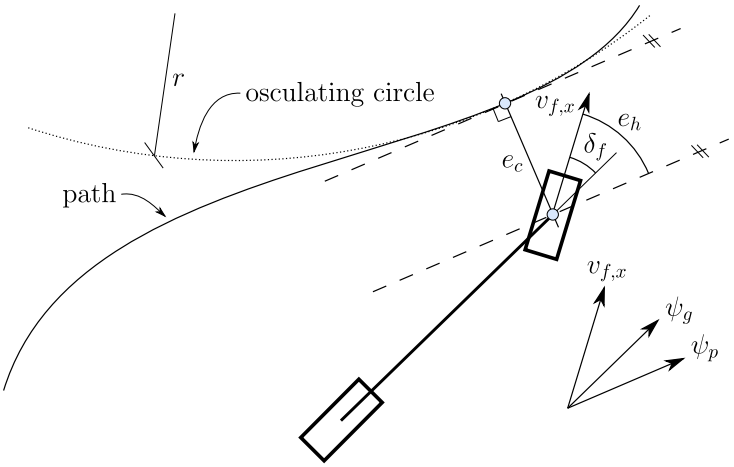

Fig. 5.9: Stanley geometry

it has become a commonly used steering controller. Unlike the Pure pursuit, it determines the output utilizing two defined errors. The first error is the heading error e_h which indicates the deviation of the vehicle yaw angle (heading) ψ_g from the desired yaw angle ψ_p:

$$e_h = \psi_g - \psi_p \tag{5.29}$$

This angle is determined from the nearest segment of the path to be tracked. The other error is the crosstrack error e_c which is the distance from the center of the front axle to the path. See Fig. 5.9 for a better understanding of described Stanley inputs.

The crosstrack error is considered as an angular error to fit the control law. This is achieved by using the tangent function which value range is $(-\pi/2, \pi/2)$. There is also used, as in the Pure pursuit, speed-dependent scaling. The basic kinematic Stanley control is given by

$$\delta_f(t) = e_h(t) + \arctan\left(\frac{k_d e_c(t)}{v(t)}\right), \tag{5.30}$$

where k_d is the gain parameter. This simple control law is sufficient only for low speed applications. At low speeds, tires behave like natural dampers attenuating lateral forces [83]. However, active damping that stabilizes the yaw dynamics is required for higher speeds. Simple, yet effective damper, is negative feedback on the yaw rate

$$\delta_{f,yaw} = k_{d,yaw}(\dot{\psi} - \dot{\psi}_p) = k_{d,yaw}(\dot{\psi} - \frac{v}{r}), \tag{5.31}$$

where $k_{d,yaw}$ is the tuned gain, $\dot{\psi}$ is the vehicle's yaw rate, and $\dot{\psi}_p$ is the computed path yaw rate from the radius of the osculating circle r and the velocity v.

The last possible issue is neglecting the curvature of the path which can cause poor tracking results for curvy roads. In order to track a bend correctly, the vehicle should

be directed towards the center of the curve, not parallel to the road. The yaw reference therefore should be nonzero. Using the simplified linear tire model

$$F_{f,y} = -C_y \alpha_f, \tag{5.32}$$

the steady state yaw can be derived from Eq. (4.6) as

$$\psi_{ref} = \frac{mv\dot{\psi}_p}{C_y\left(1 + \frac{l_f}{l_r}\right)} = k_{ss} v \dot{\psi}_p. \tag{5.33}$$

The coefficient C_y in Eq. (5.32) and Eq. (5.33) is the tire stiffness.

The complete steering law with the dynamics compensation is

$$\delta_f(t) = \underbrace{(e_h(t) - k_{ss}\frac{v^2(t)}{r(t)})}_{\text{heading control}} + \underbrace{\arctan\left(\frac{k_d e_c(t)}{k_s + v(t)}\right)}_{\text{offset control}} + \underbrace{k_{d,yaw}\left(\dot{\psi}(t) - \frac{v(t)}{r(t)}\right)}_{\text{yaw damper}}, \tag{5.34}$$

where k_{ss}, k_d, k_s, and $k_{d,yaw}$ are the controller parameters. When the vehicle is far away from the road, the second term in Eq. (5.34) turns the car toward the path. When the crosstrack error gets smaller, the error changes approximately as $\dot{e}_c(t) = -ke_c(t)$. This results in exponential convergence to the path. The asymptotic stability for the kinematic vehicle model was proven by the authors [83].

5.2.2 Other controllers

The first technique to be briefly introduced here is Sliding Mode Control (SMC). As mentioned in Section 5.2, SMC is a part of nonlinear robust control. It is considered one of the most promising methods for robust control. The principle of operation is to limit the trajectory of the system in the phase graph to the defined line (sliding surface). Nevertheless, this method suffers from the chattering due to a fast switching strategy as shown in Fig. 5.10. Control signals are discontinuous functions that are not affected by parametric uncertainties and external disturbances. One of the proposed approaches to eliminate the chattering is use of a higher order sliding mode. This approach is presented below.

The lateral error dynamics of the vehicle with respect to the path can be expressed as

$$\ddot{e} = a_y - a_{y,ref}, \tag{5.35}$$

where a_y is the vehicle's lateral acceleration and $a_{y,ref}$ is the reference lateral acceleration. The desired lateral acceleration is given by the relation for the centrifugal acceleration

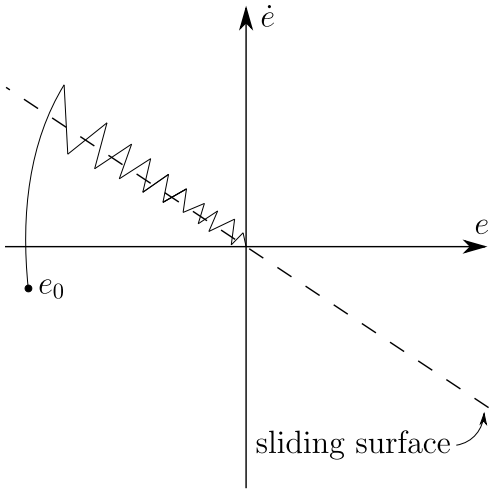

Fig. 5.10: Phase plane with the sliding surface. Chattering occurs in the basic sliding mode control.

$a_{y,ref} = v_x^2/r$, where r is the curvature. The sliding variable is selected as follows:

$$s = \dot{e} + \sigma e \tag{5.36}$$

The aim of this controller is to ensure tracking of the sliding surface defined as $s = 0$. Deriving Eq. (5.36) and substituting from Eq. (5.35), we obtain

$$\dot{s} = a_y - \frac{v_x^2}{r} + \sigma e. \tag{5.37}$$

Consider a linear parameter varying model with velocity as the varying parameter, the input δ_f and the state a_y. The linear single-track model derived in Section 4.5 can be converted into the desired form. Replacing a_y from the modified linear model results in equation

$$\dot{s}(t, s) = \Phi(t, s) + \Gamma(t, s)\delta_f(t). \tag{5.38}$$

Applying so-called super-twisting theorem, which is developed to ensure stability and reduce the chattering, the steering commands can be determined as [84]

$$u_1(t) = -\mu\sqrt{|s(t)|}\,\mathrm{sgn}(s(t)), \tag{5.39a}$$
$$\dot{u}_2(t) = -\eta\,\mathrm{sgn}(s(t)). \tag{5.39b}$$

To eliminate peaks in transient phases, a third steering command is added to the law.

This feedforward term is obtained by solving the equation $\dot{s} = 0$ in Eq. (5.38):

$$u_3(t) = -\frac{\Phi(t,s)}{\Gamma(t,s)} \tag{5.40}$$

The complete sliding mode control law is given by

$$\delta_f(t) = u_1(t) + u_2(t) + u_3(t). \tag{5.41}$$

The sliding surface can also be defined differently. For example, in [85], the sliding surface is defined as

$$s = k_1 e_c + k_2 e_h, \tag{5.42}$$

where k_1 and k_2 are weighting coefficients, e_c and e_h are the crosstrack error and the heading error respectively.

Another strategy to control the lateral dynamics of a vehicle is modified PID regulation. A PID regulator is a common controller used in industrial applications due to its simplicity. However, for fast varying dynamic systems as cars, this controller is not a suitable solution. It lacks robustness for dynamic driving as a set of parameters is tuned only for specific operating conditions. This problem can be solved by utilizing an adaptive PID controller. In case of the adaptive PID, the parameters are tuned on-line based on changing conditions.

The adaptive PID controller can tune parameters according to different criteria. One of the possible strategies is the minimum variance criterion [86]. The performance function to be minimized is defined as

$$J = \mathrm{EX}(y^2(t)), \tag{5.43}$$

where EX denotes the expectation operator and y is the system output. Consider a linear Single Input Single Output (SISO) discrete-time system

$$A(z^{-1})y(k) = z^{-1}B(z^{-1})u(k) + \omega(k), \tag{5.44}$$

where

$$A(z^{-1}) = 1 + a_1 z^{-1} + a_2 z^{-2} + ... + a_n z^{-n}, \tag{5.45a}$$
$$B(z^{-1}) = 1 + b_1 z^{-1} + b_2 z^{-2} + ... + b_n z^{-n}. \tag{5.45b}$$

The z is the shift operator ($y(k)z^{-1} = y(k-1)$) and ω is the Gaussian noise. The control

law that minimize the variance has the general form

$$u(k) = \frac{F\dot{\psi}(k) - E(z^{-1})y(k)}{B(z^{-1})D(z^{-1})}, \tag{5.46}$$

where $u(k)$ is the system input (steering angle δ_f), $y(k)$ is the system output (crosstrack error e_c), $\dot{\psi}(k)$ is the angular velocity around around the CG, and $E(z^{-1}), B(z^{-1}), D(z^{-1})$ are polynomials.

Polynomials are selected to ensure a zero steady-state error if some disturbance is present. According to the minimum variance criterion, the obtained control law is

$$\Delta\delta_f(k) = (1-z^{-1})\delta_f(k) = K(e_c(k)+e_c(k+1)+e_c(k+2))\dot{\psi}(k) - K(e_c(k-1)^2 - e_c(k-2)^2). \tag{5.47}$$

A discrete-time PID regulator has the form

$$u(k) = K_p\left(y(k) + \frac{T_d}{T_i}\sum_{j=1}^{k} y(k) + \frac{T_d}{T_s}(y(k) - y(k-1))\right). \tag{5.48}$$

After transforming the PID regulator to the incremental form and comparing to Eq. (5.47), we obtain the final control law

$$\Delta\delta_f(k) = \frac{K_p T_s}{T_i}\dot{\psi}(k) - K_p\left(1 + \frac{T_s}{T_i} + \frac{T_d}{T_s}\right)e_c(k) + K_p\left(1 + \frac{2T_d}{T_s}\right)e_c(k-1) - K_p\frac{T_d}{T_s}e_c(k-2), \tag{5.49}$$

where

$$K_p(k) = -K(e_c(k-1) + 2e_c(k-2)), \tag{5.50a}$$

$$T_i(k) = \frac{-T_s(e_c(k-1) + 2e_c(k-2))}{e_c(k) + e_c(k-1) + e_c(k-2)}, \tag{5.50b}$$

$$T_d(k) = \frac{T_s e_c(k-2)}{e_c(k-1) + 2e_c(k-2)}, \tag{5.50c}$$

are automatically tuned proportional, integral, and derivative parameters of the PID regulator. The tuning speed is modified via the constant K which is similar to the proportional gain K_p. When K is small, the system has high damping, and vice versa [86]. The last parameter T_s is the sampling period.

As already mentioned, algorithms of optimal control are not discussed here, hence we can continue to the main topic of this thesis – our implementation of combined control strategy for a racing vehicle and its verification in simulations and on the experimental vehicle.

6 Control Strategy

This chapter summarizes the implementation part of this work. Along with the next chapters, it is the main output of the thesis. Starting with this chapter, a Rear-Wheel Drive (RWD) car with front-wheel steering is assumed. The developed control strategy consists of some state-of-the-art methods and our ideas. Lateral movement is controlled by one of the algorithms discussed in the previous chapter. There are no limitations for lateral control. In contrast with speed control, lateral control works only with information about the crosstrack error and the heading error which are essential controller inputs for all algorithms of this type. Comparison of some popular lateral control methods is done in the next chapter.

Longitudinal movement, on the other hand, is controlled with respect to information about the road shape and tracking performance. We can divide the given path into two categories – straight segments and curved segments. Since the procedure is different on both parts, we will look at each part separately. At this point, we will focus on the tracking of the path centerline, thus we assume a constant curvature of all arcs. However, the proposed method can be extended to tracking of a general path. No other constraints are considered, and, for example, straight segment lengths or bend radii can be arbitrary.

6.1 Straight segments

Let us start with speed control on straight parts of the path. Because we consider a race car, the main criterion is to drive the given lap as quickly as possible. According to theory, there is the maximum speed of a car in a curve to prevent loss of stability. We parameterize this speed as

$$v_{arc} = \sqrt{cR}, \tag{6.1}$$

where c is the tuned parameter and R is the curvature. We require the car to approach the bend with the speed v_{arc}. To reach the optimal lap time, the average speed along a straight segment must be maximized.

The racing car first accelerates after leaving the previous turn and then brakes before the next turn. The point where the car starts to brake is not specified in advance, but it is determined in real time. As far as we know the average deceleration a_b created by braking, this point can be computed as follows. Let Δv denote the difference between the actual speed v and the speed v_{arc}. The time it takes to reduce the speed by Δv is $t = \Delta v / a_b$. The distance traveled by the car while braking is then given by the relation

$$s = vt - \frac{1}{2}a_b t^2 = \frac{v - v_{arc}}{a_b}\left(v - \frac{v - v_{arc}}{2}\right). \tag{6.2}$$

When the distance s is smaller than the distance to the bend with some safety margin,

Algorithm 3 Extended ABS

Require: $k \in \langle 0, 1\rangle$, $r_1 > 0$, $r_2 > 0$, $\lambda_{min} \in (0, 1)$, $\lambda_{max} \in (0, 1)$
  while Braking **do**
    if $\lambda(t) > \lambda_{min}$ **then**
      if CurrentBrakeTorque $< 0.8 \cdot T_{locking}$ **then**
        CurrentBrakeTorque $\leftarrow$ CurrentBrakeTorque $+ r_1$
      else
        CurrentBrakeTorque $\leftarrow$ CurrentBrakeTorque $+ r_2$
      end if
    else
      $T_{locking} \leftarrow$ CurrentBrakeTorque
      CurrentBrakeTorque $\leftarrow k\cdot$ CurrentBrakeTorque
      while True **do**
        if $\lambda(t) > \lambda_{max}$ **then**
          break
        end if
      end while
    end if
  end while

the car starts to brake. The car stops braking either when it reaches the speed v_{arc} or leaves the straight segment.

Acceleration is regulated by a PI regulator with saturation of the integral term to prevent windup. The same technique was used in the Stanley car to track the speed [51]. The maximum speed is provided to the controller as the reference, but this speed may not be achieved for the reasons described above. No slippage should occur when proportional and integral constants are correctly tuned. However, the constants depend on the surface, coefficient of friction respectively. Utilization of Traction Control System (TCS) is a possible improvement of our system. A similar system, Anti-lock Brake System (ABS), is nevertheless used for braking before a bend.

As a part of our faculty project, we have developed an extended version of ABS [87]. See the article for the implementation on the developed subscale vehicle. The system shown in Alg. 3 works as follows in two stages. The first stage is the braking part where the braking torque is linearly incremented. This stage ends when the slip ratio λ reaches the minimal value λ_{min}. The braking ramp is divided into two parts to keep the car in the desired area of the optimal braking torque related to the locking torque $T_{locking}$. $T_{locking}$ is a value which is loaded at the beginning of each loop. The torque is first increased by r_1 each loop. When the braking torque almost reaches $T_{locking}$ (80 % in our case), its gain is reduced to r_2 ($r_1 > r_2$).

The second stage is called tire relaxation. After the wheel crosses λ_{min}, it is assumed as a locked wheel that lost optimal adhesion with the surface. A new value of the locking torque is assigned to $T_{locking}$. This value is later used as the reference in the first phase.

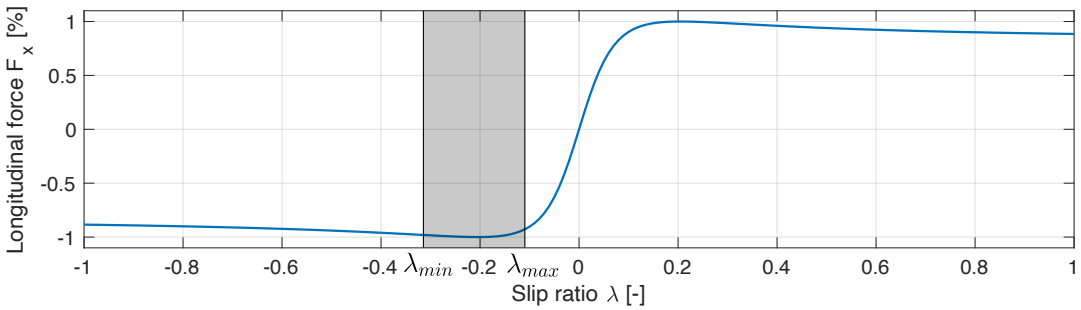

Fig. 6.1: Longitudinal slip curve with a grey area representing the operating space of ABS. The area is bounded from the left by λ_{min} and from the right by λ_{max}.

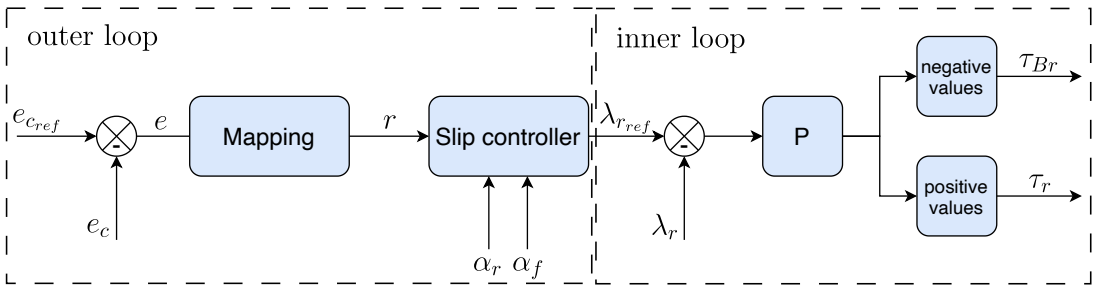

Fig. 6.2: Diagram of longitudinal control on curved segments

The braking torque is released to the value defined by the parameter k. If k is zero, braking is completely deactivated. When $k = 1$, the torque is not released, and the tire cannot relax. After the wheel starts spinning again, and the slip ratio rises above the λ_{max}, the whole loop is repeated.

6.2 Curved segments

With the first part of the longitudinal controller tuned correctly, the vehicle should approach any bend with the right speed according to Eq. (6.1). In a perfect world, the car would drive through a corner exactly on the edge of its handling limits. Due to the disturbances (e.g. the force caused by wind or an uneven surface), wrong speed, and imperfectly tuned lateral controller, the quality of path tracking is assured by an adapted slip controller. As introduced in Section 5.1.3, this controller accelerates or slows down the car depending on the position in the slip circle. We took the idea of the slip controller and customized it for our requirements.

Fig. 6.2 shows the full structure of the longitudinal controller for curved segments. The controller consists of two feedback loops. The inner loop takes the reference slip ratio $\lambda_{r_{ref}}$ and the current slip ratio λ_r, and it minimize the error $\lambda_{r_{ref}} - \lambda_r$ via a proportional regulator. Positive values of the torque are fed into the system as τ_r, whereas negative values as τ_{Br}. Since the slip ratio error is a small number less than one, and the peak torque of a real racing vehicle is five orders of magnitude higher, the proportional constant must be a high number.

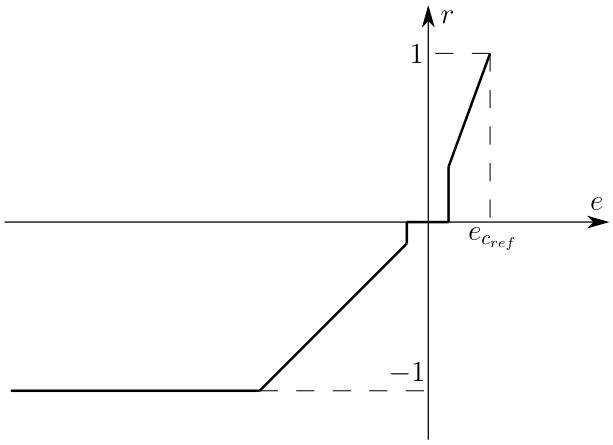

Fig. 6.3: Nonlinear mapping function $f : (-\infty, e_{c_{ref}}\rangle \rightarrow \langle -1, 1\rangle$ with deadband and saturation

Algorithm 4 Combined vehicle control

Require: ABS parameters, PI regulator parameters, lateral controller parameters, slip controller parameters, reference path

```
while True do
  v, κ, ψ̇, e_c, e_h, α_r, α_f, λ_r ← SensorFusion()
  δ_f ← LateralControl(v, κ, ψ̇, e_c, e_h)
  if In bend then
    τ_r, τ_Br ← SlipControl(α_r, α_f, λ_r, e_c)
  else
    d ← DistToBend()
    d_b ← BreakingDist()
    if d > d_b then
      τ_r ← PI(v)
    else
      τ_Br ← ABS(λ_r)
    end if
  end if
end while
```

The slip controller in the outer loop provides the reference slip ratio $\lambda_{r_{ref}}$ given the slip angles α_f, α_r, and the signal r. The slip angles are used for determining the position of the tire in the slip circle. If any slip angle is beyond the maximum value ($|\alpha/\alpha^{opt}| > 1$), the output is zero. When the slip characteristics are within the circle, the slip controller computes $\lambda_{r_{ref}}$ as

$$\lambda_{r_{ref}} = r\lambda_r^{opt}\sqrt{1 - \left|\frac{\alpha_r}{\alpha_r^{opt}}\right|^2}, \tag{6.3}$$

where r represents a nonlinear gain between -1 and 1. Zero gain means zero output of the slip controller and therefore zero motor and brake torques. On contrary, if $r = \pm 1$, the reference slip ratio equals to the maximum slip ratio on the edge in the upper half-plane of the slip circle, lower half-plane respectively.

The signal r should represent the quality of tracking of the reference path. We propose the crosstrack error e_c as the quality indicator. Furthermore, the reference crosstrack error $e_{c_{ref}}$ is used as the outer loop setpoint. A nonzero setpoint is a crucial requirement of the presented algorithm. In case of a zero setpoint, even the slightest crosstrack error would cause unnecessary braking. A small crosstrack error through the turn does not affect the lateral stability of the vehicle. The utilized mapping function is shown in Fig. 6.3. The function domain is $(-\infty, e_{c_{ref}}\rangle$ since the crosstrack error is always a nonnegative number. The function consists of two linear parts for negative error values and for positive values, saturation to limit the value, and optional deadband. The deadband prevents oscillations around the zero position due to fast gas and brake alternation. We also added averaging using a moving average before the mapping for extra smoothing. The combined vehicle control is presented in Alg. 4.

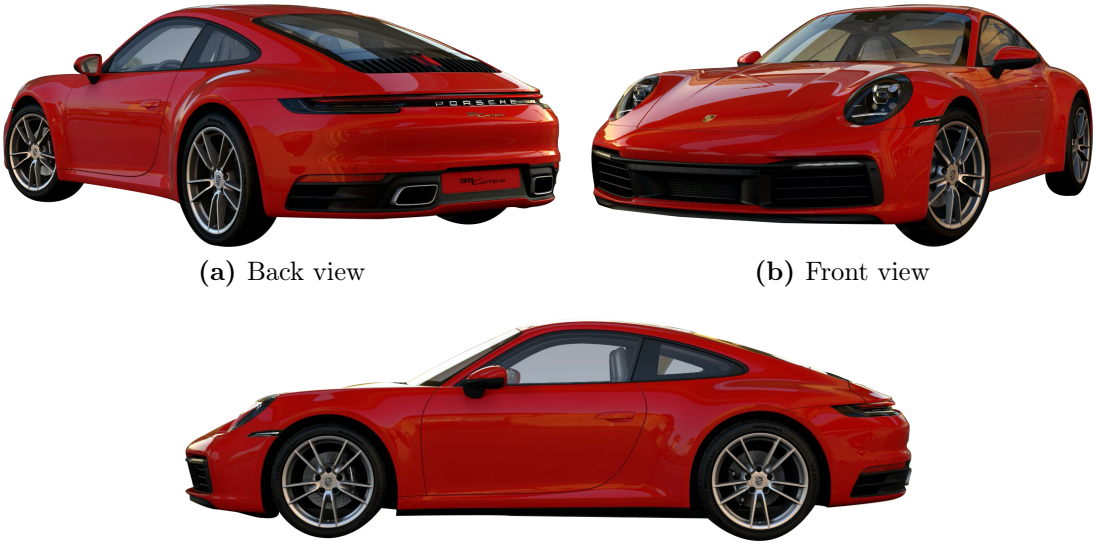

(a) Back view **(b)** Front view

(c) Side view

Fig. 7.1: Porsche 911 Carrera

7 Simulations and Experiments

Simulation is an essential tool in the development of control algorithms. This chapter is mainly devoted to simulating all parts of the proposed control strategy from the previous chapter. The first necessary task is to introduce the car used for testing. Our requirement was a high-performance car with Rear-Wheel Drive (RWD) and an engine mounted at the rear of the car. RWD layout and a heavy rear axle load were chosen considering the purpose of this work. The majority of racing cars and formulas have this type of design. The extra weight concentrated over rear wheels allows vehicles to understeer. This is particularly important for performing dynamic maneuvers on the racetrack.

We chose Porsche 911 as our testing vehicle (see Fig. 7.1). This car is a well known two-door sports car that meets all the requirements. Porsche 911 is produced in many versions which differ in its parameters and driving characteristics. The car is equipped with 20-inch front wheels and 245/35R20 tires. Rear wheels have a diameter of 21 inches, and rear tires are 305/30R21. The full list of used vehicle parameters is given in Appendix B.

7.1 Simulation framework

There are ready solutions for designing, simulating, and testing Advanced Driver Assistance System (ADAS) on the market. MATLAB/Simulink (hereinafter referred to as MATLAB) is a popular development environment not only for simulations. There is a specialized toolbox for MATLAB called Automated Driving Toolbox[9]. This toolbox offers all necessary functions including measurement simulation and road generation. Except

[9]See the website https://www.mathworks.com/products/automated-driving.html for more information.

MATLAB, there is more proprietary software like rFpro[10] which is used by car manufacturers around the world. Beside nonfree simulation software, open-source tools are also available. We can mention e.g. CARLA[11], LGSVL Simulator[12], or AirSim[13]. A new promising system is being developed at MIT [88]. A convolutional neural network is used to create a photorealistic representation of the virtual world the vehicle can respond to.

Because of previous experience, we selected MATLAB for the implementation and testing of control systems. However, we do not use the mentioned toolbox, and instead, we created our own simple simulation framework. The main reason is a better understanding of our framework. The high complexity of the Automated Driving Toolbox is unnecessary for this project. MATLAB was also chosen to integrate the works of other colleagues. The high-fidelity vehicle model has been provided through the courtesy of Denis Efremov (created in [7]). Detection of the centerline from images and subsequent measurement of errors is a thesis assignment of Burak Aydin. His system can be integrated into the simulation framework. The ABS presented in Chapter 6 was originally implemented in MATLAB by Tomáš Rutrle. The framework is captured in Fig. 7.2.

7.2 Simulation results

All parts of the control system are evaluated sequentially before simulating the entire system at once. This procedure is chosen mainly to find optimal controllers parameters. Another reason why to examine the segments separately is full insight into the controller's performance without adverse effects. The longitudinal tracking section contains the PI regulator and ABS tests on a straight path. The lateral tracking section includes a comparison of some trajectory trackers. Finally, the combined tracking section evaluates the performance of the complex control system with all features on a complete racecourse.

7.2.1 Longitudinal tracking

A PI regulator is used to accelerate to the defined speed. We performed simulations on three surfaces with different friction coefficients. The reference is a step from 1 m/s (the solution diverge at zero speed) to 20 m/s. The regulator is tested for three proportional constants – 100, 200, and 1000 on each surface. The integral term is important for precise reference tracking and therefore is set to 3 in Fig 7.3, Fig 7.4 and Fig 7.5. The effect of the integral term is shown in Fig 7.6. In addition, there is added an external longitudinal force with a mean value of −1000 N. Note that if the constant is too large, overshoot appears, and the speed decreases slowly due to the inertia effect.

[10]See the website http://www.rfpro.com/ for more information.
[11]See the website http://carla.org/ for more information.
[12]See the website https://www.lgsvlsimulator.com/ for more information.
[13]See the website https://github.com/microsoft/AirSim for more information.

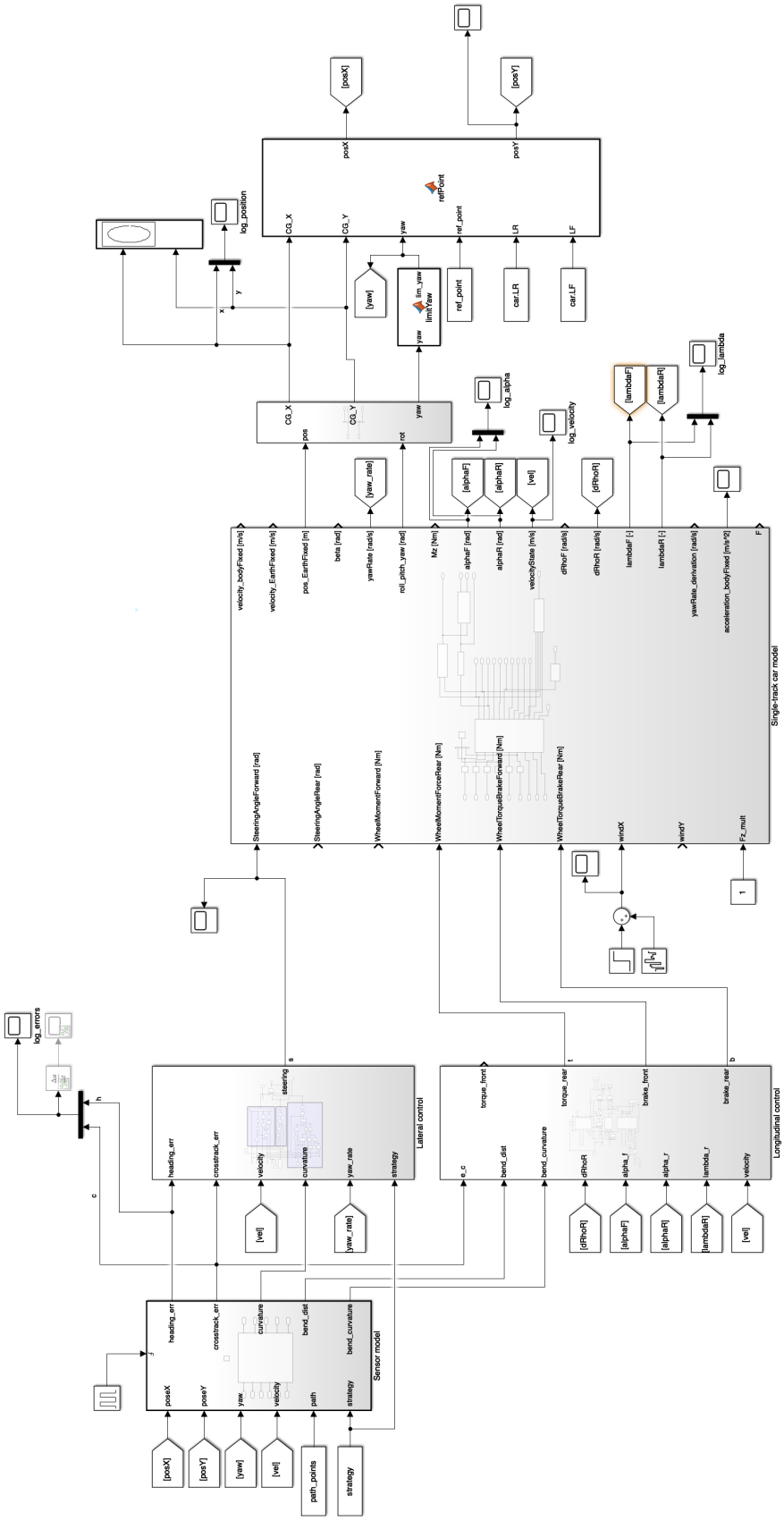

Fig. 7.2: Simulation framework. The largest block is the single-track vehicle model made by Denis Efremov. Vehicle control is divided into longitudinal control and lateral control blocks. The block with the sensor model provides simulated measurements given the reference path. The update rate is adjustable.

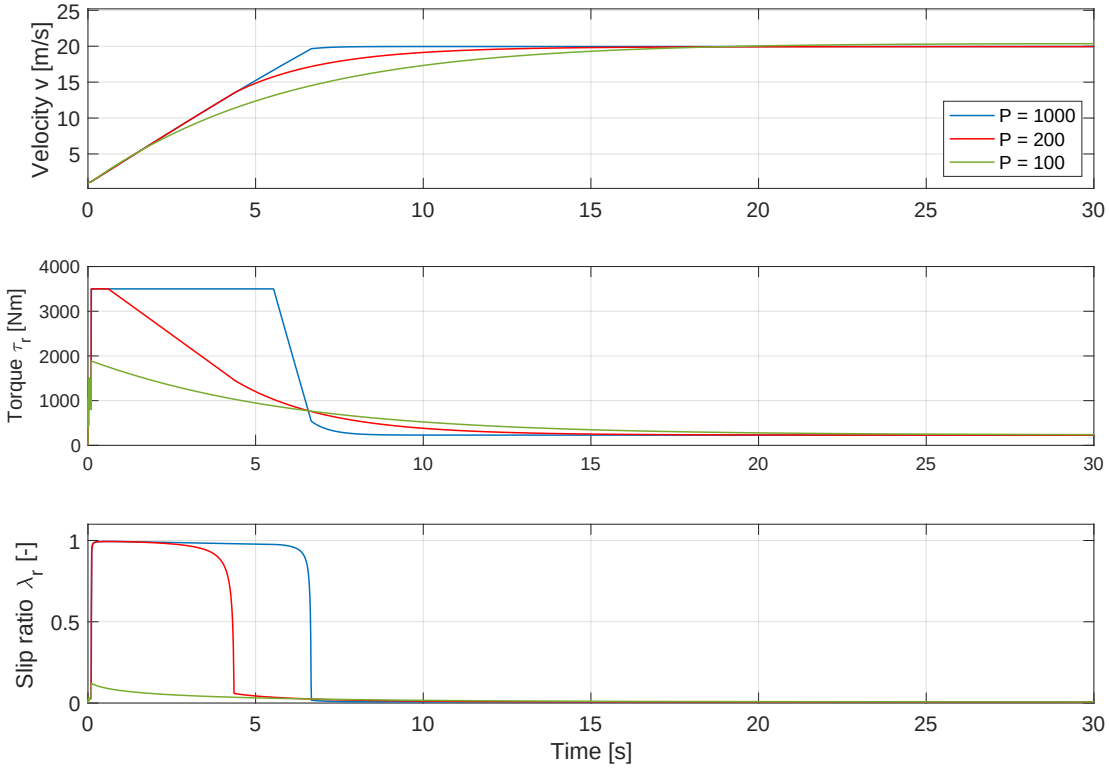

Fig. 7.3: Performance of the PI regulator on gravel ($\mu = 0.5$)

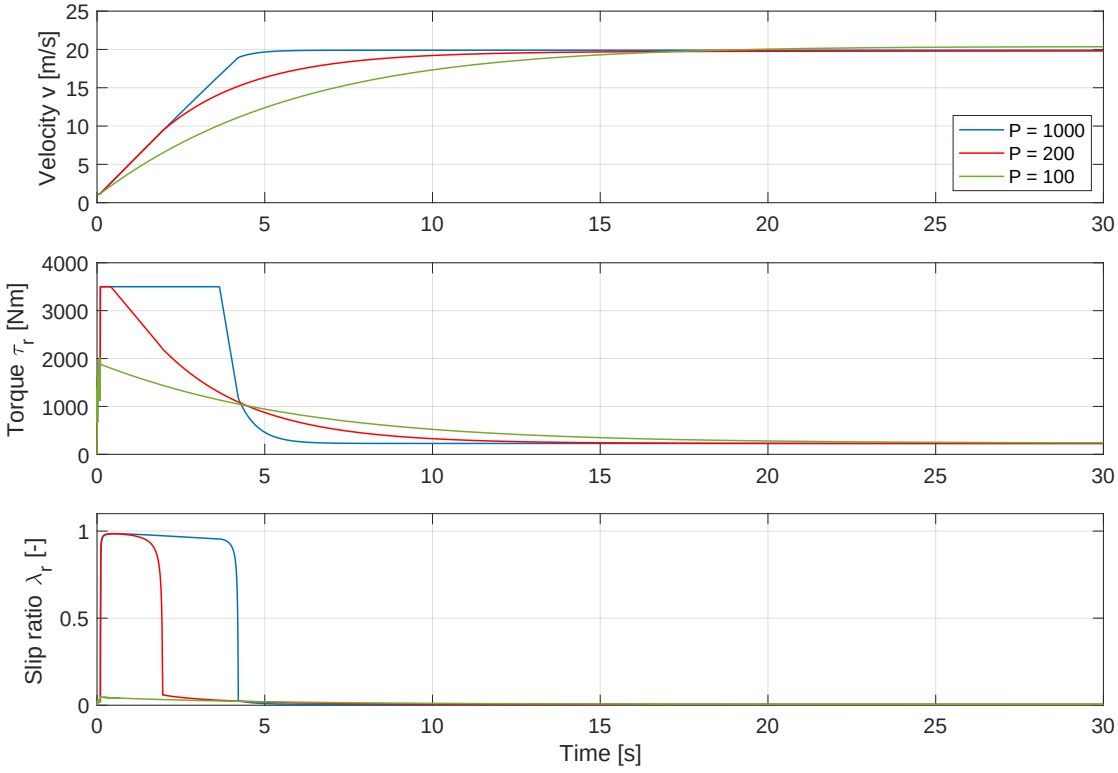

Fig. 7.4: Performance of the PI regulator on wet asphalt ($\mu = 0.75$)

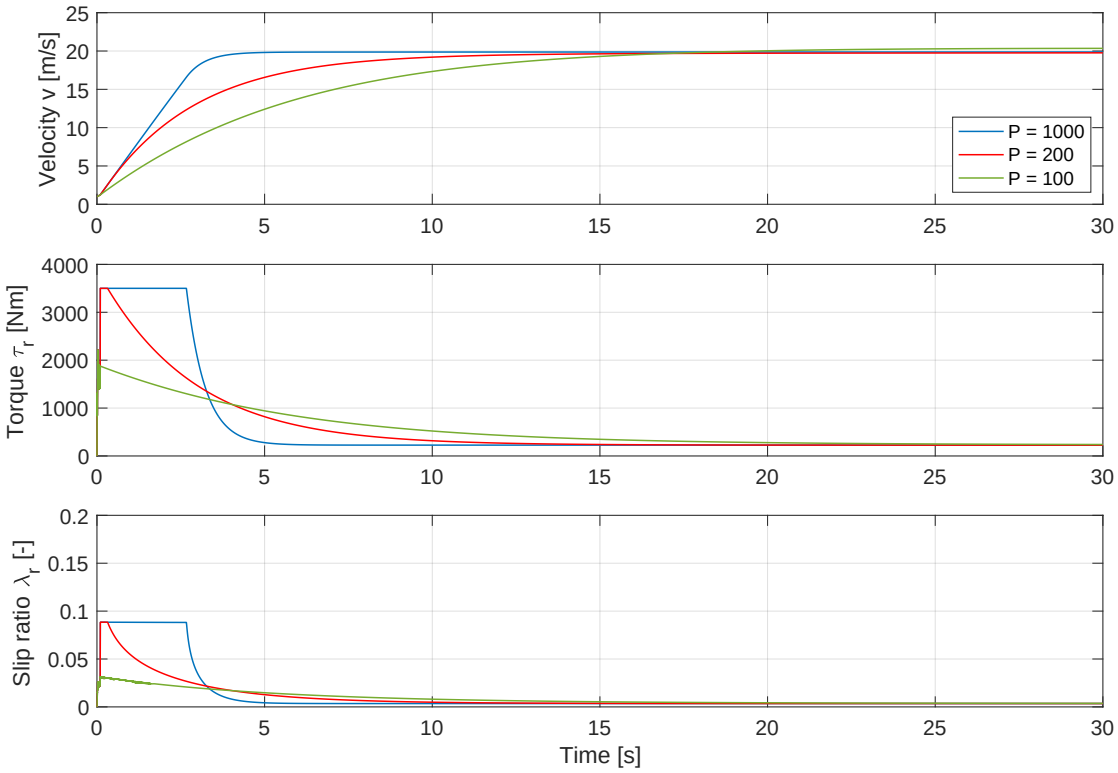

Fig. 7.5: Performance of the PI regulator on asphalt/concrete ($\mu = 1$)

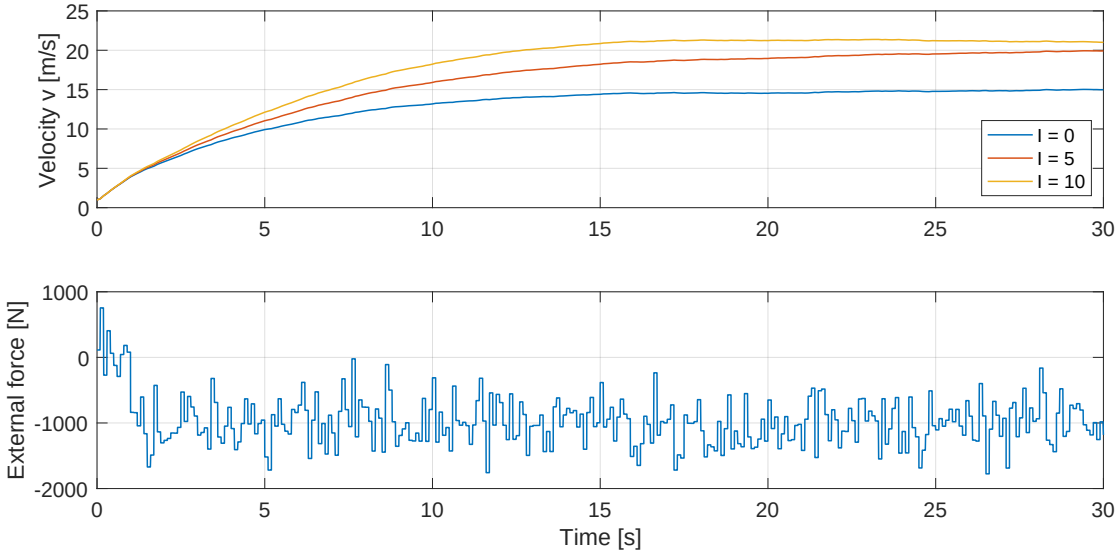

Fig. 7.6: Dependence of the parameter I on the tracking performance (P = 100, $\mu = 0.5$)

r_1 [Nm]	r_2 [Nm]	k [-]	λ_{min} [-]	λ_{max} [-]	frequency [Hz]
3	0.3	0	0.1	0.2	1000

Tab. 5: Parameters of the ABS for simulation

An important part of the longitudinal controller is ABS. The verification scenario for the ABS is designed as a straight path with friction coefficient 0.5 representing gravel. The car starts to brake at 1 s from the initial speed 30 m/s until full stop. The locking torque $T_{locking}$ is set to 2000 N. The list of all parameters is provided in Tab. 5. The braking distance difference is almost 4 m as shown in Fig. 7.7. Simulation results on a path with two different surfaces are provided in [87].

A major advantage of this braking system is better maneuverability. In the second simulation experiment, the car brakes in the same manner as in the previous experiment. In addition, the front wheels are turned by 0.3 rad to the left. This setting simulates high-speed emergency braking if an obstacle appears in front of the car. As shown in 7.8, the car without ABS has the shortest braking distance, but it slides on the surface and does not turn.

7.2.2 Lateral tracking

Lateral tracking algorithms are evaluated using the observation method (the actual path is graphically compared against the desired path) and quality indicators. The numerical expression of the tracking performance is an important method as simple observation does not provide enough information. We use one of the approaches from the review [77]. For lateral tracking, the measurement characterizing quality is the crosstrack error e_c. Let S_{ISE} define integral of square of the error as

$$S_{ISE} = \frac{1}{t_{end}} \int_0^{t_{end}} e_c^2(t)\, dt \approx \frac{1}{N} \sum_{n=1}^{N} e_c^2(n). \tag{7.1}$$

Since we work in a discrete world, the integral is approximated by sum through all measurements. The second indicator is integral of the absolute magnitude of the error S_{IAE} defined as

$$S_{IAE} = \frac{1}{t_{end}} \int_0^{t_{end}} |e_c(t)|\, dt \approx \frac{1}{N} \sum_{n=1}^{N} |e_c(n)|. \tag{7.2}$$

The last indicator is based on the steering angle generated by the lateral controller along the path. It expresses the amount of consumed energy for turning the vehicle. Controller effort is defined as

$$E_\delta = \sum_{n=1}^{N} \delta_f(n). \tag{7.3}$$

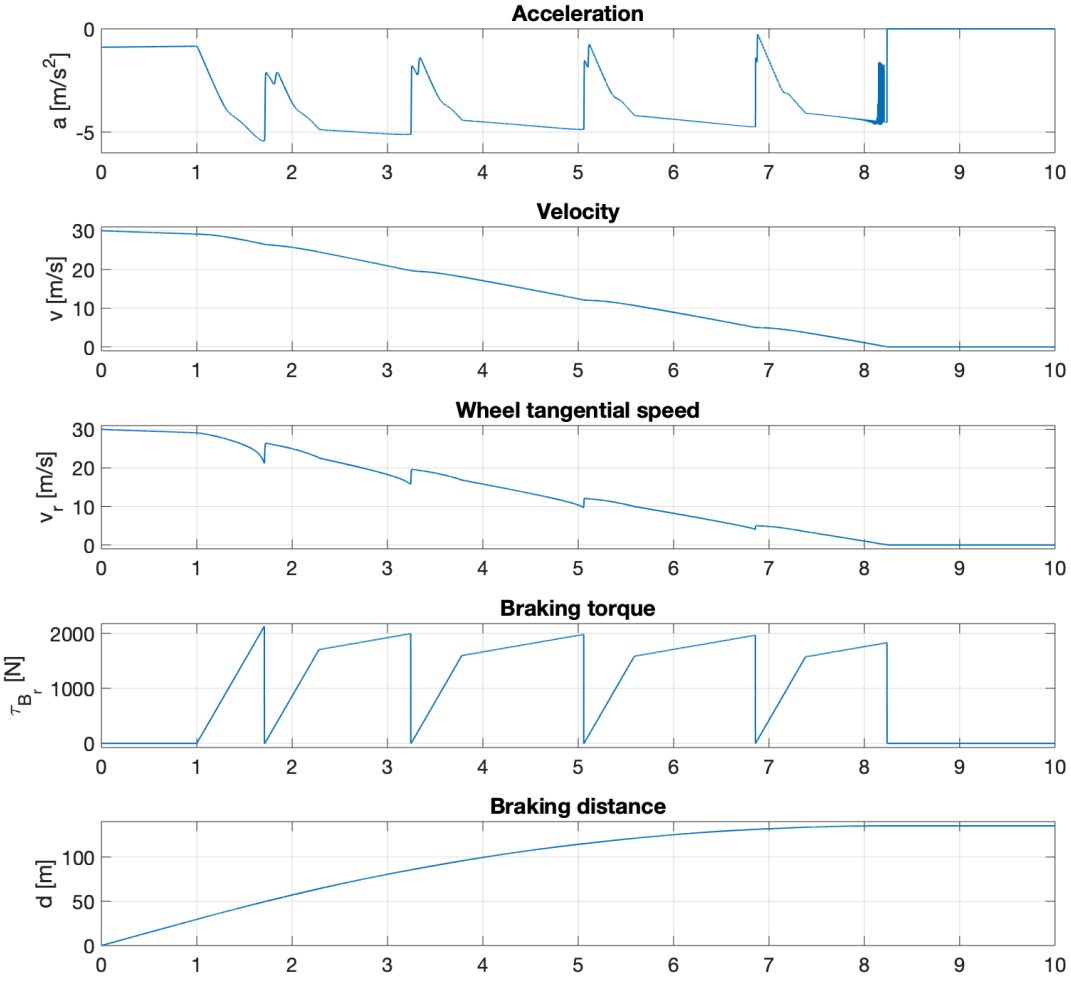

Fig. 7.7: Vehicle variables for braking with ABS

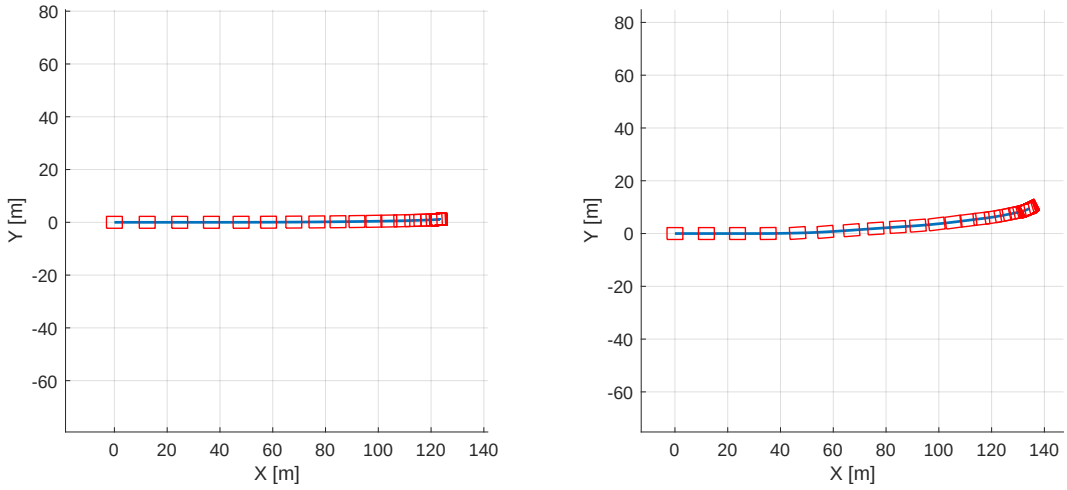

(a) No ABS **(b)** Classical ABS

Fig. 7.8: Top view of the actual path when cornering and braking

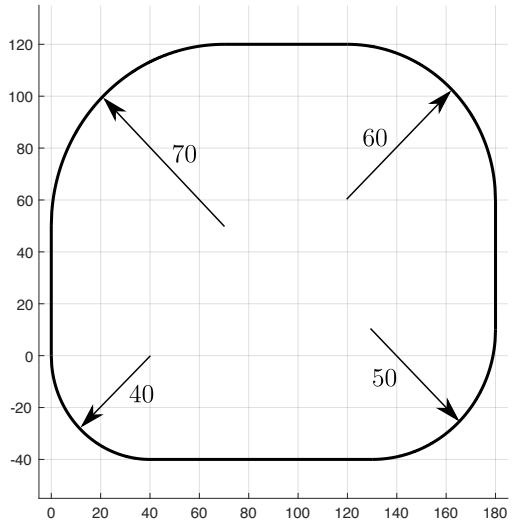

Fig. 7.9: Testing lap for lateral controllers

The integral indicators are normalized by the number of measurements N. We further divide the S_{ISE} to $S_{ISE} - S$ (on straight segments) and $S_{ISE} - B$ (in a bend). The same division applies to S_{IAE}.

We designed a testing lap with four bends with different curvatures (see Fig. 7.9). The maximal bend radius is 70 m, and it decreases linearly by ten meters up to 40 m which is the maximum bend radius for a car traveling at speed 20 m/s. The testing car employs the PI regulator on straight segments to accelerate to this speed. The car does not accelerate or brake in bends as it would affect the measurements. The starting point is $(0, 0)$, as well as the endpoint. A lateral force (mean value 1000 N + white noise) representing side wind is applied to the car.

Our main interest is in geometric path trackers introduced in Section 5.2.1. The actual path of the car with the Pure pursuit algorithm is shown in Fig 7.10 (the color represents the speed). The comparison is made depending on the constant k_d which influences the look-ahead distance. A similar comparison is made for the Stanley controller (see Fig. 7.11). In this case, the variable parameters are the gain k_d and the constant influencing the heading reference k_{ss}. Parameters $k_{d,yaw}$ and k_s are zero. Tab. 6 and Tab. 7 shows the described indicators on the testing lap for both controllers.

Too small k_d results in oscillation as shown in Fig. 7.10a. As the parameter increases, the path is smoothed. However, tracking is less accurate as the look-ahead distance increases. The car equipped with the Pure pursuit cannot pass the smallest turn without an offset even with the smallest look-ahead distance. That is given by the properties of the algorithm. Overall, the Stanley produces better results as it is also designed for the dynamic vehicle model, not only for the kinematic model. The nonzero heading error reference ensures better tracking quality in bends (Fig. 7.11a vs Fig. 7.11b). The problem

k_d	$S_{ISE} - S$ ①	$S_{ISE} - B$ ②	$S_{IAE} - S$ ③	$S_{IAE} - B$ ④	E_δ
0.5	0.047	0.830	0.095	0.506	307.8
1	0.050	1.196	0.100	0.660	279.9
2	1.256	1.063	0.598	0.684	269.7
4	11.004	6.718	1.981	1.596	262.3

Tab. 6: Pure pursuit quality indicators

k_d	k_{ss}	$S_{ISE} - S$ ①	$S_{ISE} - B$ ②	$S_{IAE} - S$ ③	$S_{IAE} - B$ ④	E_δ
0.5	**0**	0.200	1.682	0.245	0.914	283.4
2	**0**	0.003	0.849	0.025	0.492	311.6
5	**0**	0.041	0.113	0.077	0.203	468.5
0.5	**0.01**	0.010	0.287	0.050	0.279	297.1
2	**0.01**	0.001	0.428	0.020	0.258	297.5
5	**0.01**	0.003	0.047	0.032	0.135	382.0

Tab. 7: Stanley quality indicators

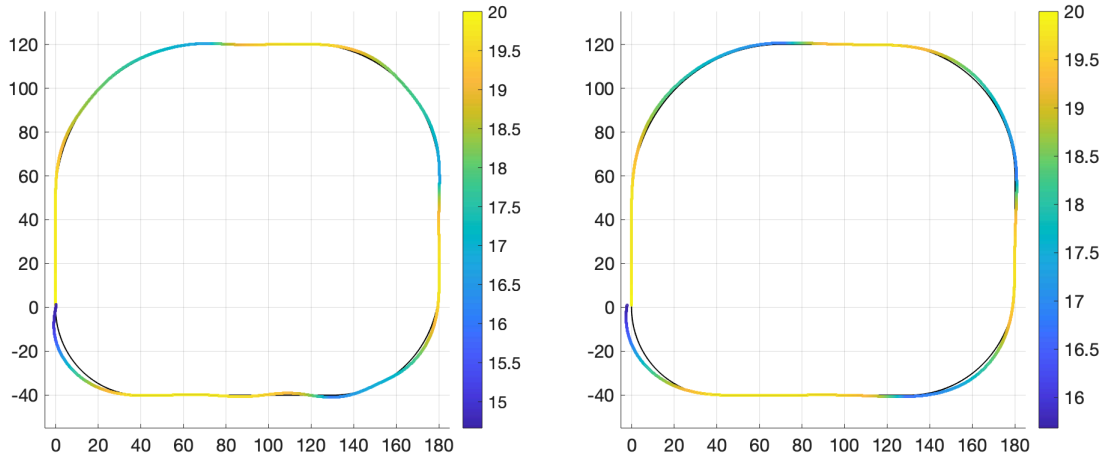

(a) $k_d = 0.5$ **(b)** $k_d = 1$

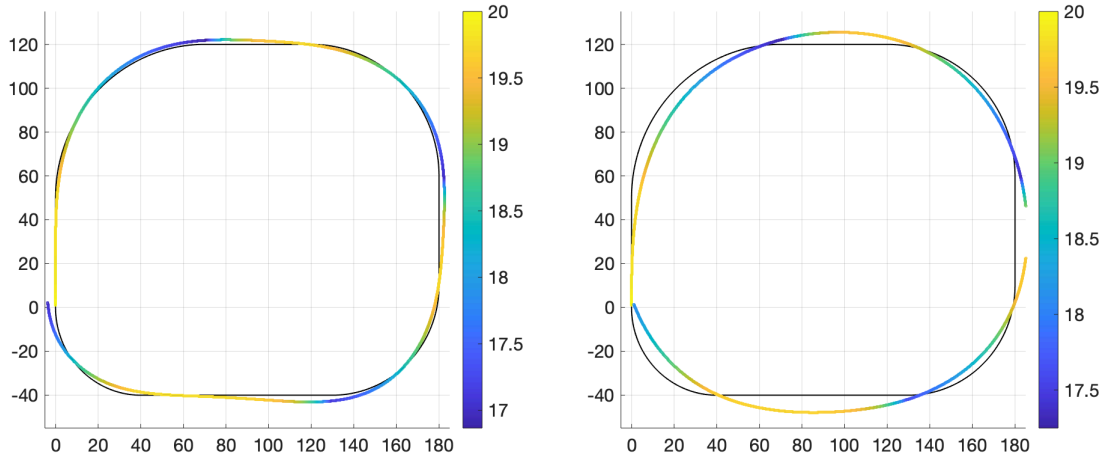

(c) $k_d = 2$ **(d)** $k_d = 4$

Fig. 7.10: Pure pursuit tracking quality for different constants k_d

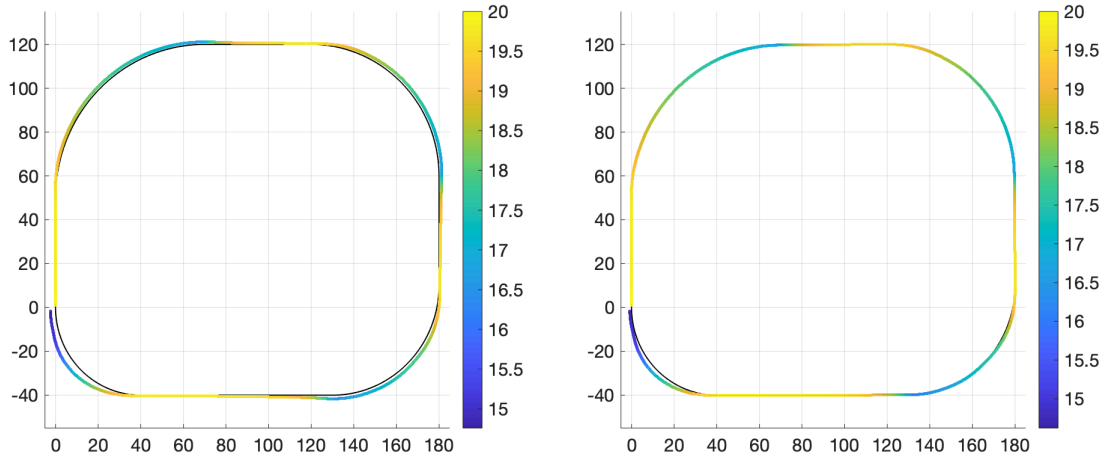

(a) $k_d = 0.5, k_{ss} = 0$ **(b)** $k_d = 0.5, k_{ss} = 0.01$

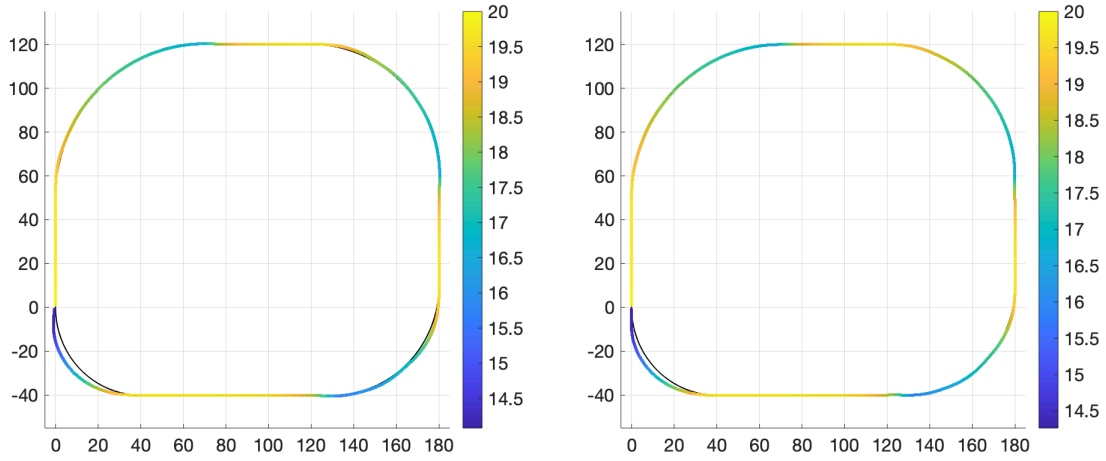

(c) $k_d = 2, k_{ss} = 0$ **(d)** $k_d = 2, k_{ss} = 0.01$

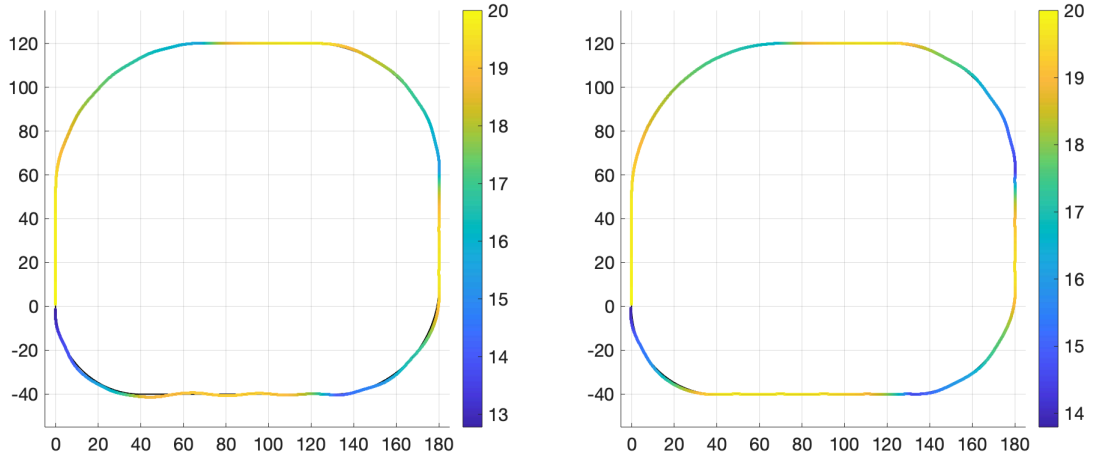

(e) $k_d = 5, k_{ss} = 0$ **(f)** $k_d = 5, k_{ss} = 0.01$

Fig. 7.11: Stanley tracking quality for different constants k_d and k_{ss}

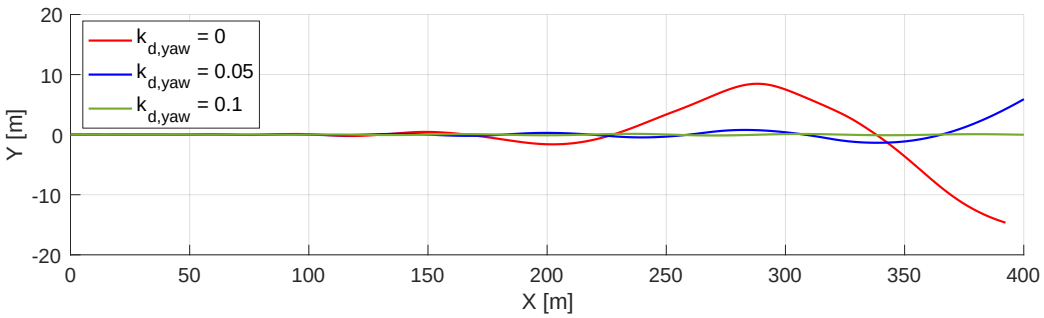

Fig. 7.12: Dependence of the parameter $k_{d,yaw}$ on the performance of Stanley controller with high gain k_d

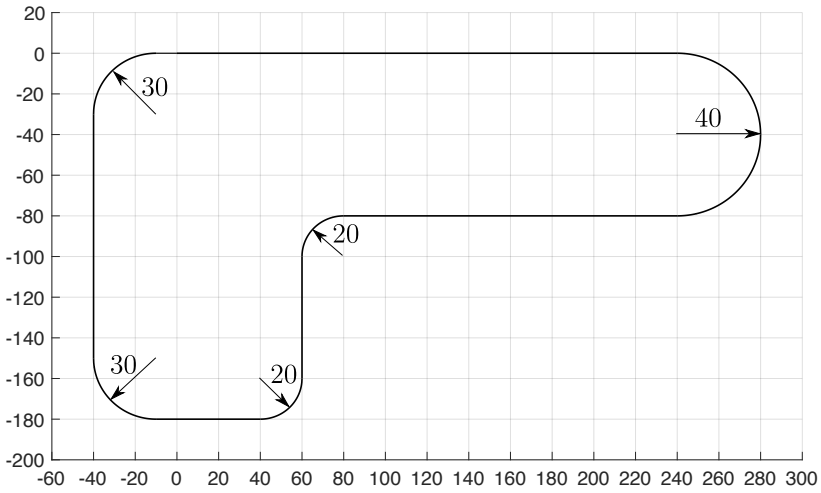

Fig. 7.13: Testing lap for combined control

with the offset in bends with relatively large curvatures can be solved by tuning the parameter k_d.

The usefulness of the damping parameter $k_{d,yaw}$ is shown in Fig. 7.12. Here, the vehicle accelerates on a straight path. When the vehicle crosses approximately 30 m/s (X = 100 in the graph), oscillations start to appear, and tracking accuracy decreases rapidly. When the yaw damping is utilized, the car is stable even with high speeds of about 60 m/s. Considering the performed measurements, the Stanley is chosen as the lateral controller for next simulations.

7.2.3 Combined tracking

For combined tracking (trajectory tracking), quality measurement is extended by the throttle effort E_τ and the brake effort E_{τ_B}:

$$E_\tau = \sum_{n=1}^{N} \tau_r(n), \; E_{\tau_B} = \sum_{n=1}^{N} \tau_{Br}(n). \tag{7.4}$$

P	①	②	③	④	E_δ	$10^5 E_\tau$	$10^5 E_{\tau_B}$	avg. v [m/s]	time [s]
0	0.004	0.009	0.039	0.046	5113.2	1248.5	795.8	18.65	50.09
25000	0.009	0.012	0.054	0.049	5662.6	1326.8	806.5	19.21	48.54
50000	0.031	0.015	0.093	0.053	6531.1	1350.8	816.8	19.29	48.19
75000	0.027	0.019	0.084	0.057	6292.7	1353.0	814.8	19.42	47.83
100000	0.028	0.017	0.090	0.056	6410.1	1362.5	827.6	19.41	47.94
125000	0.067	0.022	0.118	0.065	7482.3	1394.0	834.6	19.29	48.19

Tab. 8: Quality indicators of the proposed controller without disturbances

The map for testing the complete system was designed to contain straight segments with different lengths and curved segments with different radii (see Fig. 7.13). This map is suitable for the verification of used control systems. The total length of the track is 902.7 m. Fig. 7.14 illustrates car behavior when the controllers are properly tuned and when they are not. In Fig. 7.14b, we can see a lateral offset caused by the parameter k_{ss}. In Fig. 7.14c, the bend approach speed is too high which may even result in instability of the vehicle in some specific cases. This is either caused by incorrectly calculated braking distance or a wrong parameter c in Eq. 6.1.

The first simulation experiment is autonomous driving on the track without external forces. The variable parameter is the output gain P of the slip-based controller. The table with results is shown in Tab. 8. The marks in circles correspond to marks in Tab. 7. The corresponding slip circles are shown in Fig. 7.15 (the color indicates time). When the slip controller is off, the lap time is 50.09 s, and the tracking is very precise as seen on the indicators. If the slip controller is turned on and $P = 25000$, the quality is affected insignificantly but the lap time is improved to 48.54 s. That is a significant improvement on such a short track. We can see that the time can be improved even more at the cost of losing accuracy. There is always a trade-off between accuracy and time.

In the next simulation experiment, a negative longitudinal force was applied to the car. The quality was tested for three forces (-100 N, -500 N, -1000 N). The results are shown in Tab. 9. A better lap time is always achieved with the slip controller. The greater the force, the greater the time difference. The relative difference between the quality indicators also decreases with increasing force. The slip circle for $F = -1000$ N in Fig. 7.16 shows a noticeable change when using the slip controller.

The slip controller can also be used for faster response to external disturbances. In Fig. 7.17, a positive longitudinal force 500 N is applied. Also, the approach speed is higher than it should be. Therefore, the car leaves the path for a while. If a sufficient α^{opt} is set and the slip controller is on, the car sticks to the path earlier than when it is off. This operation, however, results in a loss of speed. The controller allows changing its functionality according to the requirements for accuracy and speed.

Fig. 7.18 illustrates the typical behavior of the car on the racetrack. The graphs show all relevant vehicle variables. In the case of the classic path tracking without the slip control, the speed decreases while cornering. While the slip control is activated, the

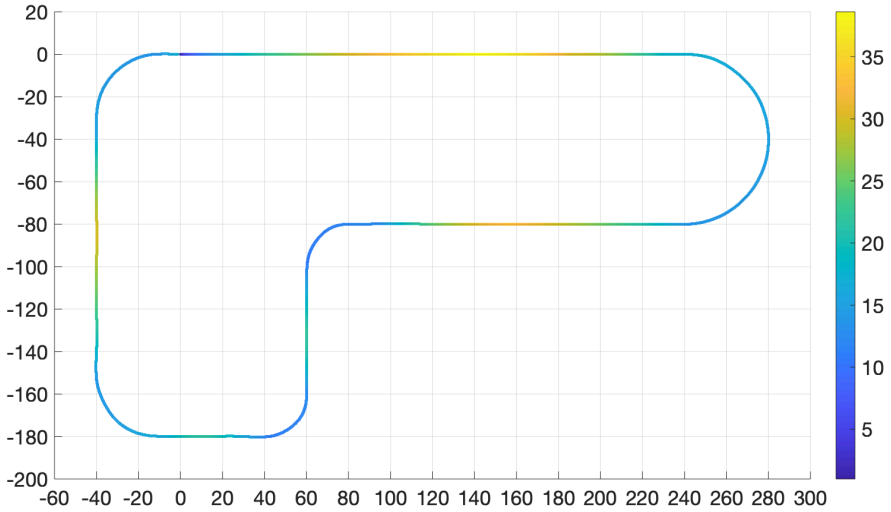

(a) Correct settings

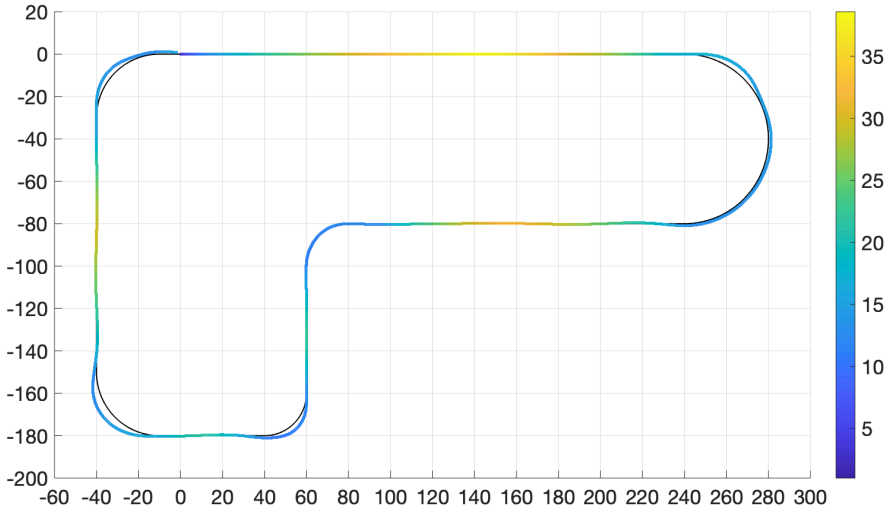

(b) No heading error reference

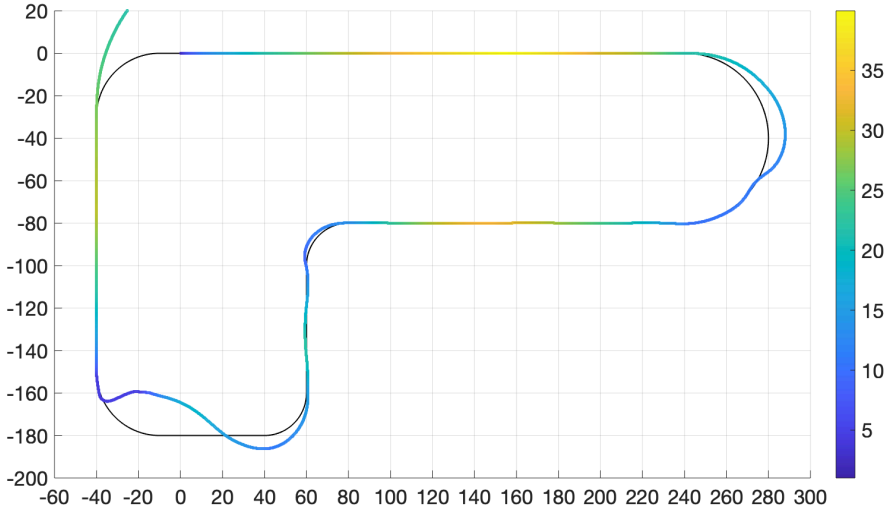

(c) Too high approach speed

Fig. 7.14: Tracking quality of the proposed controller in three different cases

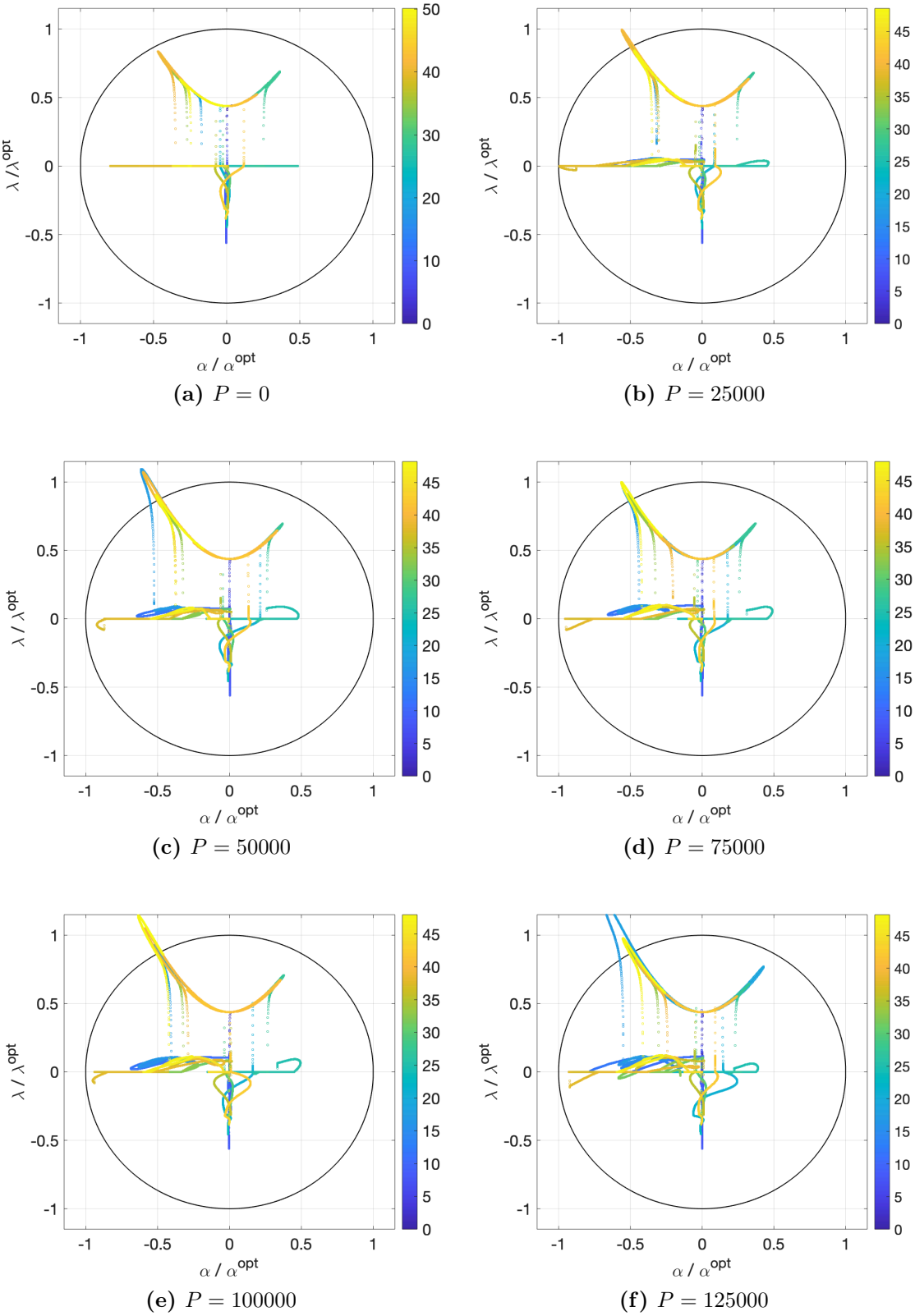

(a) $P = 0$ **(b)** $P = 25000$

(c) $P = 50000$ **(d)** $P = 75000$

(e) $P = 100000$ **(f)** $P = 125000$

Fig. 7.15: Slip circles of the proposed controller for a changing parameter P

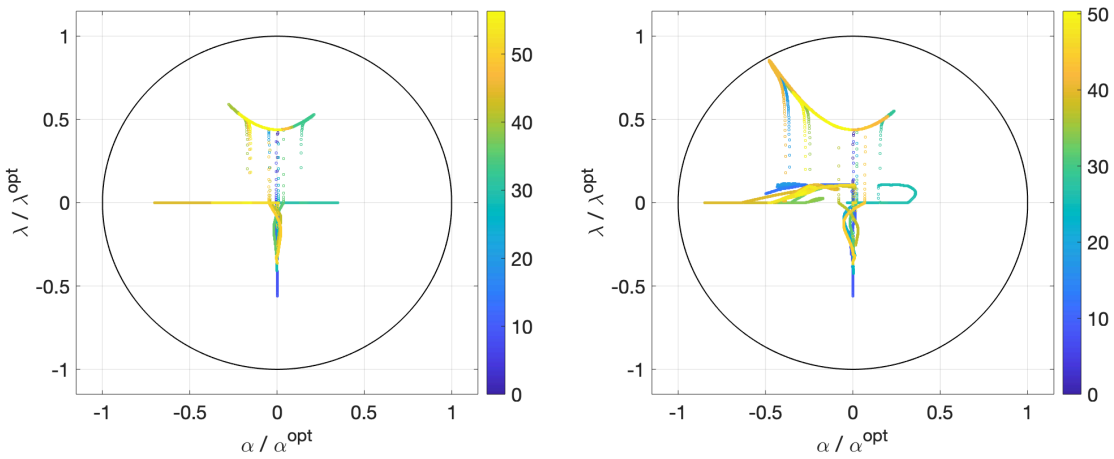

(a) $P = 0$ **(b)** $P = 75000$

Fig. 7.16: Slip circles of the car affected by a negative longitudinal force

P	F [N]	①	②	③	④	E_δ	$10^5 E_\tau$	$10^5 E_{\tau_B}$	avg. v [m/s]	time [s]
0	**-100**	0.002	0.008	0.032	0.043	4791.7	1262.1	774.2	18.46	50.59
75000	**-100**	0.033	0.015	0.096	0.054	6655.9	1382.4	802.7	19.33	48.24
0	**-500**	0.001	0.009	0.027	0.046	4927.9	1345.1	731.0	17.75	52.64
75000	**-500**	0.008	0.009	0.052	0.043	5203.6	1455.0	754.2	18.97	48.94
0	**-1000**	0.001	0.007	0.021	0.044	4962.9	1469.0	650.3	16.68	56.09
75000	**-1000**	0.003	0.008	0.035	0.041	4753.1	1561.7	693.7	18.36	50.59

Tab. 9: Quality indicators of the proposed controller with a negative longitudinal force

vehicle maintains its speed, and it can even slightly increase the speed as shown in the first graph.

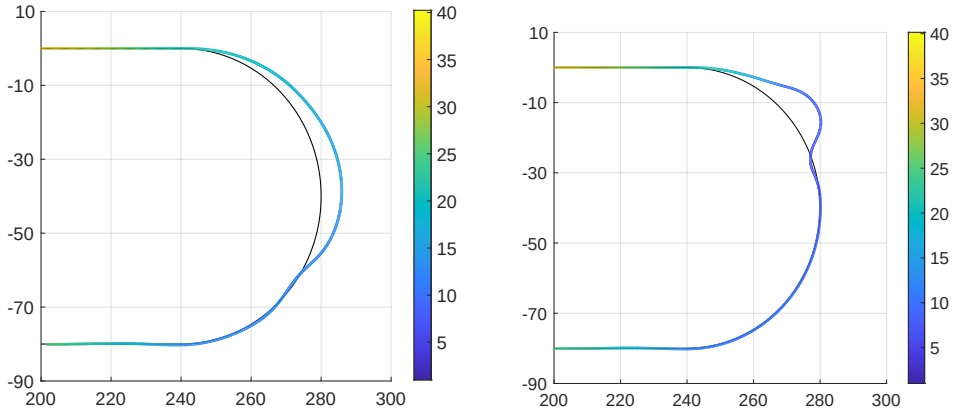

(a) Slip control off **(b)** Slip control on

Fig. 7.17: Tracking quality of the proposed method in a bend with the car affected by a positive longitudinal force

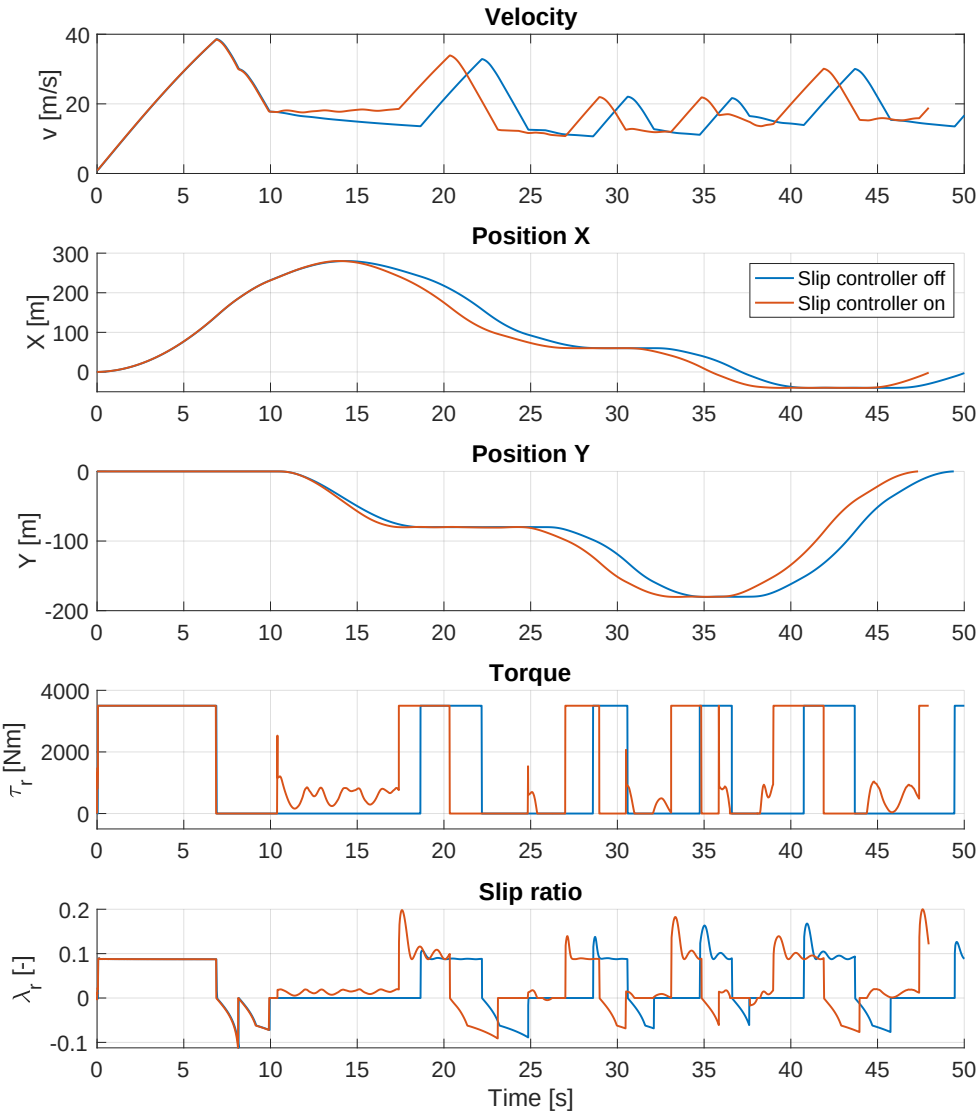

Fig. 7.18: Comparison of vehicle variables without the slip controller and with the slip controller

8 Results

All thesis goals stated in Chapter 2 have been completed. Specifically:

- Longitudinal control options have been explored in Section 5.1. The chapter contains an analysis of existing longitudinal control solutions and lateral control solutions. Before it is possible to track the desired path, a trajectory (path + speed profile) must be generated. This can be done either off-line by solving a differential equation or an optimization problem, or on-line while driving. The second approach is utilized in our solution. Active safety systems such as ABS, TCS, and ESC are also introduced here. We use a novel version of ABS which has information about the surface in addition to the generic information, in our solution.

- We became familiar with existing lateral control solutions for autonomous vehicles in Section 5.2. Two widely used lateral control algorithms (Pure pursuit, Stanley), together with two more complex methods Sliding Mode Control (SMC) and adaptive PID, are introduced in the chapter. The advantage of the Pure pursuit and Stanley, which are used in our solution, is their geometric derivation and the resulting simplicity. The disadvantage is a possible issue with the dynamic vehicle model.

- The simulation framework for autonomous racing was created in MATLAB/Simulink in Section 7.1. It includes control methods from previous objectives. A comparison of the Pure pursuit and Stanley was made in the simulation framework, and the results are presented in Section 7.2. Simulation of ABS was also performed in this chapter. Finally, the complete control system was thoroughly tested using a high-performance car Porsche 911 on the designed racetrack. The simulation experiments have shown that the slip controller improves the lap time if set correctly.

- The developed ABS was validated on the experimental subscale vehicle platform in [87]. Unfortunately, due to the COVID-19 pandemic in 2020, it was not possible to prepare other experiments. However, the control laws were thoroughly tested in the simulation model in Chapter 7.

9 Conclusion

The master thesis *Control Laws for Autonomous Racing* explored the possibilities of longitudinal and lateral control of a racing vehicle. The work starts with an opening chapter where general aspects of self-driving cars are discussed. History, classification, legislation, and autonomous racing are topics covered in this chapter. Then, it continues with a theoretical part containing mathematical modeling of a road vehicle. Two most common vehicle models are the single-track model and the twin-track model. Each model has its advantages and disadvantages, and the first model is used here for sufficient accuracy and simplicity. Linearization of the single-track model is also provided as it is a major task in designing of classical control systems. The part with control algorithms follows this chapter.

The work is based on the faculty project where the experimental 1:5 RC platform was developed. This project was financially supported by Toyota, and to this day, it is still being improved. The visually-assisted ABS, which is also part of the presented method, was verified using the platform. The platform is currently used for testing of control algorithms, localization methods, and machine perception. Our motivation is mainly the autonomous formula race where the first formula developed by Czech Technical University in Prague will be introduced in the summer of 2020.

The control system developed in this thesis consists of the Stanley controller for lateral tracking, a PI regulator with ABS for longitudinal tracking, and the slip-based controller for optimizing cornering performance. The slip controller processes information about tires slip and accelerates or decelerates the car accordingly. Simulations with a sports car having formula-like properties showed that the principle of the system is promising for further development. The system can be improved by the full traction control on straight path segments. In case of tracking of the optimal path, not centerline (simplification used for this work), the principle remains the same, but more research and testing is needed.

A List of Acronyms and Symbols

Acronyms

ABS Anti-lock Brake System. III–V, 5, 9, 19, 23–26, 33, 44, 45, 50, 54, 55, 65, 67

ACC Adaptive Cruise Control. 9–11, 23

ADAS Advanced Driver Assistance System. 12, 49

ADS Automated Driving System. 8, 9, 12

AI Artificial Intelligence. 1, 13

ALC Automated Lane Centering. 11

ALV Autonomous Land driven Vehicle. 8

CAS Collision Avoidance System. 9, 10

CG Center of Gravity. 15–17, 42, 70, 71

CPU Central Processing Unit. 2

CTU Czech Technical University in Prague. 1, 2, 14, 15, 67

DARPA Defense Advanced Research Projects Agency. 7, 8, 13, 14, 37

DOF Degrees of Freedom. 15, 17, 30

DOT Department of Transportation. 12

ESC Electronic Stability Control. V, 5, 25, 26, 65

EU European Union. 11–13

FEE Faculty of Electrical Engineering. 1, 2, 14, 15

GPS Global Positioning System. 2, 3, 26

GPU Graphics Processing Unit. 2

IMU Inertial Measurement Unit. 2, 3, 26

LiDAR Light Detection And Ranging. 7, 8

LKA Lane Keeping Assistant. 9–11

LQR Linear Quadratic Control. 30

LTVs Light Trucks and Vans. V, 24, 25

MPC Model Predictive Control. 30

NHTSA National Highway Traffic Safety Administration. 9, 12, 23–27

RC Remote Control. III, 1, 2, 5, 14, 25, 67

RWD Rear-Wheel Drive. 43, 49

SAE Society of Automotive Engineers. 9

SISO Single Input Single Output. 41

SLAM Simultaneous Localization And Mapping. 13

SMC Sliding Mode Control. 34, 39, 65

STRIA Strategic Transport Research and Innovation Agenda. 12

TCS Traction Control System. 23, 25, 44, 65

US United States. III, 1, 7, 8, 12–14

Symbols

Note: Generic notation is used to reduce number of equations. A_i denotes the variable A in the direction i ($i \in \{x, y\}$). A_j denotes the variable A for the wheel j ($j \in \{r, f\}$).

Other symbols

κ	Curvature
μ	Friction coefficient
e_c	Crosstrack error
e_h	Heading error
g	Gravitational constant

Vehicle parameters

I	Vehicle's moment of inertia about the Z axis
J_j	Moment of inertia around the axis that passes through the center of the wheel
k_j	Coefficient of the road drag
m	Vehicle's mass
R_j	Wheel's radius

Vehicle variables

α_j	Slip angle
β	Side-slip angle
δ_j	Steering angle
λ_j	Slip ratio
ψ	Yaw angle
ρ_j	Angular position
τ_j	Torque produced by the engine
τ_{Bj}	Braking torque produced by the brakes
$\vec{a}$	Acceleration of the CG ($\vec{a} = (a_x, a_y, 0)^{\mathrm{T}}$)
$\vec{v}$	Velocity of the CG ($\vec{v} = (v_x, v_y, 0)^{\mathrm{T}}$)
F_i	Force acting on the CG (in the vehicle's coordinate system)
$F_{j,i}$	Force acting on the wheel (in the wheel's coordinate system)
l_j	Distance from the axle to the CG
M	Aligning moment about the Z axis

B Vehicle Parameters in Simulations

Description	Notation	Unit	Value
Total mass	m	kg	1547
Mass above the front axle	-	kg	286
Mass above the rear axle	-	kg	871
Mass above the center	-	kg	390
Moment of inertia of the vehicle	I	$\mathrm{kg\,m^2}$	3520
Moment of inertia of the front wheel	J_f	$\mathrm{kg\,m^2}$	0.5
Moment of inertia of the rear wheel	J_r	$\mathrm{kg\,m^2}$	0.5
Radius of the front wheel	R_f	m	0.34
Radius of the rear wheel	R_r	m	0.37
Wheelbase	L	m	2.5
Distance from the front axle to the CG	l_f	m	1.72
Distance from the rear axle to the CG	l_r	m	0.78
Tire stiffness factor (long. dynamics)	B_x	-	12
Tire shape factor (long. dynamics)	C_x	-	1.4
Tire peak factor (long. dynamics)	D_x	-	1
Tire curvature factor (long. dynamics)	E_x	-	0.1
Tire stiffness factor (lat. dynamics)	B_y	-	0.15
Tire shape factor (lat. dynamics)	C_y	-	2
Tire peak factor (lat. dynamics)	D_y	-	1
Tire curvature factor (lat. dynamics)	E_y	-	0.95
Maximum torque	τ_{max}	N m	3500
Maximum braking torque	$\tau_{B,max}$	N m	5000
Maximum steering angle	$\delta_{f,max}$	rad	0.6

C Content of the Attached Disc

The attached disc contains following directories:

- *text* – A PDF file with the thesis
- *sim* – MATLAB/Simulink files and source codes with the simulation framework

References

[1] C. B. Frey and M. A. Osborne, "The future of employment: How susceptible are jobs to computerisation?," *Technological forecasting and social change*, vol. 114, pp. 254–280, 2017.

[2] "Investments to driverless cars." https://www.leasingoptions.co.uk/driverless-cars/index.html#investments. [Online; accessed 28-February-2020].

[3] S. Pandi, F. H. Fitzek, C. Lehmann, D. Nophut, D. Kiss, V. Kovacs, A. Nagy, G. Csorvasi, M. Tóth, T. Rajacsis, *et al.*, "Joint design of communication and control for connected cars in 5g communication systems," in *2016 IEEE Globecom Workshops (GC Wkshps)*, pp. 1–7, IEEE, 2016.

[4] M. Gerla, E.-K. Lee, G. Pau, and U. Lee, "Internet of vehicles: From intelligent grid to autonomous cars and vehicular clouds," in *2014 IEEE world forum on internet of things (WF-IoT)*, pp. 241–246, IEEE, 2014.

[5] M. Maurer, J. C. Gerdes, B. Lenz, H. Winner, *et al.*, "Autonomous driving," *Berlin, Germany: Springer Berlin Heidelberg*, vol. 10, pp. 978–3, 2016.

[6] Burak Aydin, Michal Bahnik, Dominik Filyo, David Pekarek, Srinath Sharma, Martin Vlasimsky, Jan Cech, Martin Hromcik, "Multi-sensor unit for autonomous driving: Experimental subscale vehicle platform," tech. rep., Czech Technical University in Prague, Faculty of Electrical Engineering, 2019.

[7] D. Efremov, "Unstable ground vehicles and artificial stability systems," Master's thesis, Czech Technical University in Prague, Faculty of Electrical Engineering, Czech Republic, 2018.

[8] J. Filip, "Trajectory Tracking for Autonomous Vehicles," Master's thesis, Czech Technical University in Prague, Faculty of Electrical Engineering, Czech Republic, 2018.

[9] L. Hostacny, "Vehicle Measurement System," Master's thesis, Czech Technical University in Prague, Faculty of Electrical Engineering, Czech Republic, 2019.

[10] M. Taiebat, A. L. Brown, H. R. Safford, S. Qu, and M. Xu, "A review on energy, environmental, and sustainability implications of connected and automated vehicles," *Environmental science & technology*, vol. 52, no. 20, pp. 11449–11465, 2018.

[11] G. Meyer and S. Beiker, *Road vehicle automation*. Springer, 2019.

[12] R. Okuda, Y. Kajiwara, and K. Terashima, "A survey of technical trend of adas and autonomous driving," in *Technical Papers of 2014 International Symposium on VLSI Design, Automation and Test*, pp. 1–4, IEEE, 2014.

[13] E. Yurtsever, J. Lambert, A. Carballo, and K. Takeda, "A survey of autonomous driving: common practices and emerging technologies," *arXiv preprint arXiv:1906.05113*, 2019.

[14] "'phantom auto' will tour city." The Milwaukee Sentinel. 8 December 1926. Retrieved 23 July 2013.

[15] "History of self-driving cars." https://en.wikipedia.org/wiki/History_of_self-driving_cars. [Online; accessed 1-March-2020].

[16] A. M. López, A. Imiya, T. Pajdla, and J. M. Álvarez, *Computer Vision in Vehicle Technology: Land, Sea, and Air*. John Wiley & Sons, 2017.

[17] K. Biss, R. T. Chien, F. Stahl, and S. J. Weissman, "Semantic modeling for deductive question-answering," *IEEE Transactions on Computers*, no. 4, pp. 358–366, 1976.

[18] J. W. Lowrie, M. Thomas, K. Gremban, and M. Turk, "The autonomous land vehicle (alv) preliminary road-following demonstration," in *Intelligent Robots and Computer Vision IV*, vol. 579, pp. 336–350, International Society for Optics and Photonics, 1985.

[19] A. Waxman, J. LeMoigne, L. Davis, B. Srinivasan, T. Kushner, E. Liang, and T. Siddalingaiah, "A visual navigation system for autonomous land vehicles," *IEEE Journal on Robotics and Automation*, vol. 3, no. 2, pp. 124–141, 1987.

[20] M. A. Turk, D. G. Morgenthaler, K. D. Gremban, and M. Marra, "Vits-a vision system for autonomous land vehicle navigation," *IEEE Transactions on Pattern Analysis and Machine Intelligence*, vol. 10, no. 3, pp. 342–361, 1988.

[21] D. A. Pomerleau, "Alvinn: An autonomous land vehicle in a neural network," in *Advances in neural information processing systems*, pp. 305–313, 1989.

[22] Z.-S. Hou and Z. Wang, "From model-based control to data-driven control: Survey, classification and perspective," *Information Sciences*, vol. 235, pp. 3–35, 2013.

[23] E. D. Dickmanns, *Dynamic vision for perception and control of motion*. Springer Science & Business Media, 2007.

[24] "Back to the future: Autonomous driving in 1995." https://www.roboticsbusinessreview.com/slideshow/

back_to_the_future_autonomous_driving_in_1995/. [Online; accessed 2-March-2020].

[25] D. Pomerleau, "Ralph: Rapidly adapting lateral position handler," in *Proceedings of the Intelligent Vehicles' 95. Symposium*, pp. 506–511, IEEE, 1995.

[26] N. R. Council *et al.*, *Technology Development for Army Unmanned Ground Vehicles*. National Academies Press, 2003.

[27] "Who is to blame for 'self-driving car' deaths?." https://www.bbc.com/news/business-44159581. [Online; accessed 3-March-2020].

[28] N. H. T. S. Administration *et al.*, "Us department of transportation releases policy on automated vehicle development," *Policy*, pp. 14–13, 2013.

[29] S. O.-R. A. V. S. Committee *et al.*, "Taxonomy and definitions for terms related to on-road motor vehicle automated driving systems," *SAE Standard J*, vol. 3016, pp. 1–16, 2014.

[30] "Tesla level 5: Autopilot." https://towardsdatascience.com/tesla-level-5-autopilot-669f6ac6ee63. [Online; accessed 4-March-2020].

[31] "How to read the stars." https://www.euroncap.com/en/about-euro-ncap/how-to-read-the-stars/. [Online; accessed 4-March-2020].

[32] G. Gunter, D. Gloudemans, R. E. Stern, S. McQuade, R. Bhadani, M. Bunting, M. L. D. Monache, R. Lysecky, B. Seibold, J. Sprinkle, *et al.*, "Are commercially implemented adaptive cruise control systems string stable?," *arXiv preprint arXiv:1905.02108*, 2019.

[33] "Why every car maker should skip level 3." https://driverless.wonderhowto.com/news/waymo-was-right-why-every-car-maker-should-skip-level-3-0178497/. [Online; accessed 5-March-2020].

[34] "Automated vehicles for safety." https://www.nhtsa.gov/technology-innovation/automated-vehicles-safety. [Online; accessed 5-March-2020].

[35] E. R. T. R. A. Council, "Automated driving roadmap," 2017.

[36] T. Litman, *Autonomous vehicle implementation predictions*. Victoria Transport Policy Institute Victoria, Canada, 2017.

[37] N. H. T. S. Administration *et al.*, "Automated driving systems 2.0: A vision for safety," *Washington, DC: US Department of Transportation, DOT HS*, vol. 812, p. 442, 2017.

[38] R. Frisoni, A. Dall'Oglio, C. Nelson, J. Long, C. Vollath, D. Ranghetti, S. McMinimy, and S. D. Gleave, "Research for tran committee–self-piloted cars: The future of road transport?," *European Parliament, Directorate-consortium and shall not be distributed or reproduced without the formal approval of the Partners*, 2016.

[39] G. Meyer, V. Blervaque, and P. Haikkola, "Stria roadmap on connected and automated transport: Road, rail and waterborne," 2019.

[40] N. H. T. S. Administration *et al.*, *Federal automated vehicles policy: Accelerating the next revolution in roadway safety*. US Department of Transportation, 2016.

[41] B. Canis, "Issues in autonomous vehicle testing and deployment," tech. rep., 2019.

[42] T. Evas, C. Rohr, F. Dunkerley, and D. Howarth, "A common eu approach to liability rules and insurance for connected and autonomous vehicles," *European Parliamentary Research Service Study*, 2018.

[43] "Eu and eea member states sign up for cross border experiments on cooperative, connected and automated mobility." https://ec.europa.eu/digital-single-market/en/news/eu-and-eea-member-states-sign-cross-border-experiments-cooperative-connected-and-automated. [Online; accessed 7-March-2020].

[44] N. Nevejans, "European civil law rules in robotics," *European Union*, 2017.

[45] "Connected and automated mobility: three 5g corridor trial projects to be launched at ict 2018 event." https://ec.europa.eu/digital-single-market/en/news/connected-and-automated-mobility-three-5g-corridor-trial-projects-be-launched-ict-2018-event. [Online; accessed 7-March-2020].

[46] P. Lin, "Why ethics matters for autonomous cars," in *Autonomous driving*, pp. 69–85, Springer, Berlin, Heidelberg, 2016.

[47] A. Hevelke and J. Nida-Rümelin, "Responsibility for crashes of autonomous vehicles: an ethical analysis," *Science and engineering ethics*, vol. 21, no. 3, pp. 619–630, 2015.

[48] "Autonomous racing leagues/competitions." https://diyrobocars.com/autonomous-racing-leaguescompetitions/. [Online; accessed 15-March-2020].

[49] "Darpa grand challenge." https://en.wikipedia.org/wiki/DARPA_Grand_Challenge. [Online; accessed 16-March-2020].

[50] M. Buehler, K. Iagnemma, and S. Singh, *The 2005 DARPA grand challenge: the great robot race*, vol. 36. Springer, 2007.

[51] S. Thrun, M. Montemerlo, H. Dahlkamp, D. Stavens, A. Aron, J. Diebel, P. Fong, J. Gale, M. Halpenny, G. Hoffmann, *et al.*, "Stanley: The robot that won the darpa grand challenge," *Journal of field Robotics*, vol. 23, no. 9, pp. 661–692, 2006.

[52] "Robocar: Watch the world's fastest autonomous car reach its record-breaking 282 km/h." https://www.guinnessworldrecords.com/news/2019/10/robocar-watch-the-worlds-fastest-autonomous-car-reach-its-record-breaking-282-k/. [Online; accessed 16-March-2020].

[53] M. O'Kelly, V. Sukhil, H. Abbas, J. Harkins, C. Kao, Y. V. Pant, R. Mangharam, D. Agarwal, M. Behl, P. Burgio, *et al.*, "F1/10: An open-source autonomous cyber-physical platform," *arXiv preprint arXiv:1901.08567*, 2019.

[54] P. Riekert and T.-E. Schunck, "Zur fahrmechanik des gummibereiften kraftfahrzeugs," *Ingenieur-Archiv*, vol. 11, no. 3, pp. 210–224, 1940.

[55] D. Schramm, M. Hiller, and R. Bardini, "Vehicle dynamics," in *Modeling and Simulation*, p. 151, Springer, 2014.

[56] J. Ackermann, J. Guldner, W. Sienel, R. Steinhauser, and V. I. Utkin, "Linear and nonlinear controller design for robust automatic steering," *IEEE Transactions on control systems technology*, vol. 3, no. 1, pp. 132–143, 1995.

[57] H. Pacejka, *Tire and vehicle dynamics*. Elsevier, 2005.

[58] P. Nguyen and E. Case, "Tire friction models and their effect on simulated vehicle dynamics," in *Proceedings of a Symposium on Commercial Vehicle Braking and Handling, number UM-HSRI-PF-75-6*, pp. 245–312, 1975.

[59] J. Svendenius, *Tire modeling and friction estimation*. PhD thesis, Department of Automatic Control, Lund University Lund, Sweden, 2007.

[60] E. Bakker, L. Nyborg, and H. B. Pacejka, "Tyre modelling for use in vehicle dynamics studies," *SAE Transactions*, pp. 190–204, 1987.

[61] H. B. Pacejka and E. Bakker, "The magic formula tyre model," *Vehicle system dynamics*, vol. 21, no. S1, pp. 1–18, 1992.

[62] J. Svendenius and B. Wittenmark, "Brush tire model with increased flexibility," in *2003 European Control Conference (ECC)*, pp. 1863–1868, IEEE, 2003.

[63] R. Attia, R. Orjuela, and M. Basset, "Combined longitudinal and lateral control for automated vehicle guidance," *Vehicle System Dynamics*, vol. 52, no. 2, pp. 261–279, 2014.

[64] K. C. Dey, L. Yan, X. Wang, Y. Wang, H. Shen, M. Chowdhury, L. Yu, C. Qiu, and V. Soundararaj, "A review of communication, driver characteristics, and controls aspects of cooperative adaptive cruise control (cacc)," *IEEE Transactions on Intelligent Transportation Systems*, vol. 17, no. 2, pp. 491–509, 2015.

[65] C. J. Kahane and J. N. Dang, "The long-term effect of abs in passenger cars and ltvs," tech. rep., 2009.

[66] "How anti-lock brakes work." https://auto.howstuffworks.com/auto-parts/brakes/brake-types/anti-lock-brake2.htm. [Online; accessed 20-March-2020].

[67] Michal Bahnik, Dominik Filyo, David Pekarek, Martin Vlasimsky, Jan Cech, Martin Hromcik, "Visually-assisted vehicle dynamic control (progress report)," tech. rep., Czech Technical University in Prague, Faculty of Electrical Engineering, 2019.

[68] R. Attia, R. Orjuela, and M. Basset, "Coupled longitudinal and lateral control strategy improving lateral stability for autonomous vehicle," in *2012 American Control Conference (ACC)*, pp. 6509–6514, IEEE, 2012.

[69] K. Kritayakirana and J. C. Gerdes, *Autonomous vehicle control at the limits of handling*. PhD thesis, Stanford University Stanford, CA, 2012.

[70] J. He, D. A. Crolla, M. Levesley, and W. Manning, "Coordination of active steering, driveline, and braking for integrated vehicle dynamics control," *Proceedings of the Institution of Mechanical Engineers, Part D: Journal of Automobile Engineering*, vol. 220, no. 10, pp. 1401–1420, 2006.

[71] J. He, *Integrated vehicle dynamics control using active steering, driveline and braking*. PhD thesis, University of Leeds, 2005.

[72] P. F. Lima, *Optimization-based motion planning and model predictive control for autonomous driving: With experimental evaluation on a heavy-duty construction truck*. PhD thesis, KTH Royal Institute of Technology, 2018.

[73] M. Marcano, J. A. Matute, R. Lattarulo, E. Martí, and J. Pérez, "Low speed longitudinal control algorithms for automated vehicles in simulation and real platforms," *Complexity*, vol. 2018, 2018.

[74] W. Farag, "Complex trajectory tracking using pid control for autonomous driving," *International Journal of Intelligent Transportation Systems Research*, pp. 1–11, 2019.

[75] L. Nouveliere *et al.*, "Experimental vehicle longitudinal control using a second order sliding mode technique," *Control Engineering Practice*, vol. 15, no. 8, pp. 943–954, 2007.

[76] R. Attia, R. Orjuela, and M. Basset, "Longitudinal control for automated vehicle guidance," *IFAC Proceedings Volumes*, vol. 45, no. 30, pp. 65–71, 2012.

[77] N. H. Amer, H. Zamzuri, K. Hudha, and Z. A. Kadir, "Modelling and control strategies in path tracking control for autonomous ground vehicles: a review of state of the art and challenges," *Journal of intelligent & robotic systems*, vol. 86, no. 2, pp. 225–254, 2017.

[78] J. M. Snider *et al.*, "Automatic steering methods for autonomous automobile path tracking," *Robotics Institute, Pittsburgh, PA, Tech. Rep. CMU-RITR-09-08*, 2009.

[79] R. C. Coulter, "Implementation of the pure pursuit path tracking algorithm," tech. rep., Carnegie-Mellon UNIV Pittsburgh PA Robotics INST, 1992.

[80] M. Samuel, M. Hussein, and M. B. Mohamad, "A review of some pure-pursuit based path tracking techniques for control of autonomous vehicle," *International Journal of Computer Applications*, vol. 135, no. 1, pp. 35–38, 2016.

[81] J. Wit, C. D. Crane III, and D. Armstrong, "Autonomous ground vehicle path tracking," *Journal of Robotic Systems*, vol. 21, no. 8, pp. 439–449, 2004.

[82] A. Ollero and G. Heredia, "Stability analysis of mobile robot path tracking," in *Proceedings 1995 IEEE/RSJ International Conference on Intelligent Robots and Systems. Human Robot Interaction and Cooperative Robots*, vol. 3, pp. 461–466, IEEE, 1995.

[83] G. M. Hoffmann, C. J. Tomlin, M. Montemerlo, and S. Thrun, "Autonomous automobile trajectory tracking for off-road driving: Controller design, experimental validation and racing," in *2007 American Control Conference*, pp. 2296–2301, IEEE, 2007.

[84] G. Tagne, R. Talj, and A. Charara, "Higher-order sliding mode control for lateral dynamics of autonomous vehicles, with experimental validation," in *2013 IEEE Intelligent Vehicles Symposium (IV)*, pp. 678–683, IEEE, 2013.

[85] S. Dominguez, A. Ali, G. Garcia, and P. Martinet, "Comparison of lateral controllers for autonomous vehicle: Experimental results," in *2016 IEEE 19th International Conference on Intelligent Transportation Systems (ITSC)*, pp. 1418–1423, IEEE, 2016.

[86] P. Zhao, J. Chen, Y. Song, X. Tao, T. Xu, and T. Mei, "Design of a control system for an autonomous vehicle based on adaptive-pid," *International Journal of Advanced Robotic Systems*, vol. 9, no. 2, p. 44, 2012.

[87] Michal Bahnik, Dominik Filyo, David Pekarek, Martin Vlasimsky, Jan Cech, Tomas Hanis, Martin Hromcik, "Visually assisted anti-lock braking system," 2020.

[88] A. Amini, I. Gilitschenski, J. Phillips, J. Moseyko, R. Banerjee, S. Karaman, and D. Rus, "Learning robust control policies for end-to-end autonomous driving from data-driven simulation," *IEEE Robotics and Automation Letters*, vol. 5, no. 2, pp. 1143–1150, 2020.